THE UNIVERSITY *of* EDINBURGH

Identification and Characterization of Ovine Herpesvirus 2 microRNAs

Claire Safrai Levy

Thesis submitted for the degree of Doctor of Philosophy

University of Edinburgh

2011

Declaration

I declare that this thesis has been composed by myself and has not been submitted for any other degree. The work described herein is my own except where otherwise indicated and all work of other authors is duly acknowledged.

Claire Levy

THE ROSLIN INSTITUTE
University of Edinburgh
Easter Bush
Midlothian EH25 9RG

Acknowledgements

The last four years have been an intense, fast-paced experience and it would not have been as useful, productive, fulfilling, or successful without the help and support of the following people. I am so appreciative that my supervisors Dr Bob Dalziel and Prof John Hopkins took me on for the project knowing I just had enthusiasm. Their open doors were always a reassurance, their input always positive, and they never ceased to think that I had more of value to say or write. Dr George Russell, Prof Ivan Morrison and Dr Amy Buck were kind enough to give cells and miRNA mimics for use in this study.

I was so lucky to enjoy my project and a big part of that was being surrounded daily by a fantastic group of people. To all those trapped in the tower, your support, wits, laughs, and office distractions all made it easy to come into work everyday. Frances Fowler made me feel welcome before I had even left California and Yvonne Ligertwood was the rock in the tumultuous sea that was the lab. To the future Drs Gill Campbell and Pete Wasson, it was a slog, and I am so happy to have gone through it with you.

Finally, the love and support of my family, The Clump, and friends back home in the Bay Area and in Edinburgh. You made home feel not so far and this task not so huge. A huge thank you to my parents for encouraging me to study abroad during my undergraduate degree, Josie Twigg for telling me to join her in Scotland, Edinburgh University Archery Club for making me want to come back and The Edinburgh Samba School for making me want to stay.

And a special thanks to Emily (because she asked me to) and to Denis - swashbuckling car chase.

Abstract

Ovine herpesvirus 2 (OvHV-2) is the causative agent of sheep-associated malignant catarrhal fever (MCF) in susceptible ruminants. Through an unknown mechanism, presence of the virus leads to proliferation of NK-like T cells that are not target-restricted by the MHC class molecules. These host cells cause the symptoms found in MCF; fever, swollen lymph nodes, and necrotic lesions of the nasal, conjunctival, and oral mucosa, which usually leads to death of the host.

MicroRNAs (miRNAs) are ~22 nt RNA molecules expressed by eukaryotes and viruses that regulate genes post-transcriptionally. Viral miRNAs have been found to regulate cellular genes to control the cell cycle and have a role in pathogenesis. It was hypothesised that OvHV-2 expresses miRNAs and these play a role in MCF pathogenesis. The aim of this project was to determine if OvHV-2 encodes miRNAs.

Bioinformatic analysis was conducted on deep sequencing data from RNA of OvHV-2-immortalised T cells. Candidate miRNAs were selected if they adhered to miRNA secondary structure. 46 candidate miRNAs were found, with three clusters on the minus strand; one at the 5' end and the other two in a 9.3 kb region that contains no predicted open reading frames. The 8 most abundant candidates were successfully validated by northern hybridisation for small RNAs. The majority of the predicted targets for the 8 validated OvHV-2 miRNAs were from the OvHV-2 genome.

This study adds OvHV-2 to the list of herpesviruses that encode miRNAs and provides another tool for studying the pathogenesis of MCF.

Table of Contents

List of Figures

List of Tables

Supplemental DVD

Abbreviations

3’	Three prime
5’	Five prime
^{32}P	Radioactive phosphorus isotope
α	Alpha
β	Beta
γ/δ	Gamma/delta
µg	Microgram
µl	Microlitre
µM	Micromolar
µm	Micrometre
~	Approximately
°C	Celsius
>	Greater than
≥	Greater than or equal to
<	Less than
%	Percent
*	Star
A	Adenine
A2M	Alpha-2-macroglobulin
Ago	Argonaute/eukaryotic translation initiation factor 2C (eIF2C)
AIDS	Acquired immune deficiency syndrome
Akt	V-akt murine thymomo viral oncogene homologue
ALDH3A2	Aldehyde dehydrogenase 3 family, member A2
AlHV-1	Alcelaphine herpesvirus 1
AMP	Ampicillin
ANK1	Ankyrin 1
ATL	Adult T cell leukaemia

ATP	Adenosine triphosphate
ATP5B	Adenosine triphosphate synthase
BALF1	*Bam*HI A leftward reading frame 1 of Epstein-Barr virus
BALF5	*Bam*HI A leftward reading frame 5 of Epstein-Barr virus
BART	*Bam*HI A rightward transcript of Epstein-Barr virus
BATF	Basic leucine zipper transcription factor
BAX	B cell lymphoma 2-associated X protein
BBC3	B cell lymphoma 2 binding component 3
bcl	B cell lymphoma
BCL2L13	B cell lymphoma 2-like 13
BCLAF1	B cell lymphoma-associated transcription factor 1
BcLF1	*Bam*HI C leftward reading frame 1 of Epstein-Barr virus
BD	Becton, Dickinson and Company
BDLF1	*Bam*HI D leftward reading frame 1 of Epstein-Barr virus
BDLF2	*Bam*HI D leftward reading frame 2 of Epstein-Barr virus
BDLF4	*Bam*HI D leftward reading frame 4 of Epstein-Barr virus
BdRF1	*Bam*HI D rightward reading frame 1 of Epstein-Barr virus
BFRF2	*Bam*HI F rightward reading frame 2 of Epstein-Barr virus
BFRF3	*Bam*HI F rightward reading frame 3 of Epstein-Barr virus
BGLF3	*Bam*HI G leftward reading frame 3 of Epstein-Barr virus
BGLF3.5	*Bam*HI G leftward reading frame 3.5 of Epstein-Barr virus
BHK	Baby hamster kidney
BILF1	*Bam*HI I leftward reading frame 1 of Epstein-Barr virus
Bim	B cell lymphoma 2-like 11
BKRF4	*Bam*HI K rightward reading frame 4 of Epstein-Barr virus
BLAST	Basic local alignment search tool
blastn	Basic local alignment search tool for nucleic acids
blastp	Basic local alignment search tool for proteins
BMLF1	*Bam*HI M leftward reading frame 1 of Epstein-Barr virus
BMRF2	*Bam*HI M rightward reading frame 2 of Epstein-Barr virus

BoHV-1	Bovine herpesvirus 1
BORF1	*Bam*HI O righward reading frame 1 of Epstein-Barr virus
bp	Base-pair
BRLF1	*Bam*HI R leftward reading frame 1 of Epstein-Barr virus
BRRF2	*Bam*HI R rightward reading frame 2 of Epstein-Barr virus
BSLF2	*Bam*HI S leftward reading frame 2 of Epstein-Barr virus
BVLF1.5	*Bam*HI V leftward reading frame 1.5 of Epstein-Barr virus
BVRF2	*Bam*HI V rightward reading frame 2 of Epstein-Barr virus
BXRF1	*Bam*HI X rightward reading frame 1 of Epstein-Barr virus
C	Cytosine
Ca	Calcium
CD	Cluster of differentiation
CDC25C	Cell division cycle 25 homologue C
CDH1	Cadherin 1/epithelial cadherin (E-cadherin)
Cdk	Cyclin-dependent kinase
cDNA	Complementary deoxyribonucleic acid
CDS	Coding sequence
CEBPβ	CCAAT/enhancer binding protein beta
CEP350	Centrosomal protein
Ci	Curie
Cl	Chloride
CMV	Cytomegalovirus
CO_2	Carbon dioxide
Col 1a2	Collagen, type 1, alpha 2
comp.	Complementary
ConA	Concanavalin A
CREB	Cyclic adenosine monophosphate responsive element binding protein
CREM	Cyclic adenosine monophosphate responsive element modulator
CXCL11/ I-TAC	Chemokine (C-X-C motif) ligand 11

CXCL12	Chemokine (C-X-C motif) ligand 12
CXCL16	Chemokine (C-X-C motif) ligand 16
CXCR4	Chemokine (C-X-C motif) receptor 4
daf	Abnormal dauer formation
DEAD	Aspartic acid-glutamic acid-alanine-aspartic acid
DENND4C	DENN/MAP-kinase activating death domain, domain containing 4C
DEPC	Diethylpyrocarbonate
DGCR8	DiGeorge syndrome critical region gene 8
DMSO	Dimethyl sulfoxide
DNA	Deoxyribonucleic acid
dNTP	Deoxyribonucleotide triphosphate
dsDNA	Double-stranded deoxyribonucleic acid
dUTP	Deoxyuridine triphosphate
E2F1	E2F transcription factor 1/retinoblastoma-associated/binding protein
EBER	Epstein-Barr virus encoded ribonucleic acid
EBNA	Epstein-Barr virus nuclear antigen
EBV	Epstein-Barr virus/human herpesvirus 4
EDC	1-ethyl-3-(3-dimethylaminopropyl)carbodiimide
EDTA	ethylenediaminetetraacetic acid
EEHV-1	Elephant endotheliotropic herpesvirus 1
e.g.	*Exempli gratia*; for example
EGFP	Enhanced green fluorescent protein
EHV-2	Equid herpesvirus 2
et al.	*Et alii*; and others
Exp-5	Exportin 5
FGARAT	Formylglycinamide ribotide amidotransferase
FoxO3a	Forkhead box O3 a
G1	Growth 1
G	Guanine
g	Gram

g/gp	Glycoprotein
GFP	Green fluorescent protein
GSK3β	Glycogen synthase kinase 3 beta
GTF2IRD2	General transcription factor 2I repeat domain 2
GTP	Guanosine triphosphate
HCMV	Human cytomegalovirus/human herpesvirus 5
HHV-6A	Human herpesvirus 6A
HHV-6B	Human herpesvirus 6B
HIVEP2	Human immunodeficiency virus type I enhancer binding protein 2
HLA II	Human leukocyte antigen class II
hr(s)	Hour(s)
HSV-1	Herpes simplex virus 1/human herpesvirus 1
HSV-2	Herpes simplex virus 2/human herpesvirus 2
HTLV-1	Human T cell lymphotropic virus 1
HV	Herpevirus
ICP	Infected-cell polypeptide
IE	Immediate-early
i.e.	*Id est*; that is
IFNγ	Interferon gamma
IL	Interleukin
ILTV	Infectious laryngotracheitis virus/gallid herpesvirus 1
IMPACT	Image analysis, multiphoton and confocal technologies
IRES	Internal ribosome entry site
JAK	Janus kinase
JC	John Cunningham
jpg	Jpeg
Jun	Jun proto-oncogene
K	Potassium
Kb	Kilobase
kbp	Kilobase-pair

KCl	Potassium chloride
KEGG	Kyoto encyclopaedia of genes and genomes
KH_2PO_4	Monopotassium phosphate
KLF4	Kruppel-like factor 4
KLHL31	Kelch-like 31
km	Kilometre
KSHV	Kaposi's sarcoma-associated herpesvirus
L	Litre
LANA	Latency-associated nuclear antigen
LARII	Luciferase assay reagent II
LB	Luria Bertani
let	Lethal
LGL	Large granular lymphocyte
Li	Lithium
lin	Abnormal cell lineage
LIP	Liver enriched inhibiting protein
LMP	Latent membrane protein
lsy	Laterally symmetric
M	Molar
MAF	Musculoaponeurotic fibrosarcoma oncogene
MAQ	Mapping and assembly with quality
Mat1	Menage a trois homologue 1
MCF	Malignant catarrhal fever
mCi	Millicurie
MCMV	Murine cytomegalovirus/murid herpesvirus 1
MDV-1	Marek's disease virus 1/gallid herpesvirus 2
MFE	Minimal folding free energy
MFEI	Minimal folding free energy index
Mg	Magnesium
mg	Milligram

$MgCl_2$	Magnesium chloride
$MgSO_4$	Magnesium sulfate
MHC	Major histocompatibility complex
MHV-68	Murine herpesvirus 68/murid herpesvirus 4
MICB	Major histocompatibility complex class I polypeptide-related sequence B
min	Minute
miRNA/miR	Micro ribonucleic acid
miRNA*/ miR*	Ribonucleic acid duplexed with micro ribonucleic acid (passenger strand)
miRNP	Micro ribonucleoprotein
ml	Millilitre
mM	Millimolar
mmol	Millimole
MOPS	3-(N-morpholino)propanesulfonic acid
mRNA	Messenger ribonucleic acid
mTOR	Mechanistic target of rapamysin
MYOHD1	Myosin XIX
Na	Sodium
$Na_2H_2PO_4$	Sodium dihydrogen phosphate
NaCl	Sodium chloride
NaOH	Sodium hydroxide
NCBI	National centre for biotechnology information
NDFIP2	Neural precursor cell expressed, developmentally downregulated 4 family interacting protein 2
NDUFB5	Nicotinamide adenine dinucleotide dehydrogenase (ubiquinone) 1 beta subcomplex 5
NEB	New England Biolabs
NECAB2	N-terminal EF-hand calcium binding protein 2
nEGFP	Nuclear enhanced green fluorescent protein
NF-κB	Nuclear factor of kappa light polypeptide gene enhancer in B cells

NFIB	Nuclear factor I/B
ng	Nanogram
nGFP	Nuclear green fluorescent protein
NH_4	Ammonium
nM	Nanomolar
nm	Nanometre
nt	Nucleotide
Oct4	Octamer-binding protein 4
OD	Optical density
oligo(dT)	Oligodeoxythymidylic acid
oncomiR	Oncogenic micro ribonucleic acid
ORF	Open reading frame or transcript derived from the designated open reading frame
orf	Protein translated from the designated open reading frame
Ov	Unique ovine herpesvirus 2 open reading frame
OvHV-2	Ovine herpesvirus 2
p	Protein
P-bodies	Processing bodies
PBS	Phosphate buffer solution
PCR	Polymerase chain reaction
PDCD6	Programmed cell death 6
pdf	Portable document format
PERP	p53 apoptosis effector related to peripheral myelin protein 22
PITRM1	Pitrilysin metallopeptidase 1
PLAC1	Placenta-specific 1
Plk1	Polo-like kinase 1
pmol	Picomole
polyA	Polyadenylation
pre-miRNA	Preliminary micro ribonucleic acid
pre-mRNA	Preliminary messenger ribonucleic acid

PRG1	Protein 53-responsive gene 1
pri-miRNA	Primary micro ribonucleic acid
PRSS2	Protease, serine 2
psi	Pounds per square inch
PTEN	Phosphatase and tensin homologue
PU.1	Spleen focus forming virus proviral integration oncogene spi 1
PUMA	Protein 53 upregulated modulator of apoptosis
Rbl2	Retinoblastoma-like 2
RC	Rolling-circle
REPS2	RalA binding protein 1 associated Eps domain containing 2
RISC	Ribonucleic acid-induced silencing complex
RNA	Ribonucleic acid
rpm	Rotations per minute
rRNA	Ribosomal ribonucleic acid
RTA	R transactivator
S	Synthesis
s	Second
SA-MCF	Sheep-associated malignant catarrhal fever
SDS	Sodium dodecyl sulfate
SEMA7A	Semaphorin 7A
SF3B14	Splicing factor 3B subunit 14
SLS	Scientific laboratory supplies
Smad2	Sma/mothers against decapentaplegic homologue 2
SOAP	Short oligonucleotide analysis package
SOC	Super optimal broth with catabolite repression
SOX2	Sex determining region Y-box 2
SPBS	Sterile phosphate buffer solution
SPP1	Secreted phosphoprotein 1
SSC	Saline sodium citrate
ssDNA	Single-stranded deoxyribonucleic acid

STAT	Signal transducer and activator of transcription
T	Thymine
TAE	Tris-acetate-ethylenediaminetetraacetic acid
TBE	Tris-borate-ethylenediaminetetraacetic acid
TE	Tris-ethylenediaminetetraacetic acid
TEMED	Tetramethylethylenediamine
TGFβ	Transforming growth factor beta
TGFR1	Transforming growth factor receptor 1
THBS1	Thrombospondin 1
TLR	Toll-like receptor
™	Trademark
TNFα	Tumour necrosis factor alpha
TRBP	Trans-activation-responsive ribonucleic acid binding protein
tRNA	Transfer ribonucleic acid
Tsc-22	Transforming growth factor beta-stimulated clone 22
TWEAKR	Tumour necrosis factor-related weak inducer of apoptosis receptor
U	Unit
U	Uracil
UBE2G1	Ubiquitin-conjugation enzyme E2G 1
U_L	Unique long open reading frame or transcript derived from the designated unique long open reading frame
u_L	Protein translated from the designated unique long open reading frame
UTP	Uridine 5'-triphosphate
UTR	Untranslated region
UV	Ultraviolet
V	Volt
VEGF	Vascular endothelial growth factor
vols	Volumes
v/v	Volume per volume
VZV	Varicella-zoster virus/human herpesvirus 3

WA-MCF	Wildebeest-associated malignant catarrhal fever
WBC	White buffy coat
WDR59	WD repeat domain 59
w/t	Weight per volume
x g	G force, relative centrifugal force
Ybx1	Y box binding protein 1
ZBED5	Zinc finger, BED-type containing 5

Chapter One: Introduction

1.1 MALIGNANT CATARRHAL FEVER

Malignant catarrhal fever (MCF) was first described in Africa in the early 1920s and in Europe in 1930 as a mostly fatal condition affecting cattle that had associated with apparently healthy wildebeest or sheep (Løken, *et al*., 1998 referring to Mettam, 1923 and Götze *et al*., 1930). Since then, this disease has been found throughout the order Artiodactyla (cloven-hoofed mammals) (Ackermann, 2006). Wildebeest-associated MCF (WA-MCF) was found in 1960 to be caused by a virus that was later classified as a gammaherpesvirus in the *Macavirus* genus; alcelaphine herpesvirus 1 (AlHV-1) (Plowright *et al*., 1960). Sheep-associated MCF (SA-MCF) was found to be caused by the antigenically related ovine herpesvirus 2 (OvHV-2) in 1993 (Rossiter, 1983, 1981). These viruses are members of a family that maintain life-long, persistent infections and this is what is observed in their natural hosts (wildebeest and sheep). So why is it that other related species develop disease? Persistence in a host requires herpesviruses to maintain a latent life stage which balances viral genome replication with immune evasion. At times of stress and suppression of the immune system, these viruses can reactivate, produce new virions and cause clinical symptoms. In the situation of sheep and cows in a pasture, stress and immunosuppression as a trigger for reactivation and the development of disease do not seem to fit. I hypothesize that the pathology of these viruses is due to an imbalance of regulatory factors that effect the expression of both viral and cellular transcripts.

1.1.1 Clinical Forms of MCF

Clinical symptoms of MCF in susceptible species appear 2-12 weeks after initial infection and can present as five overlapping syndromes; head and eye (most common) peracute, alimentary, neurological, and cutaneous (Russell *et al*., 2009). The head and eye form presents as fever, lack of appetite, diarrhoea, depression, and discharge from the nose and eyes (Figure 1.1). Additional presentations include weight loss, shivering/trembling, red urine, lethargy, loss of balance, ocular swelling, drooling,

(Picture courtesy of Dr Bob Dalziel).

Figure 1.1: A cow exhibiting clinical signs of MCF.

clouding of the cornea, bloodshot eyes, sensitivity to light, hyperventilation, increased heart rate, and/or death (Costa *et al*., 2009, Sanford *et al*., 1977). Mortality and severity of morbidity are species-dependent; deer and bison have a high mortality rate (death can occur within a few days of the appearance of clinical symptoms) while up to 50% of cattle can recover and maintain a persistent infection (Coulter *et al*., 2001, O'Toole *et al*., 1997, Powers *et al*., 2005, Russell *et al*., 2009).

1.1.2 Gross Pathology

Post-mortems of MCF fatalities show swollen lymph nodes, inflammation, ulcers and necrotic lesions of mucosal membranes, and petechial haemorrhages of the systemic mucosal epithelium (Metzler, 1991, Russell *et al*., 2009). Mucosa of the respiratory tract can be covered by a mucopurulent exudate and the digestive tract shows inflammation and gas retention (Costa *et al*., 2009). The surface of the liver, spleen and kidneys can be covered with white foci and the epi- and myocardium of the heart can be infiltrated by macrophages and lymphocytes.

1.1.3 Microscopic Pathology

Microscopic investigation shows a decrease in the number of white blood cells found in the blood due to accumulation in necrotic tissue, systemic vasculitis (due to lymphocytes) and fibrinoid degeneration of the small and medium blood vessels, and necrotic germinal centres of lymph nodes and the adrenal cortex (Costa *et al*., 2009, Metzler, 1991, Russell *et al*., 2009, Sanford *et al*., 1977). Necrotic epithelium overlies the inflamed vessels (Sanford *et al*., 1977). The most affected organs include the kidneys, heart, liver, spleen, lungs, lymph nodes, and brain (Costa *et al*., 2009). The spleen is depleted of lymphocytes and engorged with erythrocytes. The cerebrum and cerebellum of the brain show lymphocyte perivascular cuffing and there is an increase in protein deposited in the liver.

1.1.4 Proposed Model for MCF Pathogenesis

MCF is characterized by depleted levels of IL-2 in host lymphnodes and the proliferation of immortalized large granular lymphocytes (LGLs) with a lymphokine-activated killer cell phenotype, i.e. cytokines released from other lymphocytes activate these cells to begin killing other cells. These cells have the ability to infiltrate various tissues and target cells without the restriction of the major histocompatibility complex class II (MHC) (Cook *et al*., 1988, Meier-Trummer *et al*., 2009). Different alleles of MHC II have been found to be associated with susceptibility and resistance to MCF in American bison (Traul *et al*., 2007). MHC II presents antibodies from outside the cell to $CD4^+$ T cells which is unexpected in relation to the pathogenic mechanism of OvHV-2 given that MHC II is not associated with viral-induced cytotoxicity (viral-induced cytotoxicity is catalyzed by MHC I presentation of antibodies from inside the infected cell to $CD8^+$ T cells). There has not been a study on the various alleles of MHC I at present, but it appears that some effect of OvHV-2 infection can lead to an immune response against non-OvHV-2-related antigens.

The cause of the necrotic lesions in the vasculature has been hypothesized to be the OvHV-2 latently-infected γ/δ T lymphocyte subpopulation (Liggitt *et al*., 1980, Nelson *et al*., 2010, Simon *et al*., 2003). It is hypothesized that the cells may autostimulate each other via an interaction between CD2 and CD58 (Schock *et al*., 1998). The OvHV-2 transcriptome in cells of susceptible species lies somewhere between the normal gene expression patterns expected of lytic and latent virus. MCF may be a result of a lack of control over OvHV-2 gene expression in these animals (Russell *et al*., 2009); for example, OvHV-2 replication in lambs is restricted to the respiratory tract (mostly in the turbinates) whereas in cattle, OvHV-2 replication has been found in the brain, kidney, intestine, and bladder (Cunha *et al*., 2008).

1.2 HERPESVIRUSES

Herpesviruses are widespread throughout the animal kingdom and are able to control their own genome replication and virion production by encoding and expressing a large number of protein coding open reading frames (ORFs) (Roizmann *et al*., 1992).

1.2.1 Herpesvirus Structure

Herpesviruses are enveloped with a linear double-stranded DNA (dsDNA) genome contained within an icosahedral capsid (nucleocapsid) (Figure 1.2) (Roizmann *et al*., 1992). Between the envelope and nucleocapsid is a protein-filled space called the tegument. The capsids range from 100-110 nm in diameter but the size of the virions increase to 120-300 nm once the tegument and envelope are included.

The tegument of herpesviruses has yet to be clearly defined but recently there has been evidence that suggests the tegument is more structured than previously thought; the tegument consists of a densely packed inner protein layer associated with the nucleocapsid and a loosely-packed outer protein layer between the inner tegument and the envelope (Yu *et al*., 2011).

The envelope of herpesviruses is made up of a lipid biolayer (originating from the host cell it was released from) incorporated with a number of glycoproteins (g/gp) that are associated with the outer tegument to relay stimuli from the outside environment to the nucleocapsid (Roizmann *et al*., 1992).

1.2.2 Herpesvirus Genomes

As of March 2011, 45 species of herpesvirus have had their genome completely sequenced and published online (http://www.ncbi.nlm.nih.gov/); they range in size from 108,409 base-pairs (bp) (gammaherpesvirus ateline herpesvirus 3 in new world monkeys) to 295,146 bp (alloherpesvirus cyprinid herpesvirus 3 in sturgeon) and express from 69 ORFs (alphaherpesvirus suid herpesvirus 1 in pigs) to 223 ORFs (betaherpesvirus macacine herpesvirus 3 in macaques). Through the rest of this thesis,

"ORF50" (as an example) will designate open reading frame 50 or the RNA transcript transcribed from open reading frame 50 and "orf50" will designate the protein product of "ORF50". Of the ORFs encoded by herpesviruses, 43 are conserved by all members and the remainder range in specificity between sub-family (alpha, beta, and gamma) genus and species levels (McGeoch and Davison, 1999). The roles of the conserved ORFs are related to viral replication, structure, egress, and the tegument whereas the unique ORFs are related to infectivity, immune evasion and pathogenesis (McGeoch *et al*., 2006).

Herpesvirus genomes are organized in six different ways; consisting of a long unique sequence flanked or separated by sequence repeats of varying length (Roizmann *et al*., 1992). These six organizations are described with the letters A-F. A genomes have a single long unique sequence with a shorter sequence repeated exactly at both termini; B genomes have a long unique sequence with shorter sequences repeated many times at both termini; C genomes have short sequences that are repeated at both termini, but are repeated less than in B genomes and may also contain additional unrelated repeat regions that divide the long unique sequence; D genomes have a long unique sequence with two sequence repeats; one at a terminus and one within the unique sequence in an inverted orientation to that of the terminal repeat; the E genome unique sequence is flanked by two shorter sequences that are both repeated internally and inverted; F genomes do not contain repeated regions (Figure 1.3).

Upon entry of the viral genome into the host cell's nucleus, the genome becomes associated with cellular histones (forming nucleosomes) which alter the structure, and therefore the availability of ORFs to be expressed, based on the stage of the viral life cycle (Nevels *et al*., 2011).

"Plus" and "minus" can be used to describe each of the DNA strands in the herpesvirus genome. ORFs are numbered left to right based on homology within the taxonomic

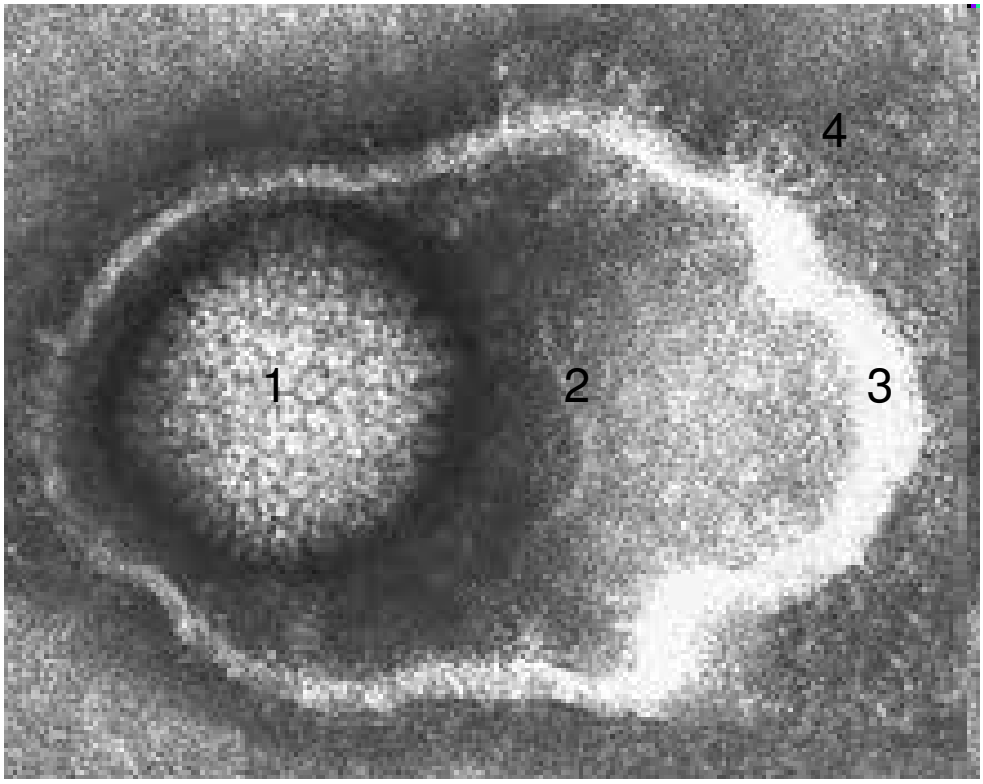

1: Nucleocapsid
2: Tegument
3: Envelope
4: Glycoproteins

Figure 1.2: The structure of a typical herpesvirus virion; herpes simplex virus is pictured here, taken from Herpesviruses 2000; http://www.stanford.edu/group/virus/herpes/2000/herpes2000.html.

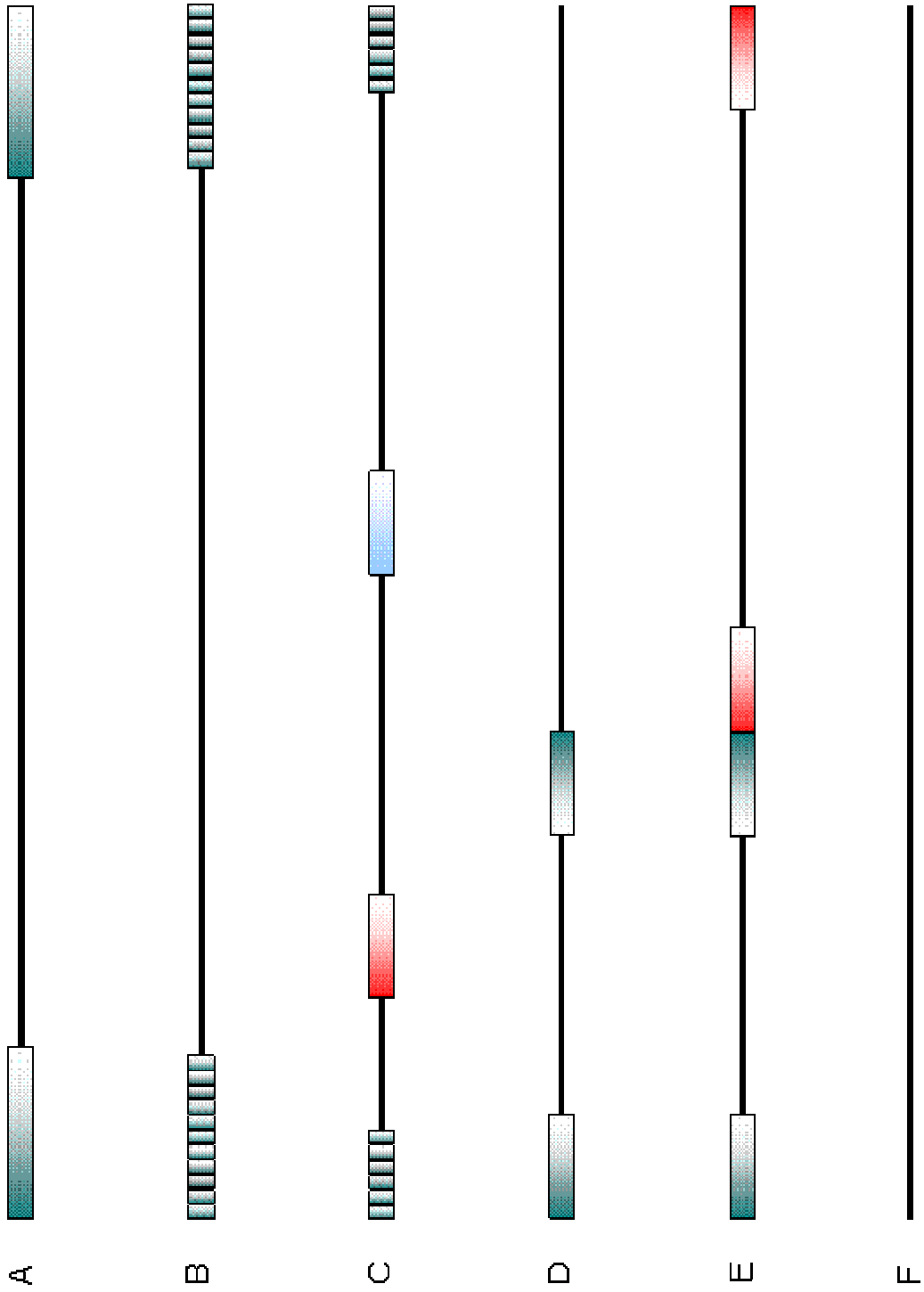

Figure 1.3: Schematic of the six different organizations (A-F) of the herpesvirus genome (adapted from Roizmann *et al*., 1992). The black line represents the unique sequence, and each box represents a repeat region; colour fade shows the direction of the repeated region.

groups. In this orientation, those that are transcribed left to right are on the plus strand and those that are transcribed right to left are on the minus strand.

1.3 HERPESVIRUS CLASSIFICATION

The herpesvirus family (Herpesviridae) is divided into three subfamilies (*Alphaherpesvirinae*, *Betaherpesvirinae*, and *Gammaherpesvirinae*) based on genome content and biological properties; range of host species and cell type, replication efficiency, and clinical symptoms where they occur.

1.3.1 Alphaherpesviruses

Alphaherpesviruses have a variable host range, they reproduce quickly, are efficient at destroying their host cells, and maintain latency in sensory ganglia (Roizmann *et al*., 1992). There are 4 genera in this sub-family comprised of 36 species; *Simplexvirus*, *Varicellovirus*, *Mardivirus*, and *Iltovirus* (Davison *et al*., 2009).

The best studied of the alphaherpesviruses are the *Simplexvirus*. Descriptions of the oral blisters (cold sores) caused by the *Simplexvirus* member herpes simplex virus 1 (human herpesvirus 1, HSV-1) have been documented since ancient Greece (Hunt, 2011). The virus is transmitted through the epithelial mucosa of the mouth or genitals and replicates in the reciprocal cells of the new host while latency is established in the sensory neurons that innervate these tissues; the trigeminal ganglia or the sacral ganglia, respectively. Reactivation of the virus is generally stress-related and results in migration of HSV-1 back down the neuron and causes a blister to form on the epithelial surface which will fill with newly replicated virions to be passed to a new host. HSV-1 can also cause more severe clinical symptoms such as eczema, ulcers, blindness (if the eye is infected), and seizures.

The *Varicellovirus* member varicella-zoster virus (human herpesvirus 3, VZV) infects most people worldwide during childhood causing varicella lesions across large areas of skin (chicken pox) (Arvin, 1996). Latency is established in the dorsal root ganglia and

reactivation in adults leads to localized lesions (herpes zoster). The chance of VZV reactivating (to cause shingles) becomes more likely as people age, if the immune system is suppressed e.g. with use of steroids. VZV is transmissible through skin-skin contact as well as through the respiratory tract and is most easily passed in temperate climates. Primary infection occurs in mucosal membranes and then migrates to lymph nodes during incubation where virions spread to $CD4^+$ and $CD8^+$ T cells. These cells enable access to the epidermis where virion replication leads to the varicella rash. In immunosuppressed individuals, VZV can infect most organs leading to varicella pneumonia, liver failure, varicella encephalitis, cerebellar ataxia, thrombocytopenia, necrotic adrenal glands, and congenital varicella syndrome when a mother is infected with VZV in early pregnancy.

The *Mardivirus* member Marek's Disease Virus 1 (gallid herpesvirus 2, MDV-1) initially infects and replicates in B lymphocytes of poultry (Mwangi *et al*., 2011). Within a week of infection, MDV establishes latency in $CD4^+$ T cells with a subpopulation infecting feather follicle epithelial cells. The epithelial cells are shed into the environment and transmit the virus through the respiratory route. Within a month of infection, $CD4^+$ T cell lymphomas can be produced throughout the entire body of the host. Vaccines have been developed that prevent tumour formation but they do not prevent infection or transmission.

The *Iltovirus* member infectious laryngotracheitis virus (gallid herpesvirus 1, ILTV) establishes latency in the central nervous system of chickens (Lee *et al*., 2010). Reactivation of the virus results in a largely fatal upper respiratory disease of the trachea involving increased mucus production and haemorrhaging.

1.3.2 Betaherpesviruses

Betaherpesviruses have a narrow host range, they reproduce slowly, infected cells become enlarged rather than lyse, and they maintain latency in lymphoreticular cells (Roizmann *et al*., 1992). Beta- and alphaherpesviruses maintain a latent infection in a

small range of cell types whereas the lytic stage of their life cycle is able to engage in the larger range of cells that they are able to infect (Ackermann, 2006). There are 4 genera in this sub-family comprised of 14 species; *Cytomegalovirus*, *Muromegalovirus*, *Roseolovirus*, and *Proboscivirus* (Davison *et al*., 2009).

The *Cytomegalovirus* member human cytomegalovirus (human herpesvirus 5, HCMV) is transmitted through body fluids and is highly seroprevalent, usually resulting in an asymptomatic infection in immunocompetent individuals (Crough *et al*., 2009). Occasionally, primary HCMV infection can lead to the presentation of a syndrome similar to that caused by primary infection of the gammaherpesvirus Epstein Barr virus (human herpesvirus 4, EBV) infectious mononucleosis. HCMV biology is still poorly understood, but latency is thought to be maintained in cells derived from bone marrow. Reactivation of HCMV occurs when these cells differentiate. The majority of pathogenic affects of HCMV are observed in children and the immunocompromised. Congenital infection can lead to sickness and death in newborns and neurological abnormalities and deafness in children. In immunocompromised individuals, HCMV disease presents as systemic inflammation.

The *Muromegalovirus* member murine cytomegalovirus (murid herpesvirus 1, MCMV) is closely related to and used as an animal model to study HCMV (Wiebusch *et al*., 2008).

The *Roseolovirus* members human herpesvirus 6A and human herpesvirus 6B (HHV-6A and HHV-6B) infect the majority of people within the first two years of life (Braun *et al*., 1997). Replication takes place in $CD4^+$ T cells and latency is established in macrophages. HHV-6A has yet to be associated with any disease but primary infection with HHV-6B causes roseola infantum in children.

The *Proboscivirus* member elephant endotheliotropic herpesvirus 1 (EEHV-1) mostly infects juvenile Asian elephants in zoos, circuses, or sanctuaries and causes systemic haemorrhaging which is usually fatal (Latimer *et al*., 2011).

1.3.3 Gammaherpesviruses

Gammaherpesviruses are limited to the family or order of their natural host and they tend to be specific for either B or T lymphocytes (Roizmann *et al*., 1992). Replication can take place in lymphoblastoid, epithelioid and fibroblastic cell lines and latency in lymphoid tissue. Differing from the other two sub-families, gammaherpesviruses preferentially maintain a latent infection once cells have been infected (Ackermann, 2006). There are 4 genera in this sub-family comprised of 34 species; *Lymphocryptovirus*, *Rhadinovirus*, *Macavirus*, and *Percavirus* (Davison *et al*., 2009).

The *Lymphocryptovirus* member EBV was first discovered in 1964 in a lymphoblastoid cell line derived from a Burkitt's lymphoma (B cell lymphoma) (Epstein *et al*., 1964). The virus is shed from epithelial cells of the tonsils and transmitted through saliva and found in the majority of people worldwide (Ascherio *et al*., 2010). Transmission during childhood does not result in the development of any clinical symptoms, whereas infection in adolescence and adulthood usually results in the development of infectious mononucleosis, a lymphoproliferative disease lasting a few weeks. The virus initially infects epithelial cells of the oropharynx for replication and then targets naïve B cells to establish latency. EBV expresses a number of viral genes that initiate the maturation of the cells to memory B cells in which EBV establishes latency without the risk of activating the host's immune response. Occasionally, infection by EBV can lead to the development of various malignancies; immunocompromised individuals can develop post-transplantation lymphoproliferative disorder, lymphomas, oral hairy leukoplakia, leiomyosarcomas, and X-linked lymphoproliferative disorder. Immunocompetent individuals can develop Burkitt's lymphoma in sub-Saharan Africa, nasopharyngeal carcinoma in northern Africa, southeast Asia, and among Inuits, and Hodgkin lymphoma in western countries.

The *Rhadinovirus* member human herpesvirus 8 (HHV-8, Kaposi's sarcoma-associated herpesvirus [KSHV]) was identified in 1994 in AIDS patients who had developed Kaposi's sarcoma (Chang *et al*., 1994); although the standard name for this virus is HHV-8, for the remainder of this thesis it will be referred to as KSHV so as to complement the microRNA nomenclature. Kaposi's sarcoma is caused by latent KSHV-infected endothelial spindle cells (Ganem, 1997). KSHV is primarily found in sub-Saharan Africa and the Mediterranean (Uldrick *et al*., 2011). KSHV virions may be produced by pharyngeal lymphoid or epithelial tissue or salivary glands and is transmitted by saliva; latency is established in B cells. Additional malignancies caused by KSHV include B cell lymphomas (such as primary effusion lymphoma), multiple myeloma and multicentric Castleman's disease.

The *Macavirus* members AlHV-1 and OvHV-2 cause the disease MCF in cloven-hoofed animals (described in section 1.1) and will be discussed in further detail below (Russell *et al*., 2009).

The *Percavirus* member equid herpesvirus 2 (EHV-2) is transmitted through the respiratory tract of horses and establishes latency in B cells (Brault *et al*., 2011). EHV-2 is thought to be the cause of respiratory disease, pharyngeal lymphoid hyperplasia, enlarged lymph nodes, inflammation of the eyes and skin, and abortion.

1.3.4 MCF Viruses

MCF can be caused by a number of gammaherpesviruses including hippotragine herpesvirus 1 (naturally infects roan antelopes) caprine herpesvirus 2 (naturally infects goats) an unidentified herpesvirus found to cause disease in white-tailed deer, and the most well known; AlHV-1 and OvHV-2 (Russell *et al*., 2009). Alcelaphids (wildebeest, hartebeest, and bonteboks) are the natural host of AlHV-1 and act as a reservoir for the virus. Genome analysis of AlHV-1 and OvHV-2 show a high degree of sequence identity (62%) extending even to the majority of unique ORFs.

Caprids (sheep and goats) are the natural host of OvHV-2 (C genome, 135135 bp). Bovids (cattle, bison, and water buffalo) cervids (deer and moose) and suids (pigs) are prone to the lymphoproliferative disease MCF. OvHV-2 DNA was first detected in susceptible host species in 1991 and in sheep in 1993 (Baxter *et al*., 1993, Bridgen *et al*., 1991). The virus initially infects and replicates in type II alveolar epithelial cells before targeting lymphocytes for latency (Baxter *et al*., 1997, Taus *et al*., 2010). Though the details of cell entry have yet to be ascertained for OvHV-2, homologues in other herpesviruses have been characterized (will be discussed in section 1.4) so it is assumed that a similar mechanism is used (Table 1.2). Latency in susceptible species is established in a subset of T cells, while in sheep B cells are also latently infected (Baxter *et al*., 1997, Taus *et al*., 2010). The T cells infected are $CD2^+$ peripheral blood mononuclear cells that are cytotoxic, with long-term latency in the $CD8^+$ subpopulation (Table 1.1) (Burrells *et al*., 1991, Kaufmann, 1996, Meier-Trummer *et al*., 2010, Thonur *et al*., 2006). It is these long-term latently-infected cells that have been hypothesized to cause MCF (Ellis *et al*., 1992, Meier-Trummer *et al*., 2009, Simon *et al*., 2003). Lytic replication from reactivated virus is initiated by orf50, orf57 and (putatively) ov6 and takes place in epithelial turbinate cells for shedding into the environment (Ackermann, 2006, Cunha *et al*., 2008). These cells undergo a single cycle of viral replication and released virions are unable to infect neighbouring epithelial cells (Li *et al*., 2004).

Table 1.1: T cell populations targeted by OvHV-2 in susceptible species.

T cell Receptor	T cell Subset	Role	Infectious
α/β	$CD4^-/CD8^+/CD2^+/T19^-$	Cytotoxic/ Suppressor	No
α/β	$CD4^+/CD8^-/CD2^+/T19^-$	Helper/Inducer	No
γ/δ	$CD4^-/CD8^+/CD2^+/T19^+$	Cytotoxic/Inducer	Yes

1.3.5 Transmission of AlHV-1 and OvHV-2 Infection

Though episodes of MCF have been observed to coincide with lambing (Collery *et al*., 1996) no evidence for an increase in viral shedding from dams has been found (Li *et al*.,

2004). Even so, it is thought that the stress of parturition in wildebeest cows and dams reactivates AlHV-1 and OvHV-2, respectively, and allows spread to the new generation. During primary infection of wildebeest calves and lambs, the viruses replicate in the respiratory tract (to a much higher degree than in adult animals) and are spread horizontally through tears and nasal secretions (Hüssy *et al*., 2002, Li *et al*., 2008, 2004, Russell *et al*., 2009). In wild pigs, incidents of venereal transmission have also been observed; boars have been found to be asymptomatic carriers that can transmit OvHV-2 to sows via virus-containing semen - the sows then go on to develop MCF (Costa *et al*., 2010).

Lambs seroconvert to OvHV-2-positive around 3 months of age and produce a peak of cell-free virus in nasal secretions around 8 months to maintain the viral reservoir (Li *et al*., 2004, 1999, 1998). Direct nose-nose contact is not necessary for transmission as outbreaks of MCF have been observed in susceptible species that have had varying contact with sheep (Moore *et al*., 2010). Transmission of OvHV-2 has been observed over a distance of at least 5 km between lambs and bison without having workers in common between the feedlots and the lambs being downwind of the bison (Li *et al*., 2008). It may be that birds act as a vector by landing in the feed of both lots and pick up and transfer virus-containing secretions with their feet. Susceptible species are dead-end hosts and cannot transmit OvHV-2 to other animals (Muller-Doblies *et al*., 2001); this is due to the cell-association of the virus they shed in comparison to the cell-free virus shed by sheep (Kim *et al*., 2003, Metzler, 1991).

1.3.6 Immunization

Treatment is difficult as death can occur within a couple days of the appearance of clinical symptoms. AlHV-1 (unlike OvHV-2 due to a lack of a permissive cell culture system) can be produced in a cell-free virulent and cell-free attenuated form; which is currently being exploited in hopes of finding a vaccine (Russell *et al*., 2009). Thus far however, exposure to attenuated AlHV-1 does not provide any protection against natural or experimental challenges. Any immunity observed in cattle has been short-lived and is

not associated with serum neutralizing antibody. Antibodies that recognize AlHV-1 antigens have been found to cross-react with those produced by OvHV-2, so theoretically a vaccine found for AlHV-1 could be effective for OvHV-2. Though sporadic, MCF is an economical issue for purveyors of American bison and Indonesian Bali cattle as they are extremely susceptible. For those locals that cannot keep sheep and susceptible species separate, OvHV-2-free sheep can be raised by separating 2 month old lambs from the OvHV-2-hosting herd (Hüssy *et al*., 2001, Li *et al*., 1999, 1998).

1.3.7 Large Granular Lymphocyte Cell Lines

Immortalized single-cell, LGL cell lines containing OvHV-2 DNA can be established from the lymph nodes of OvHV-2-infected cattle; e.g. BJ971, BJ1004, BJ1035, BJ1044, and BJ1104 (Russell *et al*., 2009, Schock *et al*., 1998). These cell lines are unresponsive to concanavalin A (ConA) stimulation unlike uninfected T cells, and contain a mixed population of latent and lytic virus. BJ1004, BJ1035, and BJ1104 are made up of $CD4^+/CD8^-$ T cells, BJ971 cells are $CD4^-/CD8^+$ T cells, and BJ1044 is a mixed population of $CD4^+/CD8^+$ cells. All five cell lines are $CD2^+/CD5^+$ and produce IFNγ, TNFα, and IL-10, and all but BJ1044 express IL-4.

1.4 HERPESVIRUS LIFE CYCLE

Given the conservation of the proteins involved in cell entry, replication, and egress between herpesviruses, research on one can suggest similar mechanisms in others. Therefore, the life cycle of herpesviruses will be described based on research on a number of viruses; where possible, proteins will be gammaherpesvirus specific because the mechanism is likely to be more accurate in regards to OvHV-2.

During initial infection, herpesviruses make cell contact using a glycoprotein to bind to a cell receptor. EBV uses gp350/220 to bind to CD21/CR2 (Carel *et al*., 1990). Once this contact is made, a complex made up of three other glycoproteins interacts with another specific receptor based on cell type; EBV gp25 (gL) gp42 and gp85 (gH) interact with

cellular human leukocyte antigen class II (HLA II) on B lymphocytes and a glycoprotein complex without gp42 is used when initiating entry into epithelial cells (epithelial cells lack HLA II) (Borza *et al*., 2002, Li *et al*., 1997, 1995, Molesworth *et al*., 2000, Wang *et al*., 1998, 1998). To initiate membrane fusion, a glycoprotein complex containing gB, gL and gH is necessary (Haddad *et al*., 1989, Miller *et al*., 1988). gB is a class III fusion protein which plays a role in attachment to target cells, fusion of the envelope with the cell membrane and viral maturation (Backovic *et al*., 2011). When endocytosed, a lysosome-independent decrease of pH within the formed vacuole causes a modest conformational change in gB that leads to the fusion of the two membranes and deenvelopment of the virion, releasing the nucleocapsid and tegument into the cytoplasm (Stampher *et al*., 2010).

For HSV-1, upon entry into the cytoplasm, phosphorylation by a tegument protein (u_L13) disassociates the outer tegument from the inner tegument and nucleocapsid (Kelly *et al*., 2009). Tegument proteins u_L36 and u_L37 remain associated with the capsid for transport to the nucleus while u_L11 and u_L14 remain in the cytoplasm. Although no interaction has yet been found, it is thought likely that transport along microtubules to the nucleus is mediated by the interaction of u_L36 and u_L37 with cellular dynein. u_L36 directs the capsid to the nucleus and interacts with the nuclear pore to aid the insertion of the viral genome into the nucleus. In HSV-1, u_L14 directs an alphaherpesvirus-specific tegument protein to the nucleus which initiates transcription of the viral genome. It is reasonable to assume that the conserved u_L14 has a similar role with a gammaherpesvirus-specific tegument protein that has yet to be characterized. Once in the nucleus, the genome circularizes and the virus initiates lytic replication and virion production or establishes latency whereby the viral episome becomes associated with cellular histones.

1.4.1 Lytic Replication

Hepesviruses can replicate upon infection of a host cell or reactivate from latency and undergo replication during times of stress, immunosuppression, and inflammation

(Crough *et al*., 2009). During reactivation the viral nucleosomes (1.1.2) become unstable and less dense, allowing access to previously blocked ORFs for transcription (Nevels *et al*., 2011). Herpesvirus replication is achieved through three waves of viral ORF expression; immediate-early (peak 2-4 hrs post-infection) early (peak 5-7 hrs post-infection) and late (peak 7-15 hrs post-infection) (Alwine *et al*., 1974, Boehmer *et al*., 1997). EBV BGLF3.5 (functional homologue to HSV-1 u_L14) catalyzes the transcription of the immediate-early ORFs (BRLF1, BSLF2/BMLF1, and a species specific gene) which once translated, initiate the transcription of the early ORFs that replicate the viral episome (Ackermann, 2006). The immediate-early ORFs initiate the transcription of early genes including the virally encoded DNA polymerase (OvHV-2 ORF9) ssDNA-binding protein (OvHV-2 Ov4.5) DNA helicase-primase (made up of OvHV-2 ORF40, ORF44 and ORF56) an origin-binding protein (as yet undefined in OvHV-2) and enzymes associated with nucleotide metabolism (Boehmer *et al*., 1997).

Initially, the episome undergoes origin-dependent theta replication, but then switches (by an as yet unknown mechanism) to sigma/rolling-circle replication (RC) (Boehmer *et al*., 1997). Theta replication describes the denaturing of the dsDNA of the episome at the origin of replication allowing binding of an RNA primer which facilitates coupled-DNA synthesis of the leading and lagging strands (del Solar *et al*., 1998). RC replication involves uncoupled-DNA synthesis whereby the leading strand is replicated before the lagging strand resulting in an intermediate state where the parental plus strand is single-stranded and the parental minus strand is double-stranded with the newly synthesized plus strand. The whole mechanism results in concatamers of the genome which are fed into the capsid and cleaved at the terminus of one unit length.

Genome replication initiates transcription of the late ORFs which encode for the structural proteins that make up the capsid in which the newly produced genome will be packaged. Once translated in response to viral DNA replication, the late structural capsid proteins (EBV BdRF1 complexed with BcLF1, BFRF3 (HSV-1 u_L35) and BVRF2 and BORF1 complexed with BDLF1,) are shuttled to the nucleus (Henson *et al*.,

2009). BdRF1 acts as a scaffold on which BcLF1, BFRF3, BORF1 and BDLF1 form a spherical procapsid. This structure interacts with the DNA packaging complex and BVRF2 cleaves the BdRF1 scaffolding as the newly replicated viral DNA is packed inside, resulting in the formation of a mature icosahedral nucleocapsid. DNA packaging and capsid maturation are ATP-dependent, in part to disassociate the viral DNA from the cellular histones (Dasgupta *et al*., 1999, Paulus *et al*., 2010).

Once the nucleocapsid is formed, it exits the nucleus by budding through the nuclear membrane (becoming enveloped at the inner nuclear membrane and deenveloped at the outer nuclear membrane) and enters the cytoplasm for association with tegument proteins, reenvelopment by the Golgi, and release into the extracellular space by exocytosis (Kelly *et al*., 2009). For HSV-1, the nucleocapsid is docked to the inner nuclear surface by u_L31 and u_L34 and enters the perinuclear space upon destabilization of the nuclear surface by u_L13. Once in the cytoplasm, the nucleocapsid is transported to the Golgi where it becomes associated with u_L36 and u_L37 which form the first layer of the tegument. The outer tegument layer, made up of u_L11, u_L16, and u_L21, is necessary for reenvelopment (Johnson *et al*., 2011).

EBV gB and gH facilitate deenvelopment of the nucleocapsid at the outer nuclear membrane and release into the cytoplasm and BcLF1 facilitates the association of the nucleocapsid with the inner tegument proteins (Kelly *et al*., 2009). Reenvelopment of the nucleocapsid and tegument at the Golgi is facilitated by gB (Johnson *et al*., 2011). The glycoprotein BKRF4 interacts with cellular kenesin-2 to transport the completed virion to the cell surface for exocytosis (Kelly *et al*., 2009).

1.4.2 Herpesvirus Latency

During latency, the viral nucleosomes increase in density and stability (similar to the host cell's chromatin) allowing transcription of only a minority of ORFs (Nevels *et al*., 2011, Paulus *et al*., 2010). ORF expression during latency is not conserved among herpesviruses; some express numerous ORFs whereas others may not express any

(Ackermann, 2006). Latency in gammaherpesviruses is maintained in part by homologues of EBV EBNA-1/KSHV LANA. This protein interacts with both viral and cellular proteins to achieve viral quiescence; it shuts down viral ORF expression by blocking expression of BRLF1/orf50 (1.3.1) aids in the replication and successful migration of the viral episome during cell mitosis by tethering the copies to the host's chromosomes, as well as blocking ubiquitin-dependent degradation to avoid immune detection (Cotter *et al*., 1999, Garber *et al*., 2002, Hu *et al*., 2002, Leight *et al*., 2000). To achieve this, LANA disrupts a number of cellular pathways including those that suppress tumour formation and transformation (Dittmer *et al*., 1998, Field *et al*., 2003, McCormick *et al*., 2005, Rosbottom, *et al*., 2002, Szekely *et al*., 1998, Verma *et al*., 2007, Zhong *et al*., 1996).

For EBV, latency is initially established in primary B cells where numerous latency-associated genes (EBNAs, LMPs, EBERs, and BARTs) are expressed from the Cp and Wp promoters (Ackermann, 2006, Babcock *et al*., 2000). These viral genes transform the B cells causing proliferation and protection from apoptosis (Ackermann, 2006). Long-term latency (expressed from the Qp promoter) is established in resting memory B cells in the blood where only viral LMP2A is expressed (Babcock et al., 1999) or the same B cell subset in lymph nodes where EBNA-1, LMP1, LMP2A, and LMP2B are expressed (Babcock et al., 2000). These more restricted latency states are the ones found in EBV-associated tumours (1.2.3).

Table 1.2: Described herpesvirus ORFs and their OvHV-2 homologs.

Virus	Protein	OvHV-2 Homolog
EBV	BcLF1	ORF25
	BDLF1	ORF26
	BdRF1	ORF17.5
	BFRF3	ORF65
	BGLF3.5	ORF35
	BKRF4	ORF45
	BORF1	ORF62
	BRLF1	ORF50
	BSLF2/BMLF1	ORF57
	BVRF2	ORF17
	gp350/220	Ov8
	gp42	Ov7
	gB	ORF8
	gH	ORF22
	gL	ORF47
EBV/KSHV	EBNA-1/LANA	ORF73
HSV-1	U_L11	ORF38
	U_L13	ORF36
	U_L14	ORF35
	U_L16	ORF33
	U_L21	ORF24
	U_L31	ORF69
	U_L34	ORF67
	U_L36	ORF64
	U_L37	ORF63

1.5 MICRORNAS

MicroRNAs (miRNAs) are a class of small (18-30 nt) RNA molecules that regulate gene expression post-transcriptionally (Olsen *et al*., 1999). The first miRNA was discovered in *Caenorhabditis elegans* in 1993 (Lee *et al*., 1993). It was 22 nt long, expressed by the lin-4 gene, and was found to downregulate the expression of the protein product of lin-14 by targeting seven complementary sites in the 3'UTR of the lin-14 mRNA (Wightman *et al*., 1993, 1991). In 2000, orthologs of a second miRNA found in *C. elegans* (expressed by the let-7 gene) were found in other species, which began an explosion of miRNA discovery in different organisms (Lagos-Quintana *et al*., 2001, Lau *et al*., 2001, Lee *et al*., 2001, Pasquinelli *et al*., 2000). As of April 2011, miRNAs have been found in water/slime moulds, animals, green plants, and viruses (miRBase, Release 16; http://www.mirbase.org/index.shtml). miRNAs can be highly conserved among the various groups with the exception of viruses possibly due to their accelerated response to natural selection.

1.5.1 miRNA Biogenesis

miRNAs are derived from longer RNA polymerase II and III primary transcripts (pri-miRNA) which range in size from hundreds to thousands of nt in length (Aparicio et al., 2006, Lagos-Quintana *et al*., 2001, Pfeffer *et al*, 2005). A distinguishing secondary structure of a pri-miRNA is an imperfectly duplexed, stem-loop (which includes the mature miRNA in one arm of the stem) flanked by single-stranded, unstructured RNA (Meister *et al*., 2004, Zeng *et al*., 2005). A pri-miRNA may contain a single miRNA or a cluster of distinct miRNAs within the arms of multiple stem-loops (Cai *et al*., 2004,

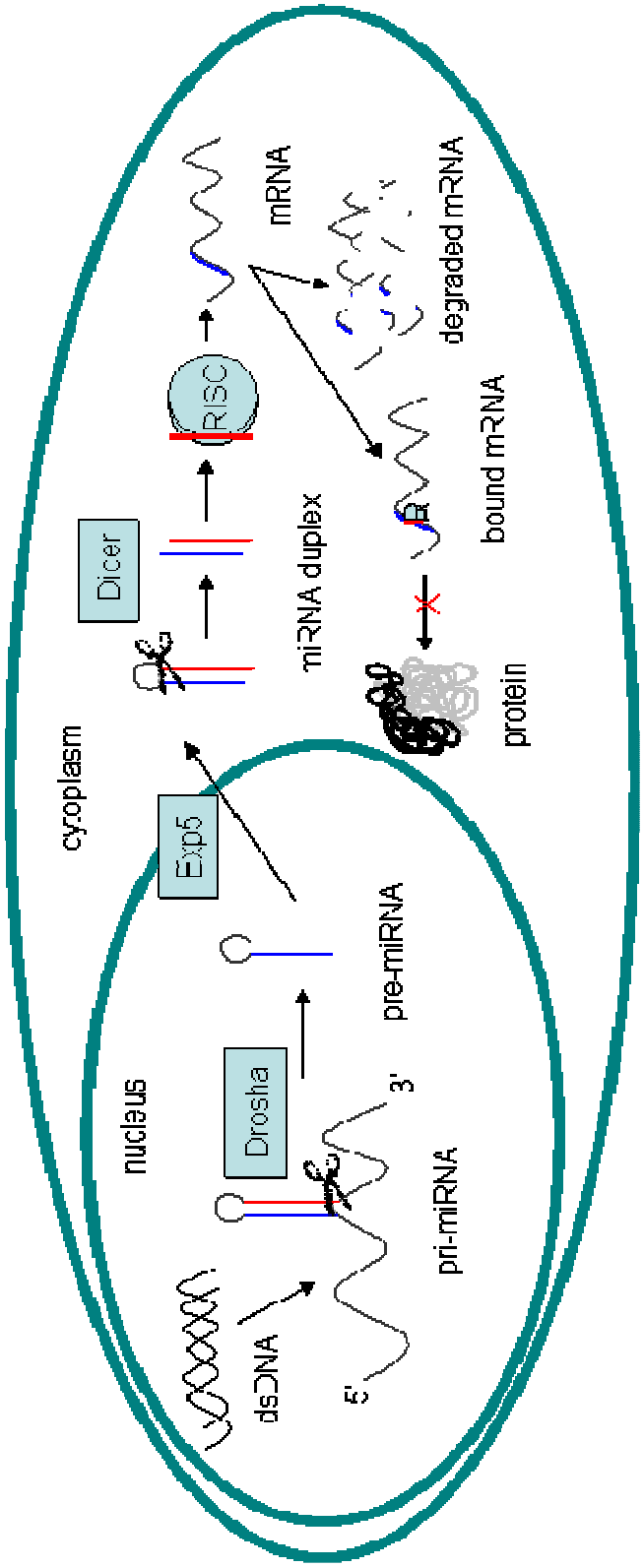

Figure 1.4: Schematic of miRNA biogenesis.

Lagos-Quintana *et al*., 2001). The unstructured flanking regions and stem-loop structure are recognized by a heterodimer made up of an RNase III enzyme (Drosha) and its cofactor (DGCR8). DGCR8 binds to the flanking regions which allows Drosha to cleave the pri-miRNA, leaving a 60-110 nt hairpin with a characteristic 5' phosphate and a 3' 2 nt overhang that defines one edge of the mature miRNA (Figure 1.4) (Basyuk *et al*., 2003, Han, *et al*., 2006, Hutvágner *et al*., 2001, Lee *et al*., 2003). Once released from Drosha, this pre-miRNA is taken up by another heterodimer made up of Exportin 5 (Exp-5) and a GTP-bound form of its cofactor (Ran) which recognizes the pre-miRNA based on the 3' 2 nt overhang and adjacent stem (Lund *et al*., 2004, Yi *et al*., 2003). Once bound, the pre-miRNA is transported from the nucleus and into the cytoplasm.

Hydrolysis of the GTP-bound Ran releases the pre-miRNA into the cytoplasm where it is bound by a heterodimer of another RNase III enzyme (Dicer) and its cofactor (TRBP) (Grishok *et al*., 2001, Hutvágner *et al*., 2001, Ketting *et al*., 2001) which also recognizes the 3' 2 nt overhang through the RNA binding domain, PAZ (piwi-argonaute-zwille) (Cerutti *et al*., 2000). Once bound, Dicer cleaves the terminal loop from the hairpin structure, leaving another 5' phosphate and a 3' 2 nt overhang. What is left is an 18-30 nt duplex that makes up the second intermediary structure.

The duplex is quite short-lived as Dicer passes it directly to a protein complex which will use the miRNA as a guide to target mRNA transcripts; RISC (RNA-induced silencing complex)/miRNP (miRNA ribonucleoprotein) (Hammond *et al*., 2000, Hutvágner *et al*., 2002, Mourelatos *et al*., 2002). The components that make up RISC have yet to be completely defined but it is known to include an Argonaute (Ago, eIF2C2) protein which interacts directly with the miRNA duplex (Liu *et al*., 2004, Maniataki *et al*., 2005). Different organisms have different numbers of Ago proteins but all Ago proteins contain two distinct domains; PAZ and PIWI (Cerutti *et al*., 2000, Meister *et al*., 2004). The specific recognition of PAZ for the unique 2 nt terminal overhangs of miRNAs reduces the chance of incorporating a non-miRNA into RISC and PIWI closely resembles members of the RNase H family and is thought to interact with

Dicer and cleave the target RNAs (Lingel *et al*., 2003, Song *et al*., 2004, 2003, Yan *et al*., 2003, Tahbaz *et al*., 2004). It is unknown how the incorporation of different Ago proteins into RISC is regulated but it is known that Ago-1-4 all associate with miRNAs (Liu *et al*., 2004).

RISC is only functional when it contains a single strand of RNA so the final step in miRNA processing, is to unwind the two RNA strands that make up the miRNA duplex, keeping one as the mature miRNA, and releasing the other strand (miRNA*) for degradation or to act as another miRNA incorporated in another RISC (Hutvágner *et al*., 2002, Okamura *et al*., 2008). The nucleotide sequence of the RNA strands that make up the miRNA duplex contribute to the bias of one strand remaining with RISC over the other; the strand whose 5' end is less tightly based paired is more energetically favoured to unwind and become incorporated into the multi-protein complex by Ago (Khvorova *et al*., 2003, Schwarz *et al*., 2003). ATP is required to initiate the unwinding of the miRNA duplex and it is thought that this may be accomplished by DEAD-box RNA helicases (Meister, 2004). Once integrated into RISC, the miRNA is used to guide the complex to target RNAs that contain sites of complementarity to the miRNA.

1.5.2 miRNA Functions

miRNA target sites can be found throughout mRNA transcripts (5'UTR, coding region and 3'UTR) and binding of RISC leads to translation inhibition (spatial interference of the translation machinery) or mRNA cleavage and degradation (Grey *et al*., 2010, Lin *et al*., 2011, Muylkens *et al*., 2010, Tang *et al*., 2009, Tay *et al*., 2008, Yekta *et al*., 2004). It may be that the expression patterns of the Ago proteins affect the degree to which the RNA silencing processes work; Ago-1 is associated with translational inhibition and Ago-2 is associated with transcript cleavage (Rossi, 2005). The mechanism of inhibition is thought to be linked to the degree of complementarity of the miRNA to the target site; in general, perfect complementarity results in cleavage whereas imperfect complementarity results in impaired translation (Zeng *et al*., 2003). Though cleavage appears to require only one RISC complex, translational inhibition appears to require the

targeting of multiple sites (Doench *et al*, 2003). Out of the ~22 nt that make up a miRNA, nucleotides 2-8 from the 5' end make up the "seed region" which is particularly important for target recognition (Doench *et al*., 2004, Gottwein *et al*., 2007, Jackson *et al*., 2003, Lai, 2002, Lewis *et al*., 2003). More than a complementary seed region is required for target recognition, but those mechanisms are presently still unknown; length variation at the 3' end of a miRNA does not appear to affect mRNA targeting. Once a target transcript is bound by RISC, the complex localizes to the cytoplasmic P-bodies for inhibition or degradation (Liu *et al*., 2005). The cleavage site of the target RNA is in the middle of the complementarity region (10 nt upstream of the nucleotide paired up with the 5' end of the miRNA) by hydrolysis of the target RNAs phosphodiester linkage, which yields a 5' phosphate and a 3' hydroxyl termini (Elbashir *et al*., 2001). This reaction requires magnesium ions but does not require ATP, though the presence of the energy-storing nucleotide causes the reaction to be more efficient (Hutvágner *et al*., 2002, Nykanen *et al*., 2001). This change in efficiency may be due to the presence of an RNA helicase, which might aid in the removal of target RNA products from RISC or reorganize the multi-protein complex so that it may bind to another target (Meister *et al*., 2004).

miRNAs regulate a large number of cellular processes by targeting mRNA transcripts of proteins with roles involved in transcription activation, embryonic development, tissue morphogenesis and differentiation, cell migration, angiogenesis, the cell-cycle, metabolism, apoptosis, tumour suppressors/oncogenes and host-virus interactions (Chen *et al*., 2004, Chen *et al*., 2011, Fish *et al*., 2008, Johnston *et al*., 2003, Otsubo *et al*., 2011, Petrocca *et al*., 2008, Reinhart *et al*., 2000, Tay *et al*., 2008, Wang *et al*., 2008, Xu, *et al*., 2009, Xu *et al*., 2003, Zheng *et al*., 2011).

A detailed discussion of the functions of all miRNAs is outside the scope of this thesis. I will however describe a few examples to illustrate the range of processes regulated by miRNAs. The presence of the *C. elegans* miRNA lsy-6 on the left side of the body during embryonic development leads to the right/left asymmetry observed in the

bilateral taste receptor neurons (Johnston *et al*., 2003). *C. elegans* let-7 is a temporal-regulating miRNA that controls the expression of a number of genes (lin-14, lin-28, lin-41, lin-42, and daf-12) so that each is present at the correct level for the given stage of development (Reinhart *et al*., 2000). Under- or overexpression of let-7 leads to a repeat of larval cell fates in the adult stage or adult cell fates in the larval stage, respectively. *Drosophila* miR-14 suppresses Reaper-dependent cell death and is necessary for fat metabolism (triacylglycerol and diacylgylcerol) (Xu *et al*., 2003).

The vertebrate miR-181 is necessary for the B cell lineage of cells to differentiate from hematopoietic cells in the bone marrow (Chen *et al*., 2004). miR-134, miR-145, miR-296 and miR-470 target transcription factors (Nanog, Oct4, KLF4 and SOX2) to push cellular differentiation and morphological changes in embryonic stem cells (Tay *et al*., 2008, Xu, *et al*., 2009). miR-92a targets CDH1 and leads to metastasis of cancerous oesophageal squamous cells (Chen *et al*., 2011). miR-126 targets negative regulators of the VEGF pathway throughout an organisms life which supports vascular expansion and integrity of the vessels (Fish *et al*., 2008, Wang *et al*., 2008). Additionally, miR-126 also targets SOX2 which leads to an increase in PLAC1 - this can lead to the development of gastric carcinoma (Otsubo *et al*., 2011). Other miRNAs have been found to be associated with gastric cancer; in a negative feedback-loop, E2F1 activates the expression of the miR-106b-25 cluster which then downregulates E2F1 (a transcription factor that controls the cell cycle and tumour suppressor proteins) and suppresses the TGFβ tumour suppressor pathway (GeneCards®, Petrocca *et al*., 2008). Human miR-101 targets cellular ATP5B resulting in the inhibition of HSV-1 replication (Zheng *et al*., 2011). A single miRNA species could target hundreds of different proteins and in combination with others could target thousands (Bartel et al., 2004, Doench *et al*., 2004) - miRNA clusters tend to be functionally associated (Kim *et al*., 2009).

1.5.3 Viruses and miRNAs

The first virus-encoded miRNAs were from EBV (Pfeffer *et al*., 2004). Given that pri-miRNA processing occurs in the cell nucleus, only those viruses that replicate and express their genomes in the nucleus can express miRNAs without running the risk of having their genomes destroyed by Drosha processing (Grundhoff *et al*., 2011, Cullen, 2006). This excludes most RNA viruses and the DNA virus group, poxviruses, as they replicate in the cytoplasm. It is also less likely that a virus would express miRNAs if it undergoes rapid replication cycles as miRNAs are only able to regulate those genes that are expressed post-infection. As has been observed, the most likely viruses to express miRNAs are nuclear DNA viruses that set up persistent latent infections; as such viral miRNAs have been discovered in polyomaviruses (BK, JC, merkel cell and simian virus 40) viruses similar to polyomaviruses and papillomaviruses (bandicoot papillomatosis carcinomatosis virus type 1 and 2) and the majority in herpesviruses (Cai *et al*., 2006, Cui *et al*., 2006, Jurak *et al*., 2010, Pfeffer *et al*, 2005, 2004, Samols *et al*., 2007).

Though the functions of the majority of herpesvirus-encoded miRNAs remain unknown, those that have been described follow the prediction that they would regulate viral and host gene expression to maintain persistent infection, support immune evasion and have a role in viral pathogenesis (Table 1.3-4). Viral targets of alpha- and betaherpesvirus miRNAs include the transcripts of immediate-early genes to support latency by suppressing those factors that would initiate gene expression, DNA replication, and virion production as well as those genes that would activate the host's immune response (Grey *et al*., 2007, Murphy *et al*., 2008, Muylkens *et al*., 2010, Stern-Ginossar *et al*., 2009, Tang *et al*., 2009, 2008, Umbach *et al*., 2008). Hsv1-miR-H6 targets ICP4, a transcription factor that initiates expression of most HSV-1 ORFs during lytic replication (Umbach *et al*., 2008). Hsv2-miR-H2, -miR-H3, and -miR-H4 target ICP34.5, a viral neurovirulence factor, and ICP0, a viral transactivator, to control latency and reactivation (Tang *et al*., 2009). Mdv1-miR-M4 targets U_L28 and U_L32 which suppresses cleavage and packaging of replicated viral DNA (Muylkens *et al*., 2010).

Hcmv-miR-U_L112-1 targets the immediate-early ORFs IE72, U_L112/113, and U_L120/U_L121 which leads to suppression of viral DNA replication and suppresses U_L114 which acts as a uracil DNA glycosylase (Grey *et al*., 2007, Murphy *et al*., 2008, Stern-Ginossar *et al*., 2009).

Gammaherpesvirus miRNAs target viral transcripts to support latency, immune evasion, those that lead to pathogenic effects in the host by suppressing DNA replication, transcription and antigens of cytotoxic T cells, and balancing pro- and anti-apoptotic functions (Barth *et al*., 2008, Bellare *et al*., 2009, Lo *et al*., 2007, Lung *et al*., 2009, Pfeffer *et al*., 2004). Ebv-miR-BART2 targets the viral DNA polymerase BALF5 and kshv-miR-K9* targets ORF50, both of which lead to the suppression of reactivation from latency (Barth *et al*., 2008, Bellare *et al*., 2009, Pfeffer *et al*., 2004). The ebv-miR-BART miRNAs target the immunogenic LMP1; this supports immune evasion but also facilitates the development of nasopharyngeal carcinoma; inhibition of LMP1 decreases the sensitivity of nasopharyngeal carcinoma cells to the chemotherapy drug cisplatin (Lo *et al*., 2007, Lung *et al*., 2009).

The suppression of cellular gene transcripts by herpesvirus miRNAs supports persistence and immune evasion, which together can lead to pathogenesis. Persistence has been shown to be supported by targeting factors that control reactivation, cell growth and proliferation, cell transformation, and apoptosis. Kshv-miR-K3 targets NFIB which suppresses activation of viral ORF50, reiterating the reactivation suppression observed by kshv-miR-K9*, and kshv-miR-K4-5p targets Rbl2 which leads to increased methylation of H3 K9 histones decreasing viral ORF expression (Lu *et al*., 2010, Lu *et al*., 2010). Kshv-miR-K1 targets p21 which decreases the cell's ability to initiate cell cycle arrest in response to p53 activation (Gottwein *et al*., 2010). Hcmv-miR-U_S25-1 targets a number of cellular cell cycle genes which leads to G1/S phase arrest (Grey *et al*., 2010). KSHV miRNAs target MAF and TGFβ which leads to a transition in lymphatic endothelial cells to a state closer to blood vessel endothelial cells and promotes angiogenesis (Hansen *et al*., 2010, Samols *et al*., 2007). The EBV BHRF1

miRNA cluster is associated with B cell transformation due to effects on both viral and cellular targets (Feederle *et al*., 2011). Suppression of apoptosis by herpesvirus miRNAs targeting cellular targets has been observed multiple times; kshv-miR-K5 targets BCLAF1 (signals apoptosis) kshv-miR-K10a targets TWEAKR (role in caspase activation) ebv-miR-BART5 targets PUMA (signals apoptosis) and mdv1-miR-M3 targets Smad2 (member of the TGFβ pathway that results in apoptosis) (Abend *et al*., 2010, Choy *et al*., 2008, Xu *et al*., 2011, Ziegelbauer *et al*., 2009).

Immune evasion can be achieved by suppressing T cell activation by targeting chemokines and membrane-bound ligands. Deletion of two mouse cytomegalovirus miRNAs leads to a reduction of virions produced in the salivary glands due to increased selectivity by natural killer and $CD4^+$ T cells (Dölken *et al*., 2010). Kshv-miR-K3 and -K7 target LIP which leads to the increased expression of IL-6 and IL-10 by macrophages which results in cell growth and immune evasion (Qin *et al*., 2010). Ebv-miR-BHRF1-3 targets CXCL11/I-TAC which decreases the motility of activated T cells (Xia *et al*., 2008). miRNAs from HCMV, KSHV, and EBV target MICB which leads to the evasion of stressed cells from attack by natural killer cells (Nachmani *et al*., 2009, Stern-Ginossar, *et al*., 2007). Kshv-miR-K10a targeting of TWEAKR also suppresses a proinflammatory response to infection (Abend *et al*., 2010). Wide spread cellular transcript regulation has also been observed by the targeting of Dicer and mimicking cellular miRNAs (Lizasa *et al*., 2010). Cellular miR-155 plays a role in lymphocyte transformation so orthologs of this miRNA found in alpha- and gammaherpesviruses could lead to the observed pathogenic effects (Gottwein *et al*., 2007, Muylkens *et al*., 2010, Skalsky *et al*., 2007, Zhao *et al*., 2009).

Thus far, the best studied virus-miRNA interactions have been with MDV-1 and although it is an alphaherpesvirus, its life cycle and pathogenesis are similar to that of gammaherpesviruses (latency is established in transformed T cells, replication takes place in epithelial and B cells, and the virus causes lymphomas) (Burnside *et al*., 2006). A number of mdv1-miRs are located in the region of the genome expressed in latently-

infected transformed and cancerous cells (including the oncomiR, mdv1-miR-M4) showing that herpesvirus miRNAs can be involved in the observed pathologies associated with herpesvirus infection (Zhao *et al*., 2011).

1.6 PROJECT OUTLINE

There is no vaccine or treatment for susceptible animals that can and/or succumb to MCF via OvHV-2 infection. At the moment the only preventative measure is keeping natural hosts away from unnatural hosts or separating newborn lambs from the rest of the herd in the hopes of raising an OvHV-2-free flock. The study of OvHV-2 continues to be held back due to a lack in ability to isolate cell-free virions in culture. The understanding of the route of transmission is still mostly due to observation of host and susceptible species and the viral role in the mechanism of the pathogenesis of MCF is still unknown. There must be something in sheep cellular biology that allows for a persistent infection that is missing in other Artiodactyla. As discussed previously, persistence requires a fine balance of gene expression and herpesviruses have adapted to this challenge by encoding and expressing miRNAs. miRNAs have been shown to regulate numerous cellular pathways and the analysis of their functions provides insight to greater cellular mechanisms. This thesis will identify whether or not OvHV-2 also expresses miRNAs. Next generation high throughput sequencing technology was used to identify the small RNA transcripts expressed by OvHV-2 in a cell line derived from an MCF-affected cow and secondary structure prediction software was used to identify if the sequenced transcripts contained the secondary structures necessary for miRNA biogenesis. MCF describes a syndrome of lymphocyte-activation to unknown antigens and OvHV-2 miRNAs could be the answer. If present, the identification of their targets and the characterization of their function could begin to unravel the mystery of MCF.

Table 1.3: Viral targets and functions of herpesvirus-encoded miRNAs.

Sub-Family	Virus	miRNA	Target	Function
α	HSV	miR-H2	ICP0	latency
	HSV-1	miR-H6	ICP4	
	HSV-2	miR-H3, -H4	ICP34.5	
	MDV-1	miR-M4	U_L28, U_L32	
β	hCMV	miR-U_L112	IE1/IE72/U_L123, U_L114	latency
γ	EBV	BART Cluster 1	LMP1	pathogenesis
		miR-BART2	BALF5	latency
		miR-BART22	LMP2A	immune evasion
	KSHV	miR-K5, -K9*	RTA/ORF50	latency

Table 1.4: Cellular targets and functions of herpesvirus-encoded miRNAs.

Sub-Family	Virus	miRNA	Target	Function
α	MDV-1	miR-M3	Smad2	anti-apoptotic
		miR-M4	PU.1, CEBPβ, HIVEP2, BCL2L13, PDCD6	pathogenesis
β	hCMV	miR-U_L112	MICB	immune evasion
		miR-U_S25-1	cyclin E2	cell cycle arrest
	mCMV	miR-M23-2	CXCL16	immune evasion
γ	EBV	miR-BART2	MICB	immune evasion
		miR-BART5	PUMA/BBC3	pathogenesis
		miR-BART6	Dicer	wide-scale cellular miRNA regulation
		miR-BHRF1-3	CXCL-11/I-TAC	immune evasion
	KSHV	miR-K1, -K3, -K6, -K11	THBS1, SPP1, PRG1	pathogenesis
		miR-K3, -K7	LIP	immune evasion, pathogenesis
		miR-K5, -K9, -K10a, -K10b	BCLAF1	reactivation
		miR-K6, -K11	MAF	cellular differentiation
		miR-K1	p21	pathogenesis
		miR-K3	NFIB	latency
		miR-K4	Rbl2	latency
		miR-K10a	TWEAKR	immune evasion, pathogenesis

Chapter Two: Materials & Methods

All buffers, solutions, plasmid maps, and PCR primer sequences and annealing conditions can be found in the Appendices.

2.1 MOLECULAR TECHNIQUES

2.1.1 Isolation of DNA

DNA was extracted from eukaryotic cells using the Qiagen DNeasy Kit according to the manufacturer's protocol. Cells were pelleted at 300 x g for 5 min at room temperature and resuspended in sterile phosphate buffer solution (SPBS). The cells were lysed with proteinase K and RNA degraded with RNase A. The lysate was combined with a chaotropic salt buffer to optimize DNA binding to the column membrane and remaining impurities were removed with two wash steps. The DNA was eluted in the provided buffer.

2.1.2 Polymerase Chain Reaction

Polymerase chain reactions (PCRs) were carried out using either *Pfu* or *Taq*. *Pfu* was the preferred DNA polymerase because of its additional proof reading function. Due to limited supplies, *Taq* was used in subsequent PCR reactions.

Pfu DNA Polymerase (Promega) was used according to the manufacturer's protocol; a reaction mix containing 1X *Pfu* DNA Polymerase Buffer with $MgSO_4$, 200 µM dNTP (each) 100 ng of both the forward and reverse primer (Eurofins MWG Operon) 1-100 ng DNA template, 1-1.5 U *Pfu* DNA Polymerase, and nuclease-free water for a total volume of 50 µl. The PCR program consisted of 35 cycles of 30 s denaturing at 96°C, 30 s annealing at a temperature specific to the primers, and 60 s extension at 72°C, with a final extension cycle of 4 min at 72°C (PCR Sprint Thermal Cycler, Thermo Scientific).

PCRs using *Taq* DNA Polymerase (Invitrogen) were carried out according to the manufacturer's hot start protocol; 1X PCR Buffer, 1.5 mM $MgCl_2$, 200 µM dNTP (each) 0.5 µM of both the forward and reverse primer, 1-100 ng DNA template, and nuclease-

free water for a total volume of 50 µl. Reactions were heated to 94°C for 3 min and then held at 80°C while 1 U *Taq* was added. The program was continued with 35 cycles of 45 s denaturing at 94°C, 45 s annealing at a specific temperature specific to the primers, and 60 s extension at 72°C, with a final extension cycle of 5 min at 72°C for 5 min. Negative controls contained water instead of DNA template. Once the PCR product was ligated into a cloning vector and amplified, it was sequenced to confirm that the product was without mutation.

2.1.3 Agarose Gel Electrophoresis

10 µl of PCR product or 1 µg plasmid DNA (made up to 10 µl with nuclease-free water) was combined with 3 µl 6X loading dye and separated by agarose (1%) gel electrophoresis (0.5 g agarose [Bioline] 50 ml 1X TAE buffer, 0.05 mg ethidium bromide [Fisher Scientific]) in 1X TAE, using 60 V for an hour; the DNA migration was visualized under UV. A DNA ladder was used for size reference (1 µl 1 Kb Plus Ladder, Invitrogen, 7 µl nuclease-free water and 6X loading dye).

2.1.4 Concentration of Nucleic Acid by Ethanol Precipitation

1/10 volume 3 M sodium acetate and 2 vols 70% ethanol was added to the nucleic acid sample, gently mixed, and then placed on dry ice for 20 min. The sample was centrifuged at 10,000 x g for 10 min, the supernatant removed, and the sample centrifuged again briefly to remove any excess supernatant. The nucleic acid sample was resuspended in nuclease-free water.

2.1.5 Restriction Digestion of Plasmid DNA

1X Buffer and 10 U of each restriction enzyme (New England Biolabs) was combined with 1 µg plasmid DNA and incubated for 2-3 hrs at 37°C. The restriction enzymes were deactivated by incubating the reaction for ~1 hr at 65°C and then a sample was separated by agarose gel electrophoresis using 1% agarose, to confirm the correct digestion pattern.

2.1.6 DNA Ligation

Two different DNA ligation methods were used depending on the vector. plZ3-CIng-ps-linker and psiCHECK™ were digested and purified and then ligated with the DNA inserts in a reaction containing 2 µl 10X Ligation Buffer, vector, insert, 1 µl T4 DNA Ligase (NEB) and made to 20 µl with water and incubated at room temperature overnight. Successful ligations resulted from vector insert ratios of 1:1 or 3:1. When using pCR®2.1-TOPO®, the TOPO TA Cloning Kit (Invitrogen) was used according to the manufacturer's protocol. 2 µl purified PCR product, 0.5 µl salt solution (1.2M NaCl, 0.06M $MgCl_2$) and 0.5 µl TOPO TA vector were combined and incubated at room temperature for 5 min (see Appendix 3 for plasmid maps).

2.1.7 Quantification of Nucleic Acid by Spectrophotometry

Nucleic acid concentrations and purities were quantified using a NanoDrop ND1000 Spectrophotometer (Thermo Scientific). Nucleic acid concentrations were calculated using an algorithm based on an absorbance at OD_{260} of 1 = 50 µg ml^{-1} DNA or 40 µg ml^{-1} RNA. Nucleic acid purity was calculated using the ratio of the absorbance at OD_{260} and OD_{280} where pure DNA has an $A_{260/280}$ = ~1.8 and pure RNA has an $A_{260/280}$ = ~2.

2.1.8 DNA Extraction from Agarose Gels

DNA was purified from 1% agarose gels using the QIAquick Gel Extraction Kit according to the manufacturer's protocol (Qiagen). The excised gel slice was dissolved in a chaotropic salt buffer, treated with isopropanol, and applied to a QIAquick spin column. The bound DNA was washed with an ethanol-containing buffer and then eluted with 50 µl of the provided buffer (10 mM Tris-Cl, pH 8.5) or water.

2.1.9 Purification of PCR Products

PCR products were purified using a QIAquick PCR Purification Kit (Qiagen) according to the manufacturer's protocol. A binding buffer was added to the PCR product, which was then applied to a spin column and centrifuged at 12000 x g for 30-60 s; primers, free nucleotides, and sample impurities passed through the column while the PCR product

became bound to the column membrane. The column was washed using an ethanol-containing buffer to remove remaining salts and the DNA was eluted with 50 µl of 10 mM Tris-Cl or water.

2.1.10 Sequencing of Plasmid DNA

Plasmid DNA was sequenced using the Big Dye® Terminator v3.1 Cycle Sequencing Kit (Applied Biosystems/Ambion). 200-500 ng in 1 µl of plasmid was added to 8.5 µl of a master mix (3.3 µl water, 2 µl 5X Sequencing Buffer, and 3.2 µl forward/reverse primer [3.2 pmol]) and 0.5 µl Big Dye. The samples were denatured at 96°C for 10 s, annealed at 50°C for 5 s, and elongated at 60°C for 2 min, for 30 cycles (Veriti 96 Well Thermal Cycler, Applied Biosystems/Ambion) and sequenced by The Genepool, University of Edinburgh. Sequences were compared to the published OvHV-2 sequence (GenBank, AY839756) using NCBI's blastn algorithm; (http://blast.ncbi.nlm.nih.gov/Blast.cgi).

2.1.11 Isolation of RNA

Cells were centrifuged at 500 x g for 10 min at room temperature. The supernatant was removed, the cells resuspended in the remaining medium, and then transferred to a 1.5 ml microcentrifuge tube on ice. The cells were centrifuged at 9000 x g for 30 s at room temperature and the remaining medium was removed. 1 ml of RNA-Bee (AMS Biotechnology) was added to homogenize the cells and degrade endogenous RNases.

200 µl chloroform (Sigma) was added to the lysate, which was then shaken vigorously by hand for 15-30 s, placed on ice for 5 min, and centrifuged at 12000 x g for 15 min at 4°C. This separated the lysate into aqueous and organic phases; isolating the RNA in the aqueous phase from the DNA and proteins in the organic phase.

The RNA-containing aqueous phase was removed to a clean 1.5 ml microcentrifuge tube and treated with 500 µl isopropanol to desalt and precipitate the RNA. The solution was incubated at room temperature for 5-10 min and then centrifuged at 12000 x g for 5 min at 4°C to pellet the RNA.

The supernatant was removed and the RNA pellet was washed with 200 µl 75% (v/v) ethanol, made with 0.1% (v/v) diethylpyrocarbonate (DEPC)-treated water (1 ml DEPC in 1 L water left overnight at room temperature and then autoclaved to deactivate the DEPC). The sample was vortexed briefly to ensure complete washing, and centrifuged at 7500 x g for 5 min at 4°C to re-pellet. Ethanol was removed and the RNA pellet was allowed to air dry for 5-10 min on ice before being re-solubilized in 50 µl 0.1% DEPC-treated 1X TE Buffer, pH 7 or 0.1% DEPC-treated water.

2.1.12 Solexa High Throughput Sequencing of Small RNA

10 µg of total RNA ($A_{260/280}$ = 2.06) was sent to The Genepool, University of Edinburgh for small RNA, paired-end, high throughput sequencing using an Illumina Solexa GAII. Although it is now routine for The Genepool to run RNA samples they receive on a bioanalyser, the RNA samples sequenced by them in this study (2.1.12-13) were sent in 2008/2009, prior to this protocol (Marian Thomson, The Genepool, communication; Supplemental DVD, The Genepool Communication). Small RNAs were isolated using a FlashPAGE Fractionator (Applied Biosystems/Ambion); total RNA was mixed with an equal volume of loading buffer, heated to denature, and then loaded onto the top of a precast gel set up in the Fractionator. The gel was run at 75-80 V for 12 min or until the loading dye began to migrate out of the gel into the Lower Buffer Chamber; the Lower Running Buffer contained the small RNA fraction (<40 nt). The small RNA was precipitated by sodium acetate and ethanol and stored at -20°C until ready to be used (2.1.4). Adapter linkers were added to the 5' and 3' ends of the small RNAs through two separate steps involving adaptor ligation and gel purification. A primer complementary to the 3' adaptor was used for reverse transcription to create a cDNA library of the adaptor-linked small RNAs and a primer equivalent to the 5' adaptor was used to amplify the library using PCR. The library was gel purified and then plated on the Illumina Solexa GAII Cluster Station Flow Cell using the 3' adaptor to bind to the surface amplification primer. The generated reads were mapped to the OvHV-2 genome (GenBank, AY839756) using SOAP (Short Oligonucleotide Analysis Package; Li *et al*.,

2008). SOAP is a tool specifically geared towards the alignment of small RNA tags sequenced from high throughput methods such as Illumina Solexa GAII. For this study, SOAP was used to align the sequenced tags that were 20-26 nt in length and contained no mismatches or gaps to the OvHV-2 genome.

2.1.13 Solexa High Throughput Sequencing of mRNA

5 µg total RNA ($A_{260/280\ Sample\ 1}$ = 2.00, $A_{260/280\ Sample\ 2}$ = 2.04, $A_{260/280\ Sample\ 3}$ = 1.97) was sent to The Genepool for paired-end, digital expression profiling via Illumina Solexa GAII sequencing. mRNA was isolated using oligo(dT) beads. A double-stranded cDNA library was generated from the bead-bound mRNA and then digested with *Nla*III; further steps apply only to 3' cDNA fragments that remained bound to the magnetic beads. A 5' adaptor containing a *Mme*I site was ligated to the *Nla*III cleavage site and then the sample was digested with *Mme*I, which cleaved downstream of the binding site, resulting in a short tag free of the magnetic bead. A 3' adaptor was ligated to the site of *Mme*I cleavage and those fragments with adaptors on both ends were amplified by PCR using primers complementary to both adaptors and gel purified. The library was bound onto the amplification primers on the flow cell surface via the 3' adaptor. The resultant tags were mapped to the OvHV-2 genome using the default parameters of MAQ (*Mapping and Assembly with Quality*, http://maq.sourceforge.net) and a mapping quality cut off of 30; i.e. the probability of each nucleotide in the alignment being wrong is 0.001.

2.2 BACTERIAL TECHNIQUES

2.2.1 Preparation of LB/Agar, AMP$^+$ Plates

7.5 g Bacto Agar (BD) was added to 500 ml Luria Bertani (LB) broth (Merck) and autoclaved. Ampicillin (AMP) was added for a final concentration of 100 µg ml^{-1} and then poured into Petri dishes (Sterilin) and allowed to solidify.

2.2.2 Transformation of One-Shot Chemically Competent *E. coli*

Two different strains of chemically competent *E. coli* were used for transformations, both according to the manufacturer's protocol. ~120 ng plasmid DNA was added to a 50 µl aliquot of XL1-Blue competent cells (Stratagene/Agilent) that had been thawed on ice. The sample was left on ice for 30 min and then heat-shocked at 42°C for 45 s. 500 µl LB broth was added to the cells and they were placed in a 37°C shaking incubator for 1hr (225 rpm). The cells were centrifuged at 1800 x g for 45 s, 400 µl supernatant was removed, the cells were resuspended in the remaining broth, plated on LB/AMP (100 µg μl^{-1}) plates and incubated at 37°C overnight.

When using TOP10 chemically competent cells (Invitrogen), 10 µl ligation reaction (2.1.6) was added to 50 µl cells (that had been allowed to thaw on ice) and left on ice for another 5 min. The sample was heat shocked at 42°C for 30 s and then placed back on ice. 250 µl SOC broth was added to the cells before they were placed in a shaking incubator at 37°C for 1 hr. 10 µl (plus 20 µl SOC broth) and 50 µl of the cells were spread on pre-warmed LB/AMP (100 µg ml^{-1}) plates and incubated at 37°C overnight.

2.2.3 Harvesting of Bacterial Colonies

A single bacterial colony was selected using a sterile metal-hoop and deposited in LB broth for further growth (2.2.4, 2.2.5).

2.2.4 Plasmid DNA Isolation from Bacteria (Small Scale)

Plasmids were extracted from bacteria using the QIAprep Spin Miniprep Kit (Qiagen). Colonies were harvested and added to 5 ml LB/AMP (100 µg ml^{-1}) broth, and placed at 37°C in a shaking incubator for ~16 hrs. The cells were centrifuged at 600 x g for 5 min and resuspended in an RNase A-containing TE buffer (0.1 mg ml^{-1}). The cells were lysed in an alkaline buffer which was neutralized before the lysate was centrifuged at 9000 x g for 10 min. The supernatant was applied to a column and centrifuged at top speed for 30-60 s and then the membrane-bound DNA was washed with a chaotropic salt solution and ethanol before being eluted in water.

2.2.5 Plasmid DNA Isolation from Bacteria (Large Scale)

Plasmid DNA was extracted from a selected clone using the PureLink™ HiPure Plasmid Maxiprep Kit according to the manufacturer's protocol (Invitrogen). A sample from a frozen glycerol stock was streaked on a pre-warmed LB/AMP agar plate and incubated at 37°C overnight. A sterile metal-hoop was used to take a sample of the streak of bacterial growth which was then harvested and added to 5 ml LB/AMP and placed in a 37°C shaking incubator for 8 hrs. 300 µl of starter culture was added to 200 ml LB/AMP and incubated at 37°C shaking overnight. The cells were centrifuged at 4000 x g for 10 min, the supernatant removed, and the cells resuspended in TE Buffer containing RNase A. The cells were lysed in an alkaline buffer containing sodium dodecyl sulphate (SDS). The lysate was neutralized and proteins precipitated with the addition of potassium acetate buffer. The entire solution was added to the HiPure Filter Maxi Column and allowed to run through the filter by gravity. The DNA was washed, eluted, and then precipitated using the PureLink™ HiPure Precipitator Module (Invitrogen). After precipitation with the addition of isopropanol, the solution was passed through a 0.22 µm filter, washed with ethanol, and eluted in 1 ml water.

2.2.6 Preparation of Bacterial Stocks for Long Term Storage

Samples of *E. coli* cultures containing validated clones (850 µl) were combined with glycerol (150 µl, autoclaved for 20 min at 15 psi on the liquid cycle) and stored at -80°C.

2.3 NORTHERN HYBRIDIZATION

2.3.1 Antisense RNA Probe Labelling

Antisense RNA Probes were constructed using the miRVana miRNA Probe Construction Kit (Applied Biosystems/Ambion) according to the manufacturer's protocol. DNA oligonucleotide templates were ordered with the same sequences as the putative miRNAs with the following addition to the 3' end; 5'-TTTTCCTGTCTC-3'; and diluted to 100 µM in nuclease-free water (Eurofins MWG Operon) (template sequence described in Appendix 2). What would be four adenine residues on the 3' end

of the RNA probe prevented cleavage by RNases A and T1. dsDNA was formed by treating the DNA templates with a T7 Promoter Primer (complementary to 5'-CCTGTCTC-3') and extending with Exo-Klenow DNA polymerase. The dsDNA template was used to transcribe a radiolabelled antisense RNA probe using α-^{32}P UTP, 800 Ci mmol^{-1}, 10 mCi ml^{-1} (PerkinElmer). Following transcription, the dsDNA template was removed by DNaseI digestion and free nucleotides were removed by column purification (miRVana Probe and Marker Kit [Applied Biosystems/Ambion]).

2.3.2 RNA Electrophoresis

20 µg total RNA was suspended in 5 µl 0.1% (v/v) DEPC-treated water and an equal volume of 100% deionized formamide (Applied Biosystems/Ambion) to remove secondary structure. 6X loading dye was added (0.25% [w/v] bromophenol blue [BDH Laboratory Supplies] in 30% [v/v] glycerol [Sigma]) to the RNA before denaturing the sample at 95°C for 1-5 min and snap-cooling on ice. The denatured sample was then loaded and run on a 15% denaturing acrylamide/bis (19:1) gel (Applied Biosystems/Ambion) containing 7 M urea, 20 mM MOPS-NaOH (pH 7) (0.06% (w/v) ammonium persulfate and 0.035% (v/v) tetramethylethylenediamine (TEMED) at 300-400 V for 2-4 hrs. Before preparing the samples, the gel was pre-run for 10 min and while the samples were snap-cooling on ice, the urea that had accumulated in the wells was flushed out with a syringe.

2.3.3 Transfer of RNA to Nitrocellulose Membrane

RNA separated by gel electrophoresis was transferred to a Hybond-NX neutral nylon membrane (GE Healthcare Life Sciences, Amersham) sandwiched between six sheets of 3 MM Paper pre-soaked in 0.1% DEPC-treated water, using a semi-dry electroblotter, run at 20 V for 20 min.

The RNA-containing membrane was laid on top of a sheet of 3 MM paper (RNA side up) saturated with 0.16 M EDC (1-ethyl-3-(3-dimethylaminopropyl)carbodiimide) hydrochloride in a 0.13 M 1-methylimidazole solution, wrapped in cling film and

incubated at 60°C for 1 hr to cross-link the RNA to the nylon membrane. The membrane was rinsed with 0.1% DEPC-treated water to remove residual cross-linking solution.

2.3.4 Probe Hybridization and Detection

The membrane-bound RNA was hybridized using ULTRAhyb-Oligo solution (Applied Biosystems/Ambion) according to the manufacturer's protocol. The membrane was placed in a hybridization tube and incubated with preheated ULTRAhyb (68°C) before 10 µl of the prepared antisense probe (2.3.1) was added and the membrane was left to incubate overnight in a rotating oven (42°C). The ULTRAhyb containing the probe was removed and the membrane washed twice with 2X SSC, 0.5% SDS for 30 min at 42°C to remove any excess probe before being wrapped in cling film, exposed to film (Sigma, Kodak BioMax MS-1) and stored at -70°C.

2.4 TISSUE CULTURE

2.4.1 Growth of Established Cell Lines

BJ1035 is an immortalized cell line, derived from the T cells of a cow naturally infected with OvHV-2 (Schock et al., 1998). These cells (a gift from Dr George Russell, Moredun Research Institute) were grown in suspension in Iscove's Modified Dulbecco's Medium (Invitrogen) supplemented with 10% (v/v) foetal calf serum (Sera Laboratories International) 1% (v/v) penicillin-streptomycin (Invitrogen) 10,000 U (in 500 ml) interleukin 2 (IL-2) (Novartis Pharmaceuticals UK Ltd) and incubated at 37°C, 5% CO_2. Once many large clumps of these suspension cells were visualized, the cells were pipetted up and down to break up the clumps and 2/3 of the volume was transferred to a new flask with 1/3 fresh medium.

BHK cells (Stoker et al., 1964) were grown in Glasgow Modified Eagle Medium supplemented with 10% (v/v) newborn calf serum (Sera Laboratories International) 10% (v/v) tryptose phosphate broth, 1% (v/v) L-glutamine and incubated at 37°C, 5% CO_2. Once these adherent cells had reached confluence, the medium was poured off and the

cells rinsed with 0.02% (w/v) EDTA. The BHK cells were harvested using 0.05% (w/v) trypsin-EDTA which was neutralized by adding 2X amount of medium once the cell layer was floating free. The cells were pelleted by centrifugation at 400 x g for 5 min at room temperature, the trypsin/medium was poured off, and the pelleted cells resuspended in fresh medium. A 1:1 mix of the cell suspension and 0.4% trypan blue (Sigma) was applied to a haemocytometer and the unstained, live cells were counted. $5x10^6$ BHK cells were used to seed a new T175 flask (Nunc).

2.4.2 Preparation of Cell Lines for Long Term Storage

$5x10^6$ cells were suspended in 1 ml freezing medium (90% foetal calf serum, 10% (v/v) DMSO) and placed in a cryovial. The vial was wrapped in cotton and placed in a Styrofoam box overnight at -80°C. The next day the vial was placed in liquid nitrogen for long term storage.

2.4.3 Growing Cell Lines from Frozen Stock

A cryovial of suspension cells was removed from long term liquid nitrogen storage and placed on dry ice until ready to use. The cells were thawed quickly in a 37°C water bath and added to a T25 flask containing 15 ml pre-warmed medium and then left to sit on end for 4 hrs in an incubator (37°C, 5% CO_2). 10 ml medium was removed carefully in order to leave the settled cells undisturbed at the bottom of the flask, and then an additional 5 ml pre-warmed medium was added to the flask and the cells returned to the incubator.

A cryovial of adherent cells was thawed as above, however the cell suspension was added to 20 ml pre-warmed medium, and centrifuged at 400 x g for 5 min and the supernatant removed. Cells were resuspended in 10 ml pre-warmed medium, seeded into a T25 flask and placed in an incubator (37°C, 5% CO_2).

2.4.4 Lipid-Based Transfection of Cell Line with Plasmid DNA

For a single plasmid transfection, $1x10^5$ cells in 500 µl normal growing medium per well were plated in a 24-well plate (with coverslips [SLS, 0.13 mm diameter]) and left to grow overnight at 37°C, 5% CO_2. In separate microcentrifuge tubes, 0.5 µg plasmid DNA and 4 µl Lipofectamine 2000 (Invitrogen) were diluted in 50 µl Opti-MEM® medium (Invitrogen) and incubated at room temperature for 5 min. The plasmid DNA and Lipofectamine 2000 were combined and incubated at room temperature for a further 20 min before 100 µl was added to each well containing 24 hr-grown cells. The plate was rocked back and forth to mix and incubated at 37°C, 5% CO_2 for a further 48 hrs.

For co-transfection with miRNA mimics (miScript miRNA Mimics, Qiagen) $6x10^4$ cells in 500 µl medium per well were prepared and placed in an incubator (37°C, 5% CO_2) while the transfection reaction was prepared (see Appendix 2 for mimic sequences). 400 ng plasmid DNA, varying titrations of the miRNA mimics (5 nM, 25 nM, 50 nM) and up to 60 µl Opti-MEM® medium were combined with 3 µl Lipofectamine 2000 and plated concurrently with the cells and incubated at 37°C, 5% CO_2 for 24 hrs.

2.4.5 Isolation of Ovine White Buffy Coat

50 ml peripheral blood was obtained by jugular venous puncture with 5 U heparin per ml as an anti-coagulant. Ten ml aliquots were centrifuged at 2000 x g for 15 min, buffy coat was carefully removed and washed with PBS.

2.4.6 Immunocytochemical Staining of Transfected Cells

Medium was removed from plated adherent cells, washed twice with sterile PBS (SPBS) and fixed with 500 µl 4% (w/v) paraformaldehyde per well at room temperature for 30 min. The cells were washed twice with SPBS, leaving the second wash on the cells during storage at 4°C.

Fixed cells were permeabilized with 0.3% (v/v) Triton-X100 (Sigma) in SPBS for 20 min and then washed for 5 min, repeated three times with SPBS. The cells were treated

with Cas-block (Invitrogen) for 30 min to prevent non-specific binding of antibodies and then treated with monoclonal murine anti-FLAG [Sigma, 1:1000]) for 90 min. Cells were washed 3 times in SPBS for 12.5 min before incubation with biotinylated rabbit anti-mouse [Dako; 1:500] for 60 min. To-pro3 [Invitrogen; 1:1000] and RNase A [Qiagen; 10 μg ml^{-1}]) were also added for nuclear staining and RNA-degradation. Cells were washed 3 times with SPBS for 12.5 min and incubated with streptavidin conjugated dye Alexa Fluor 546 (Invitrogen; 1:500) for 45 min in the dark. After two washes with SPBS for 10 min, the coverslips were mounted on slides using Pro-long Gold Antifade (Invitrogen) and viewed using a confocal microscope. All washes and staining took place at room temperature and all antibodies were diluted in Cas-block.

2.5 OTHER METHODS

2.5.1 Luciferase Activity Assay

DNA plasmid and miRNA mimic co-transfected cells (2.4.4) were lysed and prepared using the Dual-Luciferase® Reporter Assay System according the manufacturer's protocol (Promega) and luciferase levels were measured using the DLR-0-INJ Promega protocol on a GloMax® 20/20 Luminometer (Promega). The cells were lysed in 1X passive lysis buffer, which stabilized the firefly and Renilla luciferase enzymes. 20 μl of the lysate was added to LARII (activated the firefly luciferase) and read on the luminometer and then 1X Stop & Glo® was used to quench the firefly activity and activate the Renilla to be read.

2.5.2 Confocal Microscopy

Slides of immunocytochemically stained cells were viewed using a Zeiss confocal laser scanning microscope (IMPACT, University of Edinburgh) with the assistance of Trudi Gillespie.

2.6 SOFTWARE

2.6.1 The mfold Web Server

http://www.bioinfo.rpi.edu/applications/mfold

The mfold Web Server was used to predict pri-miRNA secondary structure by using an algorithm that finds the minimum free energy for each base-pair of an input RNA sequence under physiological conditions (temperature = 37°C, [Na^+, Li^+, K^+, NH_4^+] = 1 M, and [Mg^{+2}, Ca^{+2}] = 0 M) (Zuker, 2003). The output was selected in the form of a jpg or pdf file for viewing and archiving; it showed the predicted structure showing individual bases and the minimum free energy value.

2.6.2 BLAST (Basic Local Alignment Search Tool)

http://blast.ncbi.nlm.nih.gov/Blast.cgi

The nucleotide and protein blast algorithms blastn and blastp, respectively, were used to align a nucleotide or protein query against nucleotide or protein databases available in GenBank (http://blast.ncbi.nlm.nih.gov/Blast.cgi).

2.6.3 Databases

GeneCards®

http://www.genecards.org/

KEGG PATHWAY Database

http://www.genome.jp/kegg/pathway.html

SOAP

http://soap.genomics.org.cn/

2.7 BIOINFORMATIC IDENTIFICATION OF OVHV-2 MIRNAS

2.7.1 Consensus Sequence Determination

The data output produced by The Genepool (2.1.12) provided 20-26 nt cDNA sequences (tags) representing the small RNAs present in BJ1035 cells, the coordinates and strand of alignment of the tags on the OvHV-2 genome, and the number of times the tag was sequenced from the small RNA sample (reads). Minor manipulation of the tags was required to find the accurate RNA sequence from the given cDNA; those tags aligned to the plus strand of the OvHV-2 genome were given in their correct 5'-3' orientation. They were then converted to RNA sequence by changing all T → U. To obtain the RNA sequence for those tags aligned to the minus strand, the complementary RNA sequence of the cDNA tag had to be created and then inverted so as to be written 5'-3'; these manipulations were prepared by using an online sequence editor (http://www.fr33.net/seqedit.php).

Initial observation of the dataset showed that a number of tags had the same 5' coordinate (seed sequence; 1.3.2) with variation within the sequence or length at the 3' end. The tag with the most reads for each 5' coordinate was used as the consensus sequence for that location, the tags with fewest reads at that location were discarded - their read numbers were added to that of the consensus sequence.

2.7.2 Putative miRNA and miRNA* Sequence Determination

The consensus tags were grouped together based on proximity; if they overlapped or were within 30 nt of each other (pre-miRNA; 1.3.1). Read counts were used to determine the tag most likely to represent a mature miRNA and miRNA* (1.3.1); the tag with the most reads in a group was designated as the putative miRNA and the tag with the second highest number of reads (that did not overlap with the putative miRNA) was designated the putative miRNA*.

2.7.3 Secondary Structure Analysis

The OvHV-2 genome (GenBank, AY839756) and the mfold Web Server (2.6.1) were used to predict the secondary structure of the putative pri-miRNA (1.3.1) represented by each group (2.7.2). The nucleotide sequence of the OvHV-2 genome on the given strand (from 100 nt up- and downstream of the putative miRNA and miRNA*) was taken from GenBank and inputted into the RNA folding form of mfold. The putative miRNA and miRNA* sequences were mapped onto the predicted secondary structures, which were then manually analyzed for the three features associated with miRNA biogenesis that had been set as criteria for the basis of miRNA identification (Ambros *et al*., 2003); stem-loop, 3' overhangs formed by the miRNA/miRNA* duplex, and $\geq$16 bp within the miRNA/miRNA* duplex (3.3). Those groups that satisfied all three secondary structure criteria were elevated to predicted OvHV-2 miRNA status.

2.8 BIOINFORMATIC TARGET PREDICTION

2.8.1 Seed Sequence Alignment

Blastn (2.6.2) was used to align the complementary sequence to the ovhv2-miRs individually against the OvHV-2 (2.1.10) and bovine genomes (btau_4, http://www.ensembl.org/das/Bos_taurus.Btau_4.0.reference/). Hits were reported back with the nucleotide coordinates of the alignment on the searched genome. Those hits that contained the complementary seed sequence (3.7.1) were further analyzed while the others were discarded.

2.8.2 Genome Trawl

ORF annotation (5' UTR, coding region, 3' UTR) on the OvHV-2 and bovine genome was analyzed for all coordinates found in 2.8.1. Those coordinates that were annotated were designated as predicted targets for the given ovhv2-miR.

2.9 OVHV-2 TRANSCRIPTOME ANALYSIS

The data output produced by The Genepool (2.1.13) provided 21 nt cDNA sequences (tags) representing the mRNAs present in BJ1035 cells, the coordinates and strand of alignment of the tags on the OvHV-2 genome, and the number of times the tag was sequenced from the given total RNA sample (reads). Annotation of the OvHV-2 genome available online (2.1.10) allowed for manual assignment of the tags to the 73 ORFs encoded by the virus. The sum of the reads for each ORF was plotted to create an expression profile for the overall genome.

Appendix 1: Buffer & Stock Solutions

LB Broth	5 g yeast extract 10 g peptone from casein 10 g sodium chloride 12 g agar-agar up to 1 L water
Phosphate-buffered saline (PBS)	150 mM NaCl 2.5 mM KCl 10 mM $Na_2H_2PO_4$ 1 mM KH_2PO_4 (pH 7.4)
1X TAE Buffer	40 mM Tris-acetate 1 mM EDTA (pH 8.0)
10X TBE Buffer (pH 8.3)	900 mM Tris-HCl (pH 8.3) 900 mM Boric Acid 30 mM EDTA (pH 8.0)
1X TE Buffer (pH 7.0)	10 mM Tris-HCl (pH 7.0) 1 mM EDTA (pH 8.0)

Appendix 2: Sequences

DNA Templates for Construction of Antisense RNA Probes	
Ovhv2-miR	**Sequence (5'-3')**
miR-1	AAGGCTTGATAAGTAGCACTGATTTTCCTGTCTC
miR-2	ATCTTGGACGCATCTGTCAGTAGTTTTCCTGTCTC
miR-3	TCTGTATCATAGGGGTTGTGTTGTTTTCCTGTCTC
miR-4	AAGGATCCTTAAGTGACGAACGTTTTCCTGTCTC
miR-5	TGAAGTTACAGCTGCACCTGGATTTTCCTGTCTC
miR-6	TATTTTTAGCGGAGACCTCTAGGTTTTCCTGTCTC
miR-7	GAAGGCGCATCATAGACACCACTTCTTTTCCTGTCTC
miR-8	TGGCTCAGCGTGACTGCTCTTCTTTTCCTGTCTC

PCR Primers				
Name	**Dir.**	**Genome Location (5')**	**Sequence (5'-3')**	**Ann. Temp**
*Xho*I-Orf20-FLAG-*Nhe*I	F	48434	AACTCGAGCATGTTTCCGCTGCTCG	50°C
	R	3' end of FLAG	AAGCTAGCCTACTTGTCATCGTCATC	
*Xho*I-Orf20 3'UTR-*Not*I	F	40786	AACTCGAGACAACATAGTCCAGGCAAACA	54.9°C
	R	39273	AAGCGGCCGCCACCCCTGGCTGGACTAT	

OvHV-2 miRNA Mimics	
Ovhv2-miR	**Sequence (5'-3')**
miR-5	UGAAGUUACAGCUGCACCUGGAU
miR-6	UAUUUUUAGCGGAGACCUCUAGG
miR-7	GAAGGCGCAUCAUAGACACCACUUC

Appendix 3: Cloning Vectors

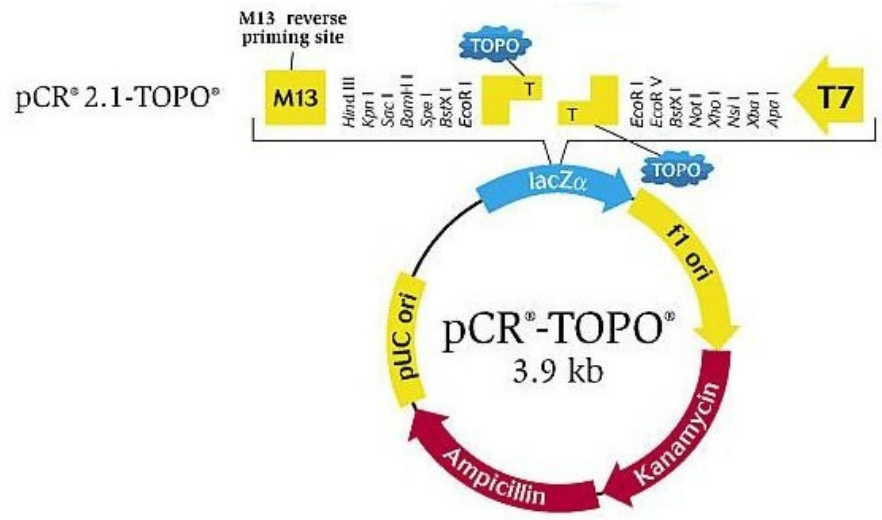

Vector pCR®2.1-TOPO® was obtained from Invitrogen as part of the TOPO TA Cloning Kit

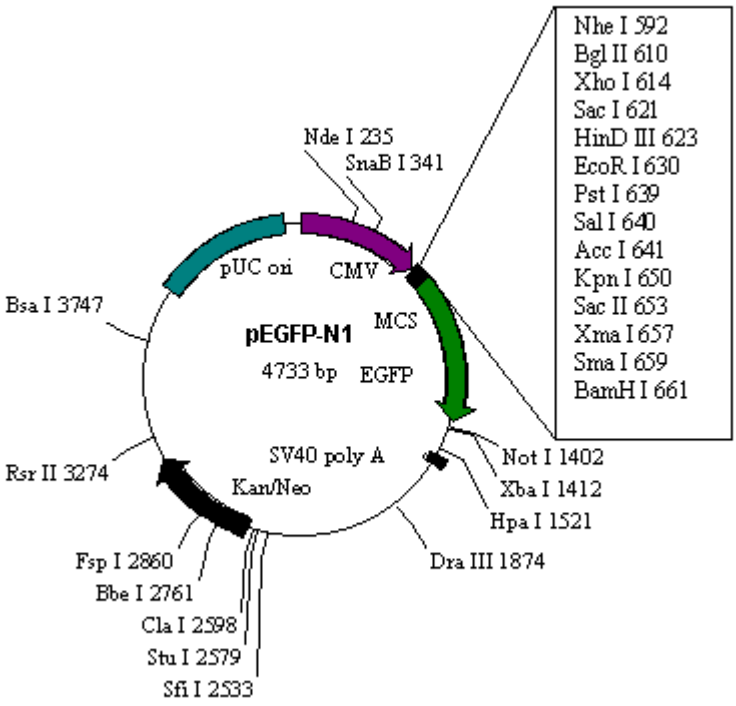

Vector pEGFP-N1 (Clontech - www.clontech.com)

.

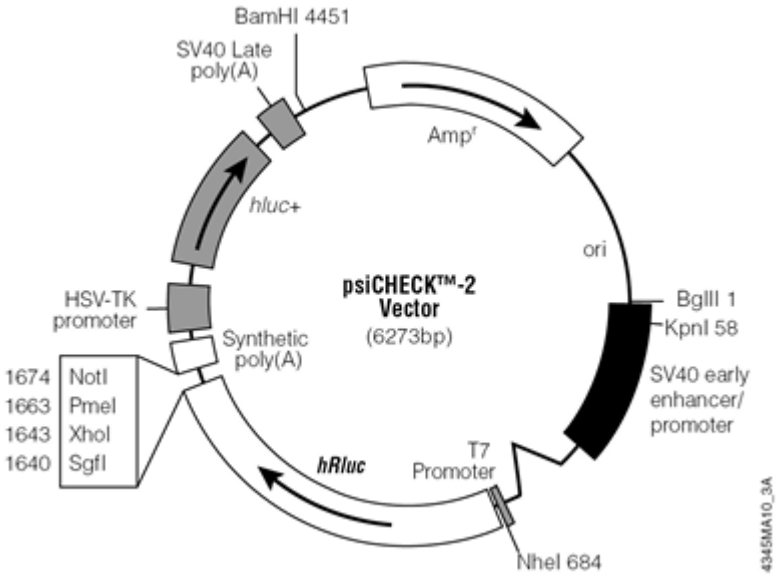

The psiCHECK™ Vector (Promega - www.promega.com).

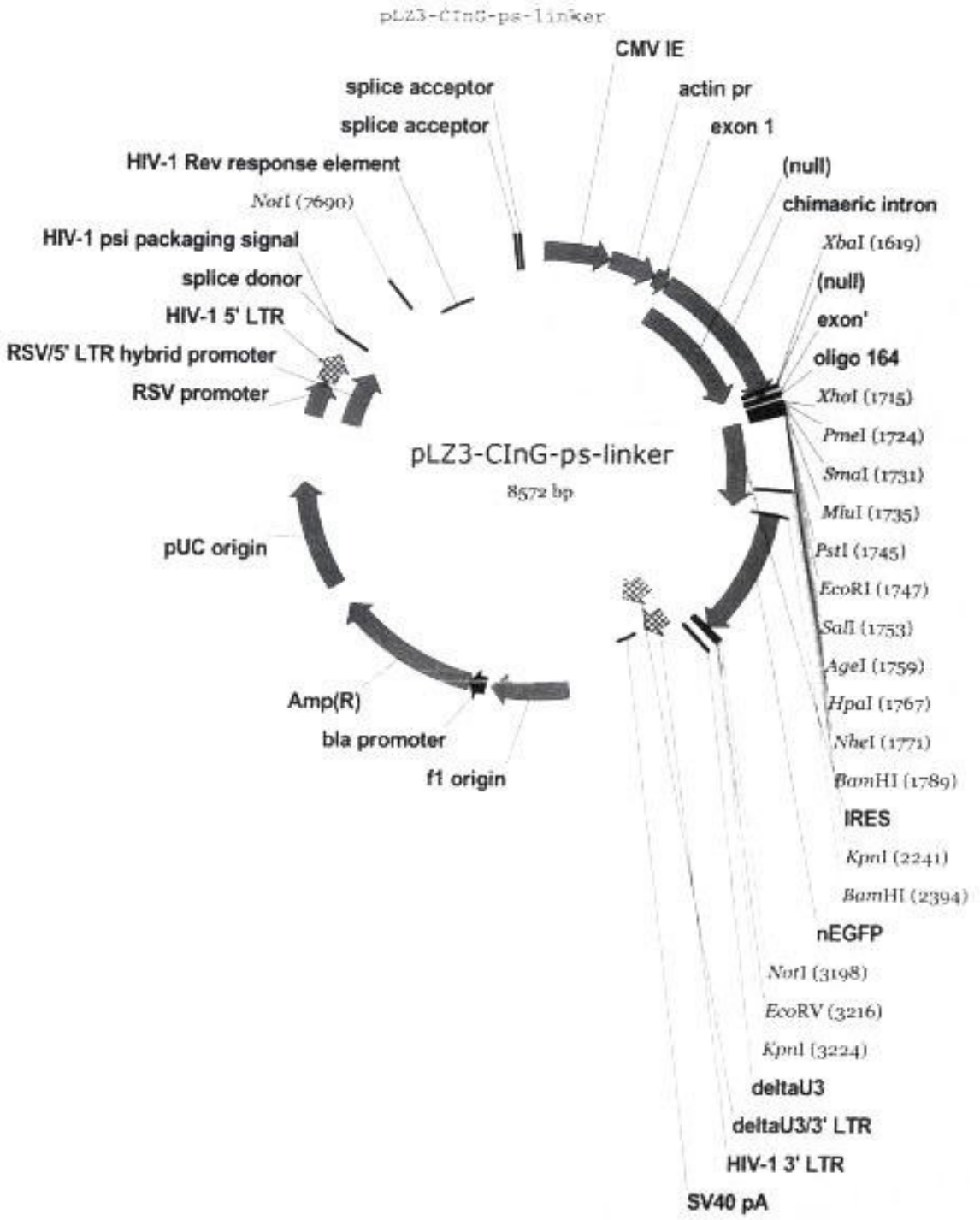

Vector pLZ3-CIng-ps-linker was obtained from Debiao Zhao at The Roslin Institute. This was based on pLenti6/V5-D-TOPO (Invitrogen) but the CMV promoter was replaced with a CAG promoter (a fusion of the CMV early enhancer element and chicken β actin promoter) along with an IRES-nGFP cassette and the blasticidin resistance gene was deleted.

Appendix 4: Commercial Suppliers

Agilent Technologies UK Ltd, 610 Wharfedale Road, Winnersh Triangle, Wokingham, Berkshire RG41 5TP, UK
http://www.home.agilent.com/agilent/home.jspx?&cc=GB&lc=eng

AMS Biotechnology (Europe) Ltd, 63B Milton Park, Abingdon OX14 4RX, UK
www.amsbio.com

Applied Biosystems/Ambion, 2130 Woodward St, Austin, TX 78744-1832, USA
www.ambion.com

BDH Laboratory Supplies, Merck Ltd, Hunter Boulevard, Magna Park, Lutterworth, Leics LE17 4XN, UK
www.bdh.com

Becton, Dickinson U.K. Ltd, The Danby Building, Edmund Halley Road, Oxford Science Park, Oxford, Oxfordshire OX4 4DQ, UK
www.bd.com/uk

Bioline Ltd, 16 The Edge Business Centre, Humber Road, London NW2 6EW, UK
www.bioline.com

Clontech Laboratories, Inc, 1290 Terra Bella Avenue, Mountain View, CA 94043, USA
www.clontech.com

DJB Labcare Ltd, 20 Howard Way, Interchange Business Park, Newport Pagnell, Buckinghamshire MK16 9QS, England
www.sigmacentrifuge.co.uk

Eurofins MWG Operon, Anzingerstr. 7a, 85560 Ebersberg, Germany
www.eurofinsdna.com

Fisher Scientific UK Ltd, Bishop Meadow Road, Loughborough, Leicestershire LE11 5RG, UK
www.fisher.co.uk

GE Healthcare Life Sciences, Amersham Place, Little Chalfont, Buckinghamshire HP7 9NA, UK
www.gelifesciences.com

The Genepool, Ashworth Laboratories, The King's Buildings, The University of Edinburgh, Edinburgh EH9 3JT, UK
http://genepool.bio.ed.ac.uk

Greiner Bio-One Ltd, Brunel Way, Stroudwater, Business Park GL10 3SX Stonehouse, UK
www.greinerbioone.com

Invitrogen Ltd, 3 Fountain Drive, Inchinnan Business Park, Paisley PA4 9RF, UK
www.invitrogen.com

Merck, Hertford Road, Hoddesdon, Hertfordshire EN11 9BU, UK
www.merck.com

LC Sciences, 2575 West Bellfort Street, Suite 270, Houston, TX 77054, USA
www.lcsciences.com

New England Biolabs (UK) Ltd, 75/77 Knowl Piece, Wilbury Way, Hitchin, Herts SG4 0TY, UK
www.neb.com

Novartis Pharmaceuticals UK Ltd, Frimley Business Park, Frimley, Camberley, Surrey GU16 7SR, UK
www.novartis.co.uk

NUNC, Thermo Fisher Scientific, Roskilde Site, Kamstrupvej 90, Postbox 280, DK-4000, Roskilde, Denmark
www.nuncbrand.com

PerkinElmer, 940 Winter Street, Waltham, Massachusetts 02451, USA
www.perkinelmer.com

Promega UK Ltd, Delta House, Chilworth Research Centre, Southhampton SO16 7NS, UK
www.promega.com

QIAGEN Ltd, QIAGEN House, Fleming Way, Crawley, West Sussex RH10 9NQ, UK
www.qiagen.com

Scientific Laboratory Supplies Ltd, Orchard House, The Square, Hessle, East Riding of Yorkshire HU13 0AE, UK
www.scientificlabs.co.uk

Sera Laboratories International Ltd, Unit 44, Bolney Grange Business Park, Haywards Heath, West Sussex RH17 5PB, UK
www.seralab.co.uk

Severn Biotech Limited, Unit 2, Park Lane, Kidderminter, Worcestershire DY11 6TJ, UK
http://www.severnbiotech.com

Sigma-Aldrich Company Ltd, Dorset, England
www.sigmaaldrich.com

Sterilin Ltd, Angel Lane, Aberbargoed, Bargoed, Caerphilly CF81 9FW, UK
www.sterilin.co.uk

Thermo Scientific, 3411 Silverside Road, Bancroft Building, Wilmington DE 19810, USA
www.nanodrop.com

Chapter Three: OvHV-2 miRNA Identification

3.1 AIMS

The aim of this project was to identify OvHV-2-encoded miRNAs by using high throughput sequencing to identify the small RNA transcripts expressed in the bovine LGL cell line BJ1035, bioinformatics to predict the secondary structure of the sequenced transcripts, and northern hybridization to validate that the sequenced transcripts were present as ~22-mers.

3.2 INTRODUCTION

miRNA identification generally involves a combination of bioinformatic analysis of transcript secondary structure and sequence conservation between organisms, and sequencing the population of small RNAs. Many miRNAs have been identified using algorithms that look for sequence conservation between species where miRNAs have already been identified. These programs are not appropriate for viral miRNA identification as there is very little sequence homology between different viruses. Therefore, for this project, the initial step was to sequence the small RNAs expressed in OvHV-2-infected cells.

Sequencing the small unknown transcripts involved attaching adapters of known sequence to both ends, and reverse transcription to create a cDNA library where the sequences of interest could be found between the sequences of the known adapters (2.1.12). For this project, high throughput sequencing was available which has the additional benefit of amplifying the adapter-bound transcripts before sequencing. This allowed for more sensitive detection of transcripts that have a low abundance of expression. An Illumina Solexa GAII (The Genepool, University of Edinburgh) was used as it specializes in sequencing short cDNA libraries and had the option of sequencing each molecule from both ends, further increasing the sensitivity of the results.

Once the small RNAs were isolated (2.1.11) and sequenced they could be aligned to the OvHV-2 genome to segregate those expressed by the virus and those from the host, and then bioinformatics could be used to predict the secondary structure of transcripts from those sequenced regions (2.7). SOAP (Short Oligonucletide Alignment Program) was used by The Genepool to align the sequenced library against the OvHV-2 genome because, as the name suggests, it specializes in aligning short sequences. The particular secondary structures inherent in miRNA biogenesis (1.5.1) lend themselves as sensitive markers for bioinformatic identification of miRNAs. Therefore, the plan was to predict the secondary structure of the OvHV-2 aligned transcripts that had been sequenced using mfold (2.6.1) as it has been used successfully in other miRNA identification studies.

3.3 RESULTS

3.3.1 Sequencing Analysis

The purification of small RNA from BJ1035s followed by the generation of the library and its subsequent sequencing (2.1.12) generated 5,702,036 sequence tags of 20-26 nt, 404,439 (7%) of which mapped to the OvHV-2 genome. Many of the 404,439 tags were replicates of each other, in fact there were only 2,260 unique tags represented by a single copy or up to 46,048 copies (reads). 348 of the 2,260 tags (0.12% of the reads) aligned to the plus strand and the remaining 1,912 tags (99.88% of the reads) aligned to the minus strand. The size distribution of the tags can be seen in Figure 3.1. The OvHV-2-mapped tags were grouped together if they had the same 5' genomic position, the sum of their reads was taken and the tag with the most reads was used as the consensus sequence (2.7.1). The 348 plus strand tags were consolidated to 283 and the 1,912 minus strand tags were consolidated to 825; Table 3.1 shows an example of the tag consolidation using the first 20 minus strand tags and Figure 3.2 shows the genome location of the consensus tags with their consolidated reads.

A

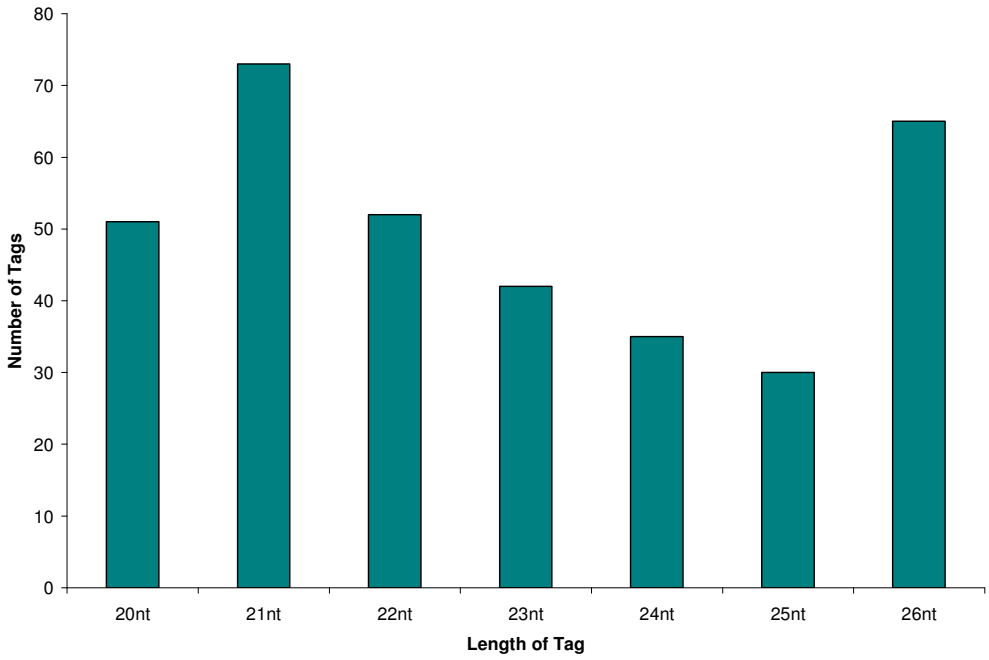

Figure 3.1A: Abundance of the 348 high throughput sequenced, OvHV-2 mapped, plus strand, small RNA tags by length. Note the difference in scale to Figure 3.1B.

B

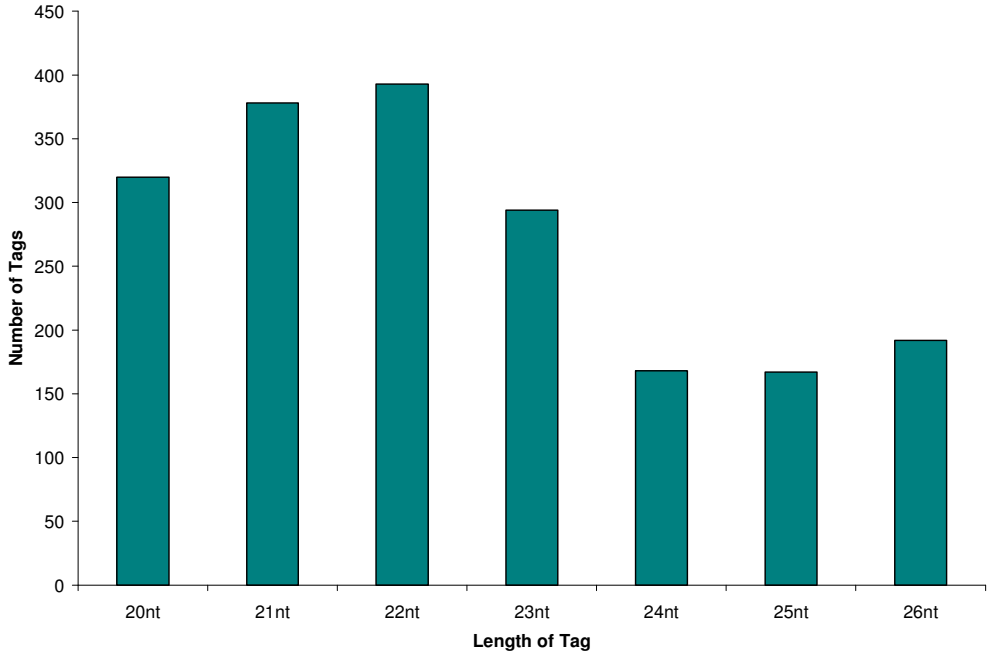

Figure 3.1B: Abundance of the 1,912 high throughput sequenced, OvHV-2-mapped, minus strand, small RNA tags by tag length. Note the difference in scale to Figure 3.1A.

Table 3.1: OvHV-2 tag consolidation; using first 20 tags aligned to the minus strand of the OvHV-2 genome as an example.

5' Start	Original Data		Consolidated Data	
	Length (nt)	Reads	Length (nt)	Reads
155	21	4	21	4
156	21	5	20	21
	20	11		
	22	5		
234	20	1	20	1
276	20	1	20	1
277	21	1	21	1
278	22	1	22	1
488	20	18	21	54
	21	36		
489	22	4	22	4
490	20	1	22	18
	21	1		
	22	16		
491	23	1	23	1
525	23	1	23	1
526	21	31	22	189
	20	27		
	22	130		
	25	1		

A

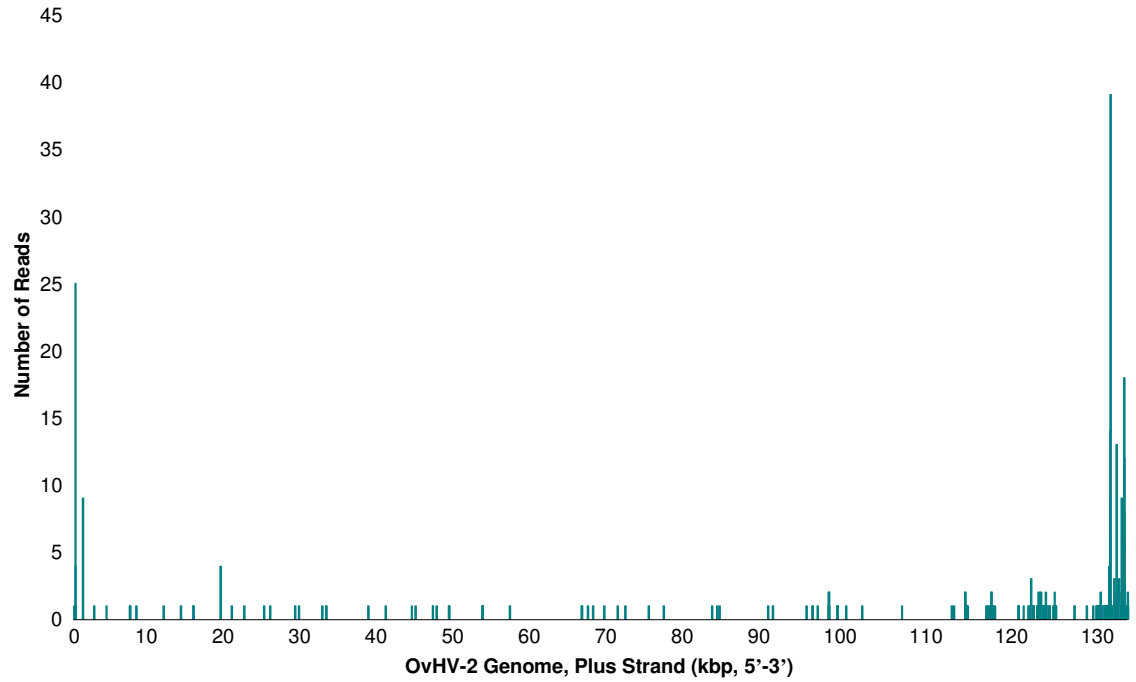

Figure 3.2A: Read count of the 283 consolidated tags generated from high-throughput sequencing plotted along the OvHV-2 genome plus strand. Note the difference in scale to Figure 3.2B.

B

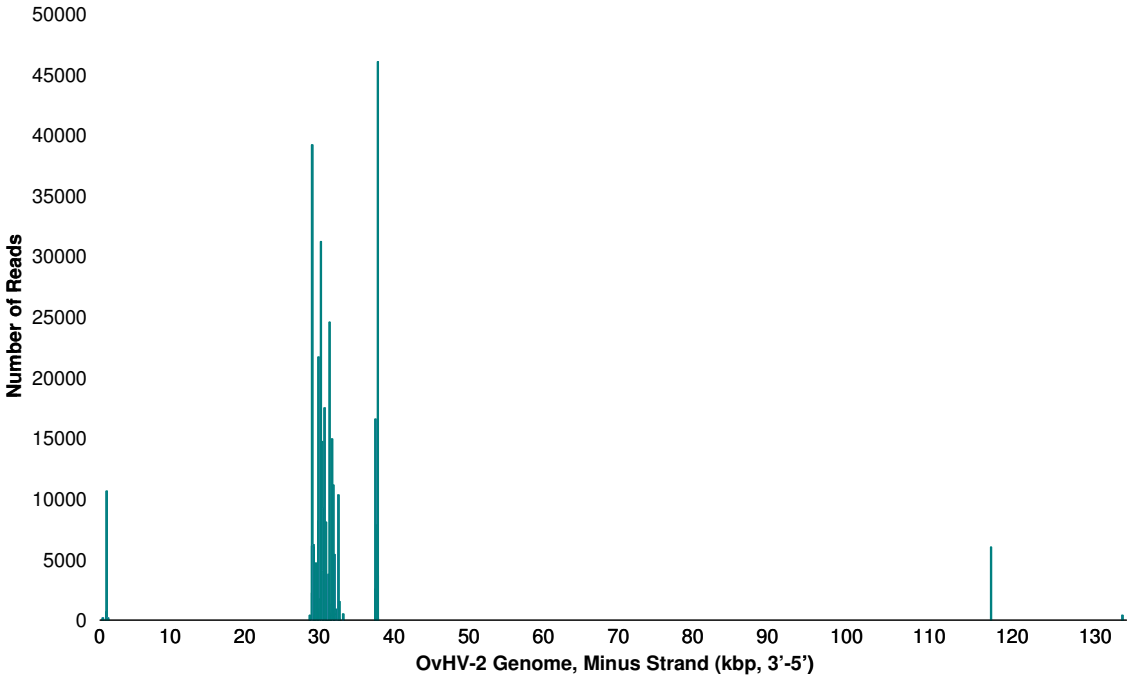

Figure 3.2B: Read count of the 825 consolidated tags generated from high-throughput sequencing plotted along the OvHV-2 genome minus strand. Note the difference in scale to Figure 3.2A.

3.3.2 miRNA Bioinformatic Analysis

The consensus tags were grouped together if they overlapped or were within 30 nt of each other (2.7.2); the 283 plus strand tags were divided into 126 groups (numbered 1-126 5' → 3') and the 825 minus strand tags were divided into 261 groups (numbered 1-261 3' → 5'). The twelve groups containing the most highly abundant tags (all from the minus strand) were analyzed initially (Table 3.2).

Table 3.2: The twelve OvHV-2 small RNA consensus tags with the most reads.

Group	5' Start of Most Abundant Tag	Reads of Most Abundant Tag
5	927	10,588
35	27903	39,169
41	28781	21,686
43	29052	31,227
44	29248	14,694
47	29637	17,508
51	30338	24,497
53	30510	14,966
56	30818	11,187
61	31462	10,378
66	36313	16,574
68	36575	46,048

The secondary structure criteria set forth by Ambros *et al*., 2003 was used to determine if these twelve groups represented candidate miRNAs by using mfold (2.6.1, 2.7.3). The required secondary structure included a stem-loop (60-110 nt, recognized by the RNase III enzyme Drosha) 3' overhangs in the miRNA/miRNA* duplex (due to cleavage by the RNase III enzymes Drosha and Dicer) and $\geq$16 bp within the miRNA/miRNA* duplex (for stability within the duplex while the pre-miRNA is transported from the nucleus to the cytoplasm, the terminal loop is cleaved by Dicer and the duplex is transferred to RISC). The most abundant tag in each group was designated the putative miRNA and the second most abundant, non-overlapping sequence as the putative miRNA*. If the mfold predicted secondary structure contained a stem-loop, the miRNA and miRNA* were mapped onto it to find the remaining structural elements (Figure 3.3 gives an example using group 47 from the minus strand).

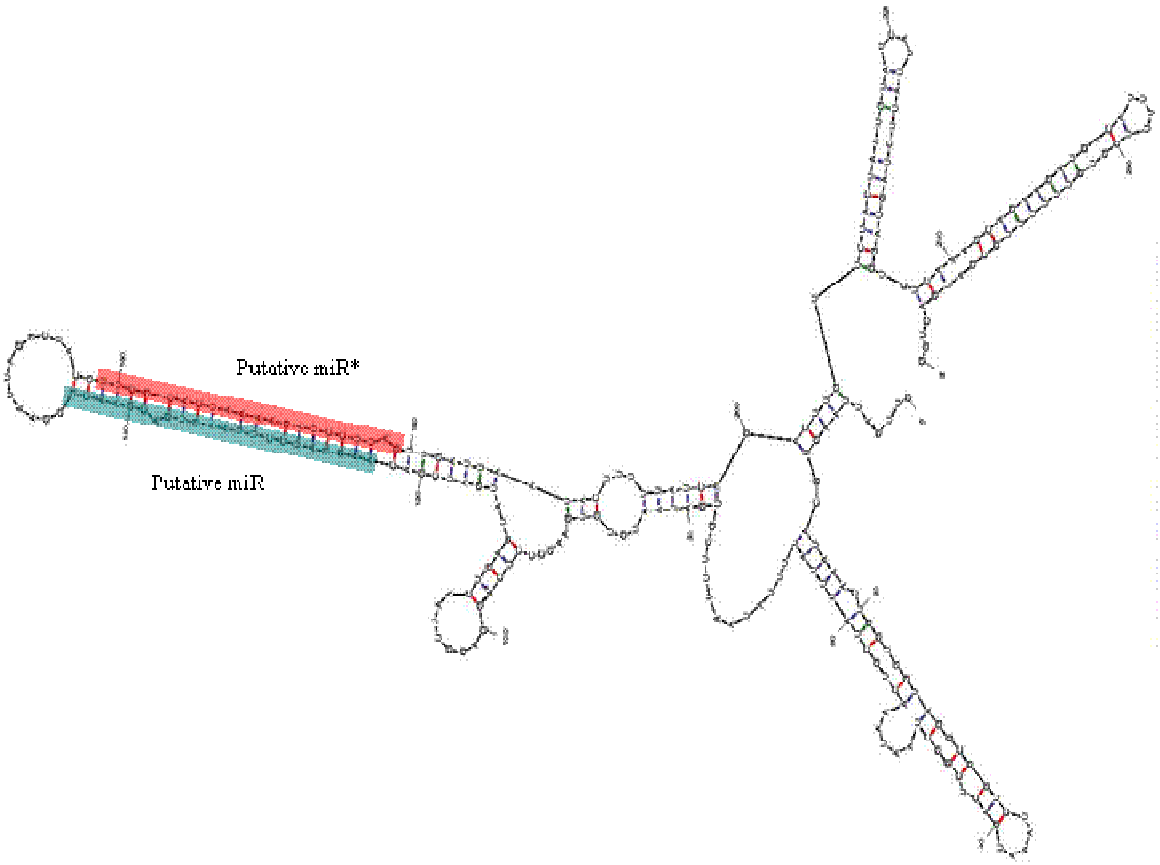

Consensus Data				miR/miR*
5' Start	cDNA Sequence (3'-5')	Length	Reads	
29600	ACTAAGGATCTTTTAGTGCGA	21	2	
29601	CTAAGGATCTTTTAGTGCGAA	21	6102	miRNA*
29636	CGTTCGTCACTTAAGGATCCT	21	15	
29637	CGTTCGTCACTTAAGGATCCTT	22	17508	miRNA
29638	CGTTCGTCACTTAAGGATCCTTG	23	50	
29639	CGTTCGTCACTTAAGGATCCTTGT	24	3	
29659	GTCGATCATACTCAGTTAACCT	22	3	

Figure 3.3: Predicted secondary structure (mfold) with stemloop of group 47 on the minus strand of the OvHV-2 genome; putative miRNA (miR; green) and miRNA* (miR*; red) are highlighted with 3' overhangs and 17 bp in the predicted miRNA duplex.

Eight out of the twelve minus strand groups initially analyzed adhered to these miRNA secondary structure standards (Table 3.3, Figure 3.4).

Table 3.3: Initial predicted OvHV-2 miRNAs. "X" signifies that the predicted secondary structure contains the given characteristic.

Group	5' Start	Stem-loop	3' Overhang	≥16 bp in Stem
5	927	X	X	X
35	27903	X	X	X
41	28781	X	X	
43	29052	X	X	
44	29248	X	X	X
47	29637	X	X	X
51	30338	X	X	
53	30510	X	X	
56	30818	X	X	X
61	31462	X	X	X
66	36313	X	X	X
68	36575	X	X	X

3.3.3 Validation of Predicted OvHV-2 miRNAs

Although the eight tags identified in section 3.3.2 met the expression (high throughput sequencing data) and biogenesis criteria (secondary structure) set by Ambros *et al*., 2003, additional supporting evidence that the tags were expressed by OvHV-2 *in vitro* was sought by northern hybridization for small RNAs using radiolabelled complementary RNA probes (2.3). Equal amounts of total RNA from BJ1035 cells, 495 TPM cells (*Theileria parva*-immortalized bovine T cell line, OvHV-2-free; a gift from Prof Ivan Morrison), and ovine leukocytes (from an OvHV-2-infected sheep) (2.1.11, 2.4.5) were separated by gel electrophoresis and probed for the eight predicted OvHV-2 miRNAs along with the ubiquitous cellular miRNA bta-mir-16a as a positive control (Figure 3.5). *T. parva* is a parasitic protozoan of cattle that causes a similar pathology to that of MCF and produces IL-2-dependent immortalized T cell lines (Schock *et al*., 1998).

No. of Reads

Group 5

```
     C       G   A                 UU
5′ GU AAGGCUU AUA GUAGCACU  GAG GU  A                    10588
3′ UA UUCCGAA UAU CAUCGUGA  CUC CA                       586
     U       G             AG   G  CA
```

Group 35

```
      AA  GAUUG       AUA        U   U               GAAUA
5′ UGG  GA     UUUUGAC   GUUUACUG ACA GUGC CCAA AUGU     U      2201
3′ ACC  CU     AAAACUG   UAGAUGAC UGU UACG GGUU UACA           39169
      GA    A          AAA            C    C    C    AAGCA
```

Group 44

```
    U             AGU       U          G     G     AAAG
5′ G CUGCU  AAAGCA   GCACUUA CUGUAUCAUA GGGUU UGUUG    U      14694
3′ C GACGA  UUUCGU   CGUGAAU GACGUAGUAU UCCAA ACAAC    U        420
          CU       G                   A           CAAG
```

Group 47

```
                    C  A    A      GGAAU
5′ UGAUCGAC AAGGAUC UU AGUG CGAACG     U                   17508
3′ AUUAGUUG UUCCUAG AA UCAC GCUUGC     A                    6102
           A       A  A           AUCGG
```

Figure 3.4A: Predicted stem-loop structure of Group 5, 35, 44, and 47 on the minus strand; consensus miRNA and miRNA* sequences are in bold, the miRNA seed sequence is underlined (number of reads of miRNA and miRNA* are on the right).

No. of Reads

Group 56

```
       A   C     G             CA    GAUACAAG
5′ UGAC GGU CGUUU AAGUUACAGCUG  CCUG        C                  11187
3′ ACUG UCG GCAGG UUCAAUGUCGGU  GGAC        C                   2241
       A   A     G             UG    AUGAAAAU
```

Group 61

```
             U    A U        G   C A          GUGUG
5′ UAUGC  GCA GAGC G UUAGGGGU UCU   AAAAAUACAU     A              89
3′ GUACG  CGU CUCG U GAUCUCCA AGG   UUUUUAUGUG     U           10378
        GU        A G        G   CGA          AAUGA
```

Group 66

```
        A      G      A    A  G          C         C      AU
5′ GAAU    CUU    GCUU CUGG AA AAGGCG CAU  AUAGACAC ACU UC  C    16574
3′ UUUA    GAA    CGAA GACC UU UUCCGU GUG  UAUCUGUG UGA GG        2598
       CGAC   AAUA         A  A      U   UA            U  GA
```

Group 68

```
             A  UC     C         U     UUA   G
5′ UGCUU UAUAG AG  GAGCA UUACGCUGA CCAAA   UUU U                3732
3′ ACGAA GUGUC UC  CUCGU AGUGCGACU GGUUU   GAA U               46048
        U     G  UU     C         C      C    A
```

Figure 3.4B: Predicted stem-loop structure of Group 56, 61, 66 and 68 on the minus strand; consensus miRNA and miRNA* sequences are in bold, the miRNA seed sequence is underlined (number of reads of miRNA and miRNA* are on the right).

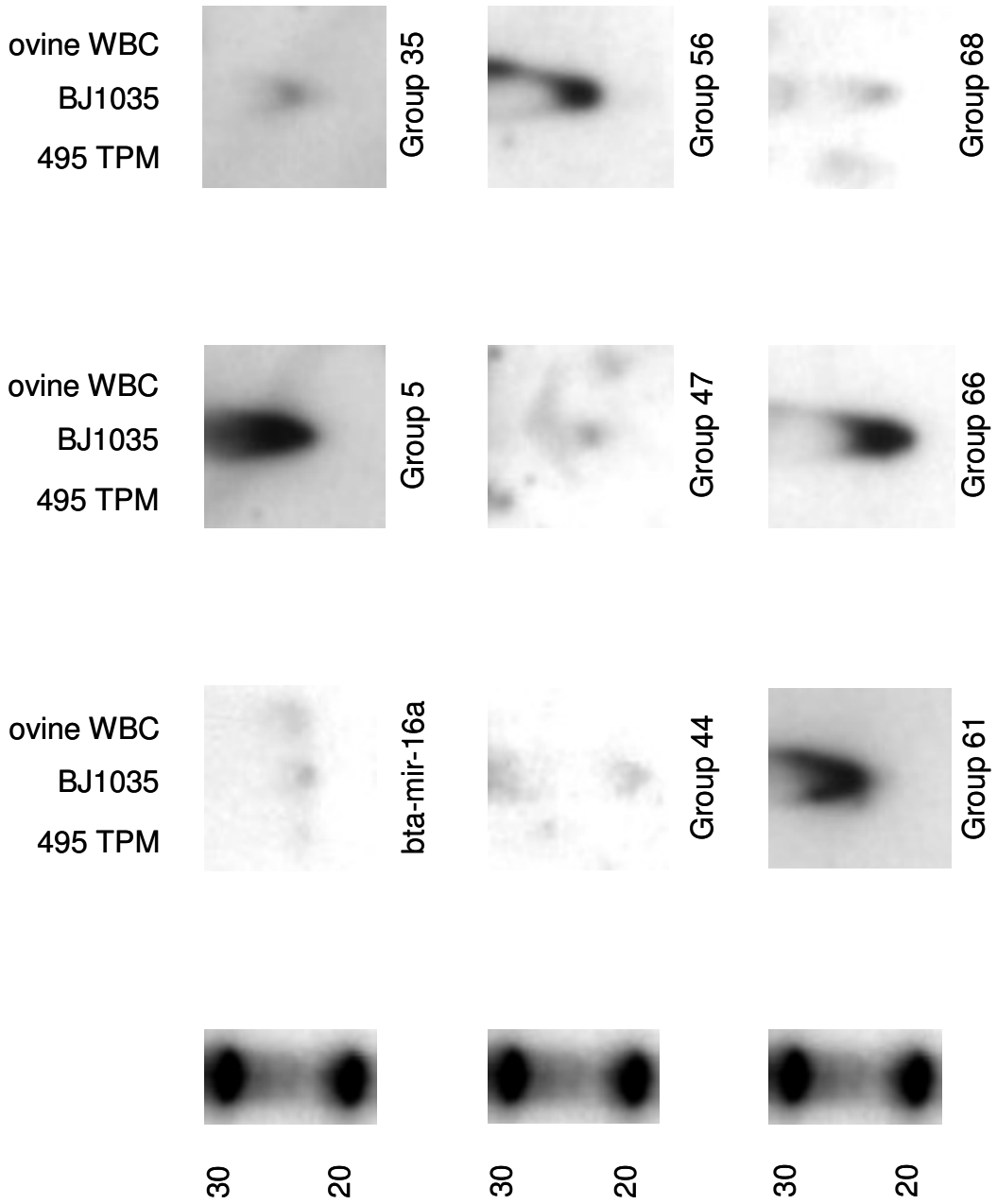

Figure 3.5: Northern hybridization for OvHV-2-encoded miRNAs in total RNA of uninfected bovine T cells (495 TPM) infected bovine T cells (BJ1035) and infected ovine leukocytes (ovine WBC).

Specific hybridization signals were observed for bta-mir-16a in all three cell types which confirmed the small RNA transfer was successful. Signals for all eight predicted miRNAs were observed only in OvHV-2-infected immortalized bovine T cells and absent in non-infected immortalized bovine T cells and ovine buffy coat (all signals were observed between 20-30 nt). The absence of a signal in the sheep cells is likely due to the fact that following a natural infection, OvHV-2 only infects a small minority of cells in the buffy coat, therefore the RNA copy number could be too low for detection by this method. The results from the northern hybridization confirmed that the eight identified tags are present in cells as ~22-mers and are expressed by OvHV-2. These are the first miRNAs found to be expressed by a virus in the *Macavirus* genus and will be referred to as ovhv2-miR-1 - miR-8.

3.3.4 Additional Predicted OvHV-2 miRNAs

The remaining tag groups were analyzed for miRNA secondary structure as described previously (Supplemental DVD; Secondary Structure Prediction and Candidate miRNAs; raw data can be found on Microarray Informatics, Accession E-MTAB-466). Groups that contained a stem-loop but did not have a putative miRNA* to use for the establishment of 3' overhangs or base-pairing within the stem were included in the list of predicted miRNAs to avoid over-stringency. Thus, the four of the 12 candidates mentioned previously that were not validated by northern hybridization due to having less than 16 bp in the miRNA/miRNA* duplex were also reconsidered as predicted miRNAs. With those four included, 38 additional predicted miRNAs were found; 3 on the plus strand and 35 on the minus strand (Table 3.4, Figure 3.6). All of the predicted miRNAs were found in noncoding regions of the genome and the 35 predicted miRNAs on the minus strand were found in three distinct clusters (it is unknown whether these miRNA clusters are expressed from a single or multiple promoters - it is currently being investigated). There was not time to find additional supporting evidence by northern hybridization for these additional predicted viral miRNAs but based on the bioinformatic criteria, it is believed that most, if not all, represent expressed miRNAs.

Table 3.4: Additional predicted OvHV-2 miRNAs.

Group	5' Start of Most Abundant Tag	Reads of Most Abundant Tag
Plus Strand		
3	182	25
64	117612	2
96	129703	1
Minus Strand		
1	156	21
3	526	196
4	724	1
6	1182	253
13	8445	1
34	27722	434
36	28066	6200
37	28209	6015
38	28381	322
39	28515	4717
40	28683	1014
41	28781	21686
42	28888	740
43	29052	31227
45	29345	6487
46	29455	9219
48	29745	8095
49	29945	2967
50	30091	3794
51	30338	24497
53	30510	14966
54	30632	1357
57	30980	5457
58	31085	942
60	31359	351
62	31603	1535
63	32075	517
67	36462	7834
83	48585	1
95	57413	1
128	79692	1
163	96435	1
181	103953	1
182	104758	1
217	117122	6064

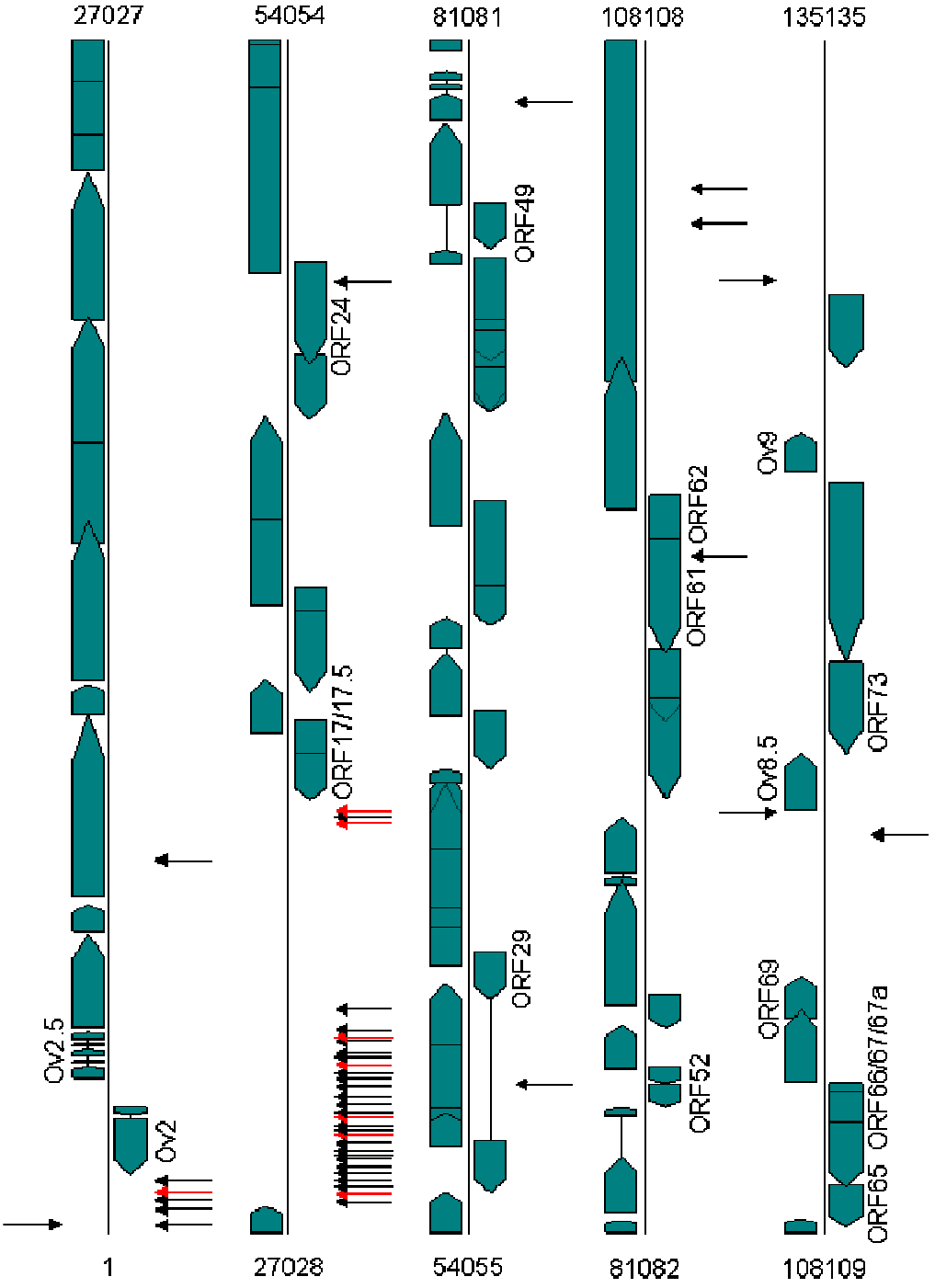

Figure 3.6A: Location of validated and predicted OvHV-2 miRNAs on an OvHV-2 genome schematic; predicted ORFs are shown with closed boxes (arrows indicating direction of transcription) miRNA sites are shown with arrows; those in red have been validated by northern hybridization. Rightward pointing arrows are transcribed from the plus strand of the genome, and leftward pointing arrows are transcribed from the minus stand. Names of ORFs flanking regions with miRNAs have been given.

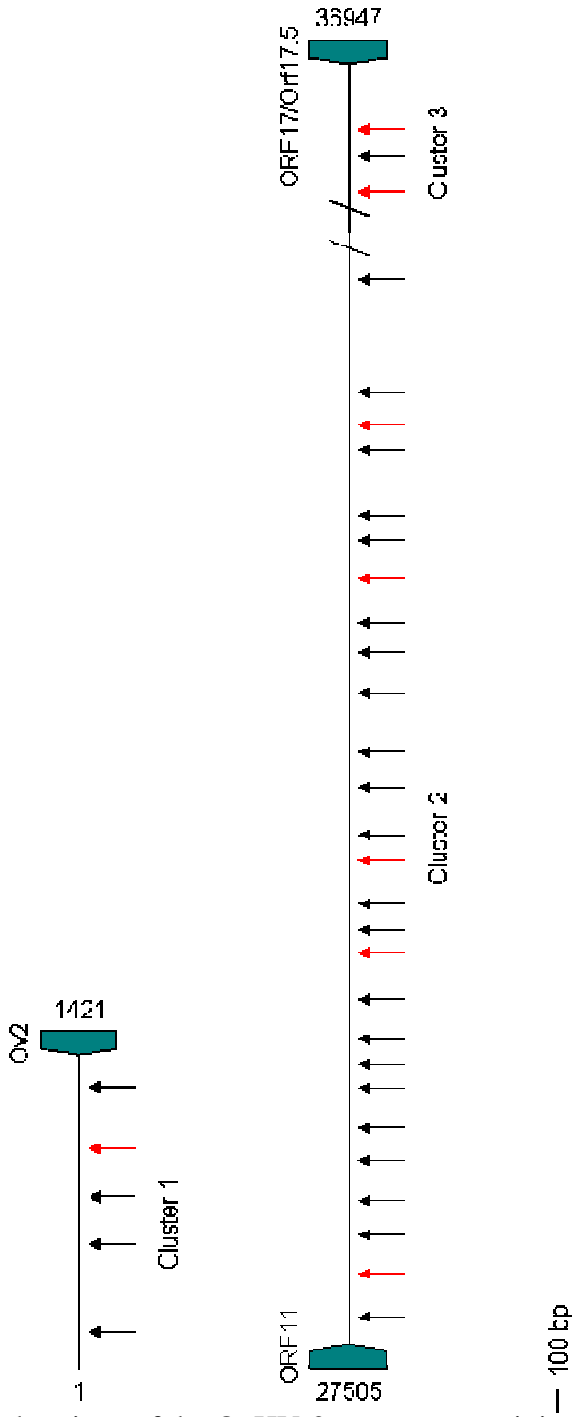

Figure 3.6B: Expanded regions of the OvHV-2 genome containing the three miRNA clusters on the minus strand that include the eight validated ovhv2-miRs (~4 kb separate Cluster 2 and Cluster 3). 100 bp of flanking orfs are shown by closed boxes (Ov2 and ORF17/17.5 are transcribed from the minus strand and ORF11 is transcribed from the plus strand).

3.3.5 LC Sciences Bioinformatic Analysis for OvHV-2 miRNAs

To complement the bioinformatic analysis used in this study, the Solexa sequence data originally generated by The Genepool was sent to LC Sciences for analysis. The data were subject to a number of filters to isolate the tags that represented predicted OvHV-2 miRNAs. The first filter eliminated those tags that matched the adaptors, were made up of mostly one nucleotide (A, C, G, or T) or had too many non-sequenced nucleotides. The second filter eliminated those tags that were less then 15 nt in length or were represented by less than three reads. The third filter eliminated tags that aligned to sequences in mRNA, repetitive DNA, or small RNA (excluding miRNA) databases, and that mapped to the bovine genome database. The resultant 294,233 reads - 5.2% of the original number of reads analyzed - aligned to the OvHV-2 genome. The OvHV-2 reads were represented by 33 unique tags (3.88% of the reads) from the plus strand of the genome and 818 unique tags (96.12% of the reads) from the minus strand (Supplemental DVD - LC Sciences). The size distribution of the tags selected by LC Sciences is shown in Figure 3.7.

Reads of tags with the same 5' start but variation in length were consolidated as described previously (3.2.1) resulting in 20 tags for the plus strand and 249 tags for the minus strand being identified (Figure 3.8).

The consensus tags were grouped together as described previously (3.3); the 20 plus strand tags were clustered into 11 groups and the 249 minus strand tags were clustered into 53. Based on the LC Sciences analysis, these groups represent OvHV-2 miRNAs; 64 compared to 46 miRNAs found by my manual analysis ($miRNAs_{C\ Levy}$) (3.3.4). For the predicted $miRNAs_{LC\ Sciences}$ on the plus strand, only one of the 11 was also a predicted $miRNA_{C\ Levy}$. The remaining ten predicted $miRNAs_{LC\ Sciences}$ on the plus strand were not determined to be $miRNAs_{C\ Levy}$ based on their predicted secondary structure; two of the $miRNAs_{LC\ Sciences}$ were represented by a single group in The Genepool dataset due to overlapping and close sequences (Figure 3.9).

A

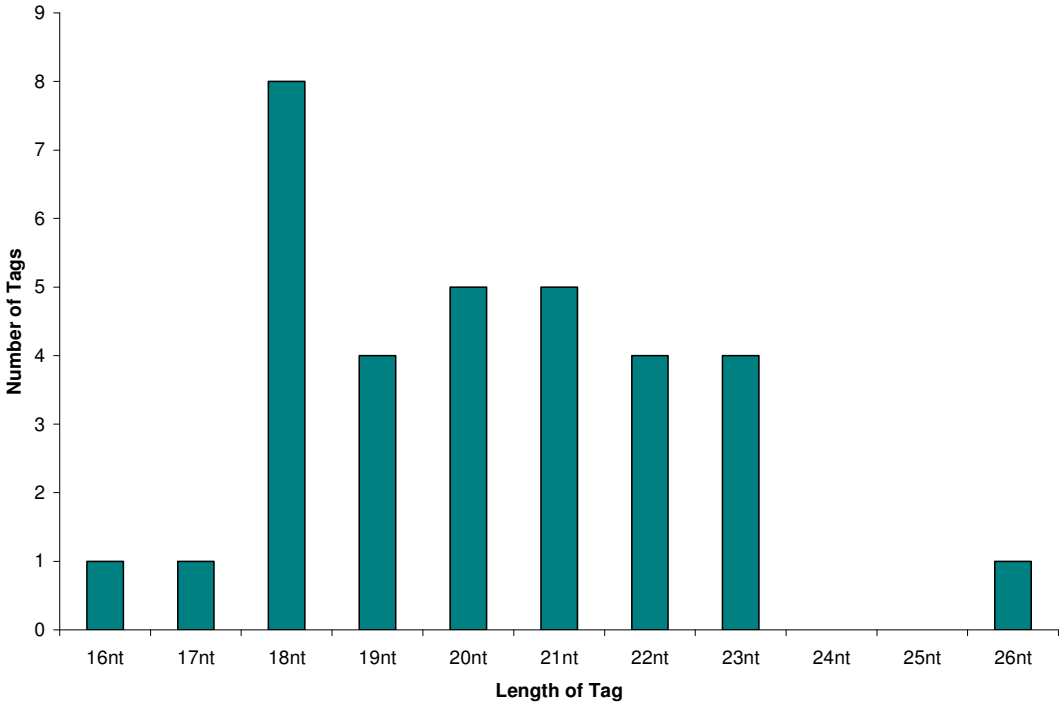

Figure 3.7A: Abundance of LC Sciences high throughput sequenced, OvHV-2-mapped, plus strand, small RNA tags by length. Note the difference in scale to Figure 3.7B.

B

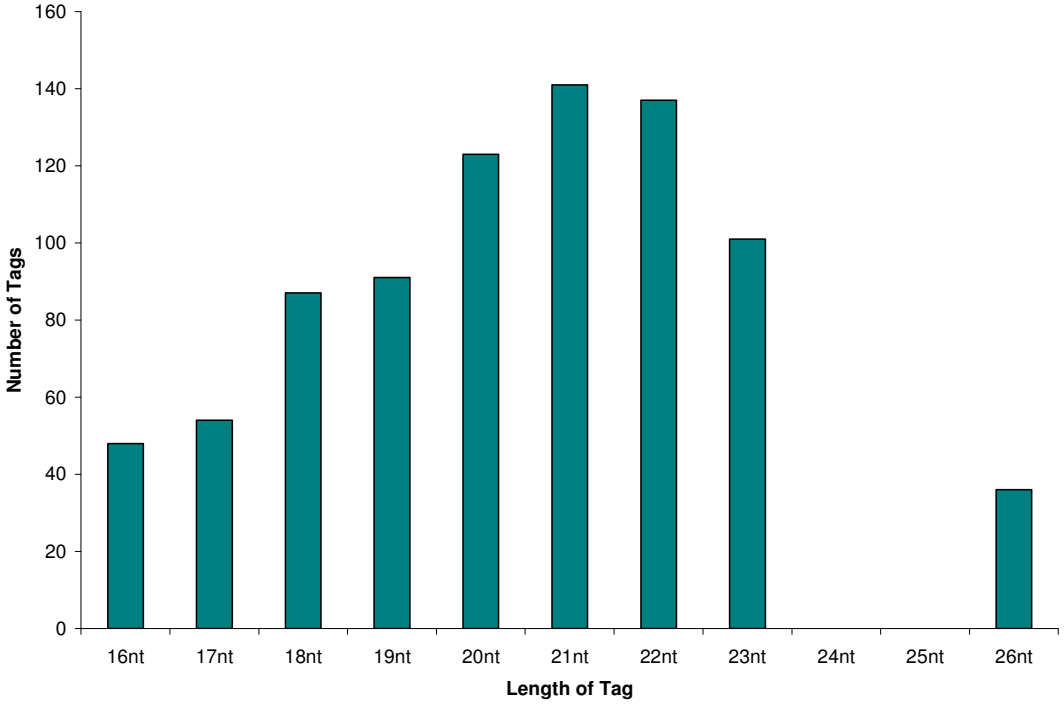

Figure 3.7B: Abundance of LC Sciences high throughput sequenced, OvHV-2-mapped, minus strand, small RNA tags by length. Note the difference in scale to Figure 3.7A.

A

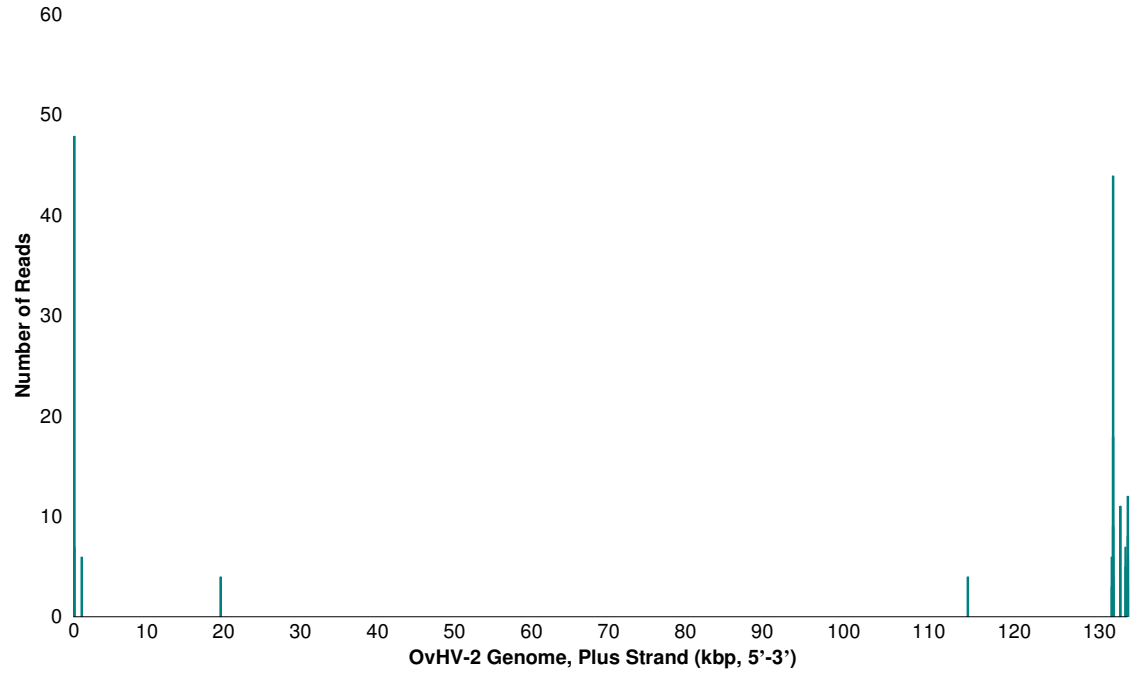

Figure 3.8A: Abundance of the 20 16-26 nt tags analyzed by LC Sciences plotted along the OvHV-2 genome plus strand. Note the difference in scale to Figure 3.8B.

B

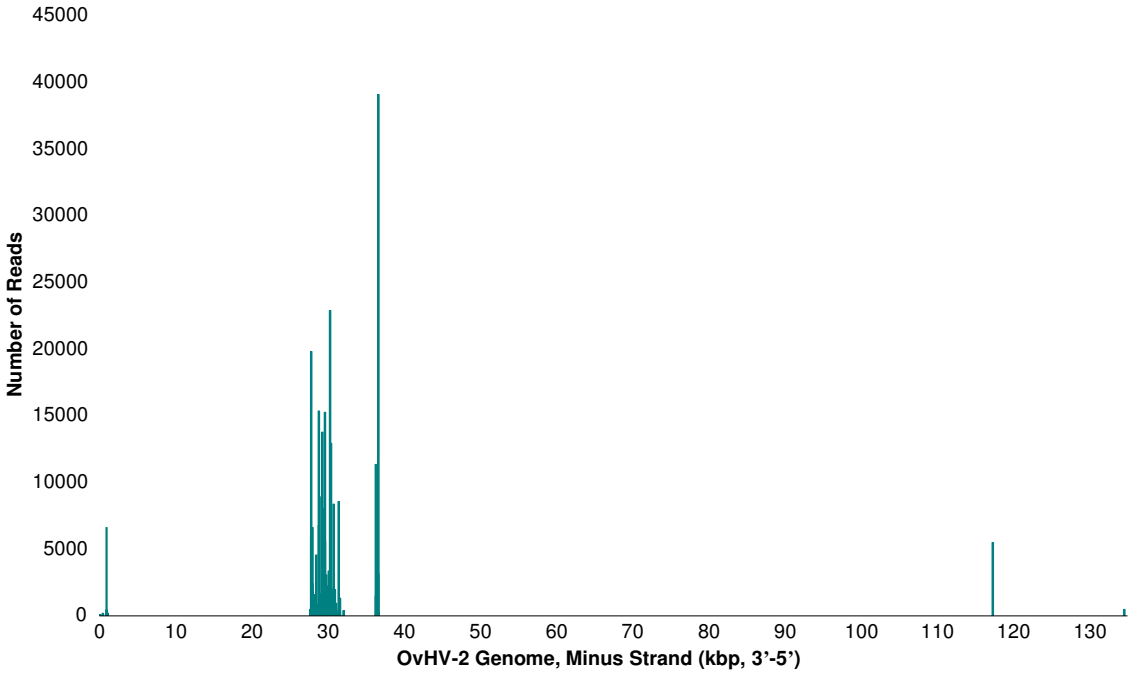

Figure 3.8B: Abundance of 249 16-26 nt tags analyzed by LC Sciences plotted along the OvHV-2 genome minus strand. Note the difference in scale to Figure 3.8A.

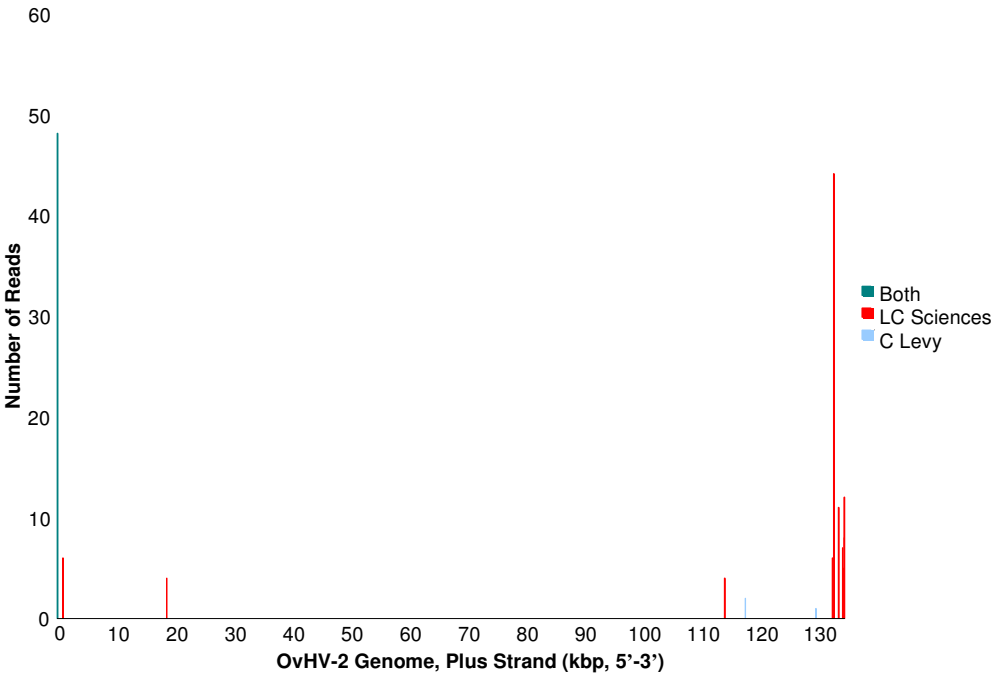

Figure 3.9A: Abundance of predicted plus strand OvHV-2 miRNAs by manual and LC Sciences analysis, mapped along the OvHV-2 genome. Note the difference in scale to Figure 3.9B.

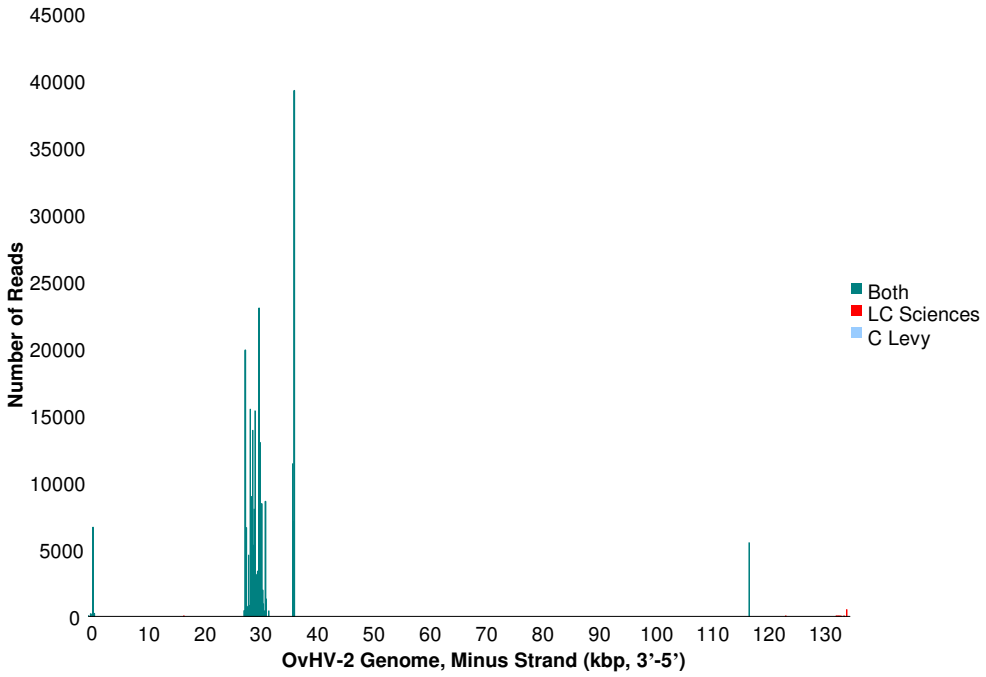

Figure 3.9B: Abundance of predicted minus strand OvHV-2 miRNAs by manual and LC Sciences analysis, mapped along the OvHV-2 genome. Note the difference in scale to Figure 3.9A.

For the miRNAs$_{LC\ Sciences}$ on the minus strand, 36 of the 53 were also predicted as miRNAs$_{C\ Levy}$ (including the 8 that were validated). Fifteen of the remaining miRNAs$_{LC\ Sciences}$ were not determined to be miRNAs$_{C\ Levy}$ based on their secondary structure, and 2 miRNAs$_{LC\ Sciences}$ were not analyzed manually as they had not passed through the filters set by The Genepool (Figure 3.10).

3.3.6 Predicted Target Bioinformatic Analysis

In order to determine what potential role these miRNAs may have in OvHV-2 biology and pathology, it is necessary to identify their target transcripts. There are a number of ways this can be accomplished; bioinformatics, microarray, and pull-down assays. Bioinformatics acknowledges the importance of the seed region in miRNA targeting and identifies complementary sequences in annotated ORFs by alignment. Microarrays can be used to measure a difference in transcript abundance between miRNA-treated and non-treated samples. Pull-down assays target the protein components of the RISC complex or the miRNA itself and pull down transcripts actively being targeted. Due to time constraints for this project, optimization and testing of microarrays or pull-down assays was not feasible; thus, bioinformatics were used to initiate the assessment of the function of OvHV-2 encoded miRNAs.

At this point in time, the cow genome has been fully sequenced with >5-fold coverage and is currently being annotated (the annotation at this point in time is not as comprehensive as the mouse and human genomes). In contrast, the sheep genome is only incompletely sequenced and has only partial and preliminary annotation. It is more likely that OvHV-2 miRNAs have evolved to target cellular transcripts of the ovine genome rather than the bovine genome as sheep appear to be its natural host given their lack of clinical symptoms upon infection. Therefore, the complementary sequences to the eight validated ovhv2-miRs were aligned against the OvHV-2 and bovine genomes to predict targets using blastn (2.6.2). Once the ovine genome is complete, it will be analyzed for OvHV-2 miRNA targets found in this study.

3.3.7 OvHV-2 Genome Targets

The blastn search found 131 to 412 putative target sites on the OvHV-2 genome for each of the eight ovhv2-miRs. Once these sites were manually filtered to include only those that involved the complementary sequence to the seed region (nucleotides 1-8, 1-7, or 2-8) the number of potential target sites decreased to between 22 and 56 for each ovhv2-miR. The complete OvHV-2 genome (2.7.3) was used to determine whether these seed target sites fell within annotated ORFs (Table 3.5).

Table 3.5: Ovhv2-miR seed alignment to OvHV-2 genome.

Group	Seed Hits	Annotated ORF Hits	Individual ORF Hits
ovhv2-miR-1	22	17	15
ovhv2-miR-2	31	21	19
ovhv2-miR-3	23	18	15
ovhv2-miR-4	31	14	14
ovhv2-miR-5	35	30	20
ovhv2-miR-6	56	28	25
ovhv2-miR-7	24	24	17
ovhv2-miR-8	56	45	33

Legend: Blastn results aligning validated ovhv2-miRs against the OvHV-2 genome; filtered for seed regions, and filtered for annotated ORFs (5' UTR, coding region, and 3' UTR). The "Annotated ORF Hits" value is the number of total target sites found for the given miRNA and the "Individual ORF Hits" value is the number of total ORF targets found for the given miRNA.

The annotation of the OvHV-2 genome allowed for the putative target sites to be assigned to the different regions of the mRNA transcript - 5' UTR, coding region, or 3' UTR. The eight ovhv2-miRs were predicted to target 65 (89.0%) of the 73 predicted viral ORFs (Table 3.6). A broad targeting range was observed over the functions of the targeted genes; targets included those involved in replication, gene expression, structure, and signalling with no particular pathway standing out.

Table 3.6A: Predicted OvHV-2 ORF targets of ovhv2-miR-1 and ovhv2-miR-2.

Ovhv2-miR	Target Site	ORF	Add. Ovhv2-miRs	Predicted Function
miR-1	5' UTR	ORF10	miR-8	Unknown
	CDS	ORF8		Glycoprotein B
		ORF9	miR-2, -6	DNA Polymerase Subunit
		Ov5	miR-8	G-Protein Coupled Receptor (putative)
		ORF23	miR-2	Tegument Protein
		ORF32	miR-2, -8	Nuclear Capsid Localization
		ORF44		Helicase
		ORF48	miR-2	EBV BRRF2
		ORF63	miR-3, -5	Tegument Protein
		ORF64 x3	miR-3, -4, -7, -8	Tegument Protein
		ORF69	miR-4, -6	Nuclear Lamina Capsid Docking Protein
		Ov8.5	miR-6, -8	Unknown
		ORF75	miR-2, -4, -7	Formylglycinamide Ribotide Amidotransferase (FGARAT), Tegument Protein
	3' UTR	ORF7	miR-8	Terminase Subunit
		ORF31	miR-2, -8	EBV BDLF4 (putative glycoprotein)
miR-2	5' UTR	ORF20	miR-5, -6, -7, -8	Nuclear Protein
		ORF75	miR-1, -4, -7	FGARAT
	CDS	Ov2	miR-4, -5	Basic Leucine Zipper Motif
		ORF6 x2	miR-4, -5, -7	ssDNA Binding Protein
		ORF9	miR-1, -6	DNA Polymerase Subunit
		ORF18	miR-7, -8	EBV BVLF1.5
		ORF21	miR-6	Thymidine Kinase
		ORF23	miR-1	Tegument Protein
		ORF26	miR-3, -5, -8	Capsid Triplex Protein
		ORF29	miR-3, -5, -6	Terminase Subunit
		ORF32	miR-1, -8	Nuclear Capsid Localization
		ORF39	miR-3	Glycoprotein M
		ORF43		Capsid Portal Protein
		ORF48	miR-1	EBV BRRF2
		ORF56	miR-4	Primase
		ORF75	miR-1, -4, -7	FGARAT
miR-2	CDS	Ov10 x2	miR-4, -5	Glycoprotein (putative)
	3' UTR	ORF25	miR-3, -4, -5, -6, -8	Major Capsid Protein
		ORF31	miR-1, -8	EBV BDLF4

Legend: OvHV-2 ORFs predicted to be targeted by the eight validated ovhv2-miRs by target region of the mRNA (5' UTR, coding region [CDS] or 3' UTR); "x#" after the ORF name indicates the number of additional target sites on that particular ORF by the given ovhv2-miR. Replication, gene expression, structural, and unknown/undesignated orf functions are colour-coded.

Table 3.6B: Predicted OvHV-2 ORF targets of ovhv2-miR-3 and ovhv2-miR-4.

Ovhv2-miR	Target Site	ORF	Add. Ovhv2-miRs	Predicted Function
miR-3	5' UTR	ORF58	miR-5, -7, -8	Multiple Membrane-Spanning Protein
	CDS	Ov3	miR-6, -8	Semaphorin (putative)
		ORF27 x2	miR-5, -8	EBV BDLF2
		ORF29	miR-2, -5, -6	Terminase Subunit
		ORF34	miR-8	EBV BGLF3
		ORF39	miR-2	Glycoprotein M
		ORF50	miR-5, -6, -8	Transcriptional Control
		Ov6	miR-8	Transcriptional Control (putative)
		ORF59	miR-5, -7, -8	DNA Polymerase Subunit
		ORF63	miR-1, -5	Tegument Protein
		ORF64	miR-1, -4, -7, -8	Tegument Protein
	3' UTR	ORF25 x2	miR-2, -4, -5, -6, -8	Major Capsid Protein
		ORF26 x2	miR-2, -5, -8	Capsid Triplex Protein
		ORF60	miR-6, -8	Ribonucleotide Reductase Subunit
		ORF65		Capsid Protein
miR-4	CDS	Ov2.5		IL-10
		ORF3	miR-8	FGARAT
		Ov4.5	miR-8	Bcl-2
		ORF6	miR-2, -5, -7	ssDNA Binding Protein
		ORF25	miR-2, -3, -5, -6, -8	Major Capsid Protein
		ORF40	miR-7, -8	Complexed with Helicase and Primase
		ORF54		Deoxyuridine Triphosphatase (dUTPase)
		ORF56	miR-2	Primase
		ORF64	miR-1, -3, -7, -8	Tegument Protein
		ORF68	miR -6	Nuclear Capsid Localization
		ORF69	miR-1, -6	Nuclear Lamina Capsid Docking Protein
		ORF75	miR-1, -2, -7	FGARAT
		Ov10	miR-2, -5	Glycoprotein (putative)
	3' UTR	Ov2	miR-2, -5	Basic Leucine Zipper Motif

Table 3.6C: Predicted OvHV-2 ORF targets of ovhv2-miR-5 and ovhv2-miR-6.

Ovhv2-miR	Target Site	ORF	Add. Ovhv2-miRs	Predicted Function
miR-5	5' UTR	ORF65	miR-3	Capsid Protein
	CDS	Ov2	miR-2, -4	Basic Leucine Zipper Motif
		ORF6 x2	miR-2, -4, -7	ssDNA Binding Protein
		ORF19	miR-6, -7	Portal Capping Protein (putative)
		ORF26 x2	miR-2, -3, -8	Capsid Triplex Protein
		ORF27	miR-3, -8	EBV BDLF2
		ORF29	miR-2, -3, -6	Terminase Subunit
		Ov8	miR-6	Glycoprotein (putative)
		ORF58	miR-3, -7, -8	Multiple Membrane-Spanning Protein
		ORF63	miR-1, -3	Tegument Protein
		ORF66 x3		EBV BFRF2
		Ov9	miR-6	Bcl-2
		Ov10	miR-2, -4	Glycoprotein (putative)
	3' UTR	ORF20	miR-2, -6, -7, -8	Nuclear Protein
		ORF25 x3	miR-2, -3, -4, -6, -8	Major Capsid Protein
		ORF26	miR-2, -3, -8	Capsid Triplex Protein
		ORF50	miR-3, -6, -8	Transcriptional Control
		ORF59	miR-3, -6, -8	DNA Polymerase Subunit
		ORF67 x3		Nuclear Lamina Capsid Docking Protein
		ORF67a x3		Terminase Cofactor
miR-6	5' UTR	ORF50	miR-3, -5, -8	Transcriptional Control
		ORF60	miR-3, -8	Ribonucleotide Reductase Subunit
		ORF73	miR-8	LANA
	CDS	Ov3	miR-3, -8	Semaphorin (putative)
		ORF9 x2	miR-1, -2	DNA Polymerase Subunit
		ORF19	miR-5, -7	Portal Capping Protein (putative)
		ORF20	miR-2, -5, -7, -8	Nuclear Protein
		ORF22		Glycoprotein H
		ORF24 x2	miR-7	HSV U_L20
		ORF25	miR-2, -3, -4, -5, -8	Major Capsid Protein
		ORF29	miR-2, -3, -5	Terminase Subunit
		ORF52		HSV U_L49
		ORF60	miR-3, -8	Ribonucleotide Reductase Subunit
		ORF68	miR-4	Nuclear Capsid Localization
		Ov9	miR-5	Bcl-2
	3' UTR	ORF19	miR-5, -7	Portal Capping Protein (putative)
		ORF20	miR-2, -5, -7, -8	Nuclear Protein
		ORF21	miR-2	Thymidine Kinase
		Orf49 x2		Transcriptional Control
		Ov8	miR-5	Glycoprotein (putative)
		Orf61	miR-7	Ribonucleotide Reductase Subunit
		Orf62	miR-7	Capsid Triplex Protein
		Orf69	miR-1, -4	Nuclear Lamina Capsid Docking Protein
		Ov8.5	miR-1, -8	Unknown
		Orf73	miR-8	LANA

Table 3.6D: Predicted OvHV-2 ORF targets of ovhv2-miR-7.

Ovhv2-miR	Target Site	ORF	Add. Ovhv2-miRs	Predicted Function
miR-7	5' UTR	Orf58	miR-3, -5, -8	Multiple Membrane-Spanning Protein
	CDS	Orf6 x2	miR-2, -4, -5	ssDNA Binding Protein
		Orf17 x2		Maturational Protease
		Orf17.5 x2		Major Scaffold Protein
		Orf18 x2	miR-2, -8	EBV BVLF1.5
		Orf19	miR-5, -6	Portal Capping Protein (putative)
		Orf24	miR-6	HSV U_L20
		Orf40	miR-4, -8	Complexed with Helicase and Primase
		Orf45		HSV U_L4
		Orf57	miR-8	Post-Transcriptional Regulator
		Orf59	miR-3, -5, -8	DNA Polymerase Subunit
		Orf61 x2	miR-6	Ribonucleotide Reductase Subunit
		Orf64 x2	miR-1, -3, -4, -8	Tegument Protein
		Orf75	miR-1, -2, -4	FGARAT
	3' UTR	Orf20	miR-2, -5, -6, -8	Nuclear Protein
		Orf46		Uracil DNA Glycosylase
		Orf62 x2	miR-6	Capsid Triplex Protein

Table 3.6E: Predicted OvHV-2 ORF targets of ovhv2-miR-8.

Ovhv2-miR	Target Site	ORF	Add. Ovhv2-miRs	Predicted Function
miR-8	5' UTR	Ov3	miR-3, -6	Semaphorin (putative)
		Orf10	miR-1	Unknown
		Orf18	miR-2, -7	EBV BVLF1.5
		Orf58 x2	miR-3, -5, -7	Multiple Membrane-Spanning Protein
		Orf73 x2	miR-6	LANA
	CDS	Orf3	miR-4	FGARAT
		Ov4.5	miR-4	Bcl-2
		Orf7	miR-1	Terminase Subunit
		Ov5	miR-1	G-Protein Coupled Receptor (putative)
		Orf20	miR-2, -5, -6, -7	Nuclear Protein
		Orf25	miR-2, -3, -4, -5, -6	Major Capsid Protein
		Orf26	miR-2, -3, -5	Capsid Triplex Protein
		Orf27	miR-3, -5	EBV BDLF2
		Orf32	miR-1, -2	Nuclear Capsid Localization
		Orf33		Tegument Protein
		Orf36		Protein Kinase
		Orf37		Deoxyribonuclease
		Orf40 x3	miR-4, -7	Complexed with Helicase and Primase
		Orf50	miR-3, -5, -6	Transcriptional Control
		Ov6 x2	miR-3	Transcriptional Control (putative)
		Orf57	miR-7	Post-Transcriptional Regulator
		Orf59	miR-3, -5, -7	DNA Polymerase Subunit
		Orf60	miR-3, -6	Ribonucleotide Reductase Subunit
		Orf64 x2	miR-1, -3, -4, -7	Tegument Protein
		Ov8.5 x2	miR-1	Unknown
	3' UTR	Orf25 x2	miR-2, -3, -4, -5, -6	Major Capsid Protein
		Orf26	miR-2, -3, -5	Capsid Triplex Protein
		Orf31 x2	miR-1, -2	EBV BDLF4
		Orf32	miR-1, -2	Nuclear Capsid Localization
		Orf34 x2	miR-3	EBV BGLF3
		Orf35 x2		Tegument Protein
		Orf36		Protein Kinase
		Ov7		Glycoprotein (putative)

3.3.8 Bovine Genome Targets

The blastn search found between 321 and 3,496 sites on the bovine genome where at least 7 consecutive nucleotides were exactly complementary to one of the eight ovhv2-miRs. Once these sites were manually filtered to include only those that involved the complementary sequence to the seed region the number of potential target sites decreased to between 13 and 635 for each ovhv2-miR. The completed bovine genome (btau_4, http://www.ensembl.org/das/Bos_taurus.Btau_4.0.reference/) was used to determine whether these seed target sites fell within annotated orfs (Table 3.7).

Table 3.7: Ovhv2-miR seed alignment to bovine genome.

Ovhv2-miR	Seed Hits	Annotated Orf Hits
miR-1	503	10
miR-2	92	1
miR-3	635	2
miR-4	515	5
miR-5	615	6
miR-6	103	0
miR-7	13	0
miR-8	278	4

Legend: Blastn results aligning validated OvHV-2-encoded miRNAs against the bovine genome; filtered for seed regions and filtered for annotated genes (5' UTR, coding region, and 3' UTR).

The ORF coordinates also allowed for the putative target sites to be assigned to the different regions of the mRNA transcript. The eight miRNAs were predicted to target 29/~25,186 (0.1%) bovine ORFs (Table 3.8).

Table 3.8: Predicted bovine ORF targets of ovhv2-miR-1 - -miR-8.

Ovhv2-miR	Target Site	Target	Description (Function)
miR-1	CDS	NDUFB5	NADH Dehydrogenase (ubiquinone) 1 Beta Subcomplex 5 (respiration)
		REPS2	RALBP1 Associated Eps Domain Containing 2 (endocytosis of growth factor receptors)
		TLR7	Toll-like Receptor 7 (pathogen recognition/innate immune system activation in lung, placenta, and spleen)
		LOC506828	Alpha-2-Macroglobulin Precursor (protease inhibitor and cytokine transporter)
		ZBED5	Zinc Finger, BED-type Containing 5 (inactive transposon)
		ALDH3A2	Aldehyde Dehydrogenase 3 Family, Member A2 (detoxifies aldehydes)
		GTF2IRD2	GTF2I Repeat Domain 2 (putative transcription factor)
	3' UTR	LOC100139782	Exportin 4 (transports proteins between nuclear and cytoplasmic compartments)
		ANK1	Ankyrin 1 (cell motility, activation, proliferation, contact, and maintaince in erythrocytes, brain, and muscle
		PERP	TP53 Apoptosis Effector (promotes desmosome assembly and apoptosis)
miR-2	CDS	PRSS2	Serine Protease 2 (secreted by pancreas, activated in small intestine, cleaves carboxyl groups off lysine or arginine)
miR-3	CDS	CEP350	Centrosomal Protein (anchors microtubules at the centrosome)
		NDFIP2	Nedd4 Family Interacting Protein 2 (activates a number of HECT domain-containing E3 ubiquitin-protein ligases)
miR-4	CDS	DENND4C	DENN/MADD Domain Containing 4C (unknown)
		LOC783920	GTPase (interferon inducer)
	3' UTR	LOC538441	Chromosome 9 Open Reading Frame 41 (unknown)
		MYOHD1	Myosin XIX (actin-based motor molecule)
		WDR59	WD Repeat Domain 59 (unknown)
miR-5	5' UTR	CDC25C	Cell Division Cycle 25 Homologue C (regulates cell division)
		KLHL31	Kelch-like 31 (Transcriptional repressor)
		LOC616520	Splicing Factor 3B Subunit (binds pre-mRNA)
		SF3B14	Splicing Factor 3B Subunit 14 (splices pre-mRNA)
	3' UTR	CREM	cAMP Responsive Element Modulator (transcription factor)
		UBE2G1	Ubiquitin-Conjugating Enzyme E2G 1 (covalently attaches ubiquitin to other proteins)
miR-8	CDS	LOC782388	Copine II (calcium-dependent membrane-binding protein)
		LOC785769	Spermatogenesis Associated 13 (unknown)
		NECAB2	N-Terminal EF-Hand Calcium Binding Protein 2 (unknown)
		PITRM1	Pitrilysin Metallopeptidase 1 (degrades mitochondrial transit peptides and unstructured peptides [ranging from 10 to 65 residues])

Legend: Bovine ORFs predicted to be targeted by the eight ovhv2-miRs; ORF names are given next to the location on the transcript that the target site was located. Note that ovhv2-mir-6 and -miR-7 do not have any predicted targets on the bovine genome.

3.4 DISCUSSION

3.4.1 Nucleotide Composition & Minimal Folding Free Energy Index

The 46 miRNAs$_{C\ Levy}$ had an average G+C content of 51%, similar to the overall OvHV-2 genome that has a G+C content of 52% (Hart *et al*., 2007). Though stem-loops are a main feature of pri-miRNA secondary structure, pri-miRNAs are not the only RNA species that can fold into this structure (for example, rRNAs, tRNAs, and mRNAs) (Zhang *et al*., 2006). To aid in deciphering if an RNA stem-loop is likely that of a pri-miRNA, Zhang *et al*., 2006 determined the minimal folding free energy index (MFEI). MFEI is calculated by taking a predicted folding energy (using mfold, 2.6.1) and adjusting it to account for nucleic acid length and G+C content;

$$MFEI = ((MFE/length_{nt})*100)/(G+C\%)$$

They found that miRNAs tend to have higher negative MFEI than other types of RNA (>0.85). This is a useful tool, but acts more as a guideline as Pan *et al.*, 2007 observed MFEI as low as 0.55 and the 46 miRNAs$_{C\ Levy}$ have MFEI between 0.42 and 1.03 (Table 3.9). The MFEI was established using plant miRNAs which have a lower G+C content than viral miRNAs; thus resulting in higher MFEI.

As of February 2011, 235 predicted viral pri-miRNAs containing 300 mature miRNAs had been published, of which 228 pri-miRNAs (288 miRNAs) were encoded by herpesviruses (miRBase v16.0 - http://www.mirbase.org). So far, many of these have not been functionally characterized. They ranged from 18-30 nt in length and the 46 miRNAs$_{C\ Levy}$ fell within this range (20-26 nt; Figure 3.10).

Due to time constraints, only the eight ovhv2-miRs that were validated by northern hybridization were aligned (via blastn) to the AlHV-1 genome. This analysis did not find any sequence conserved homologues. This was not unexpected as there has been very little sequence conservation of miRNAs found between herpesviruses; not even

Table 3.9: Nucleotide composition of the 46 predicted OvHV-2 miRNAs.

Group	A (nt)	U (nt)	G (nt)	C (nt)	Total (nt)	A+U (%)	G+C (%)	MFEI
Plus Strand								
3	3	4	8	5	20	35.0	65.0	0.81
64	4	5	8	3	20	45.0	55.0	0.43
96	5	6	8	3	22	50.0	50.0	0.53
Minus Strand								
1	3	4	8	5	20	35.0	65.0	1.01
3	2	6	10	4	22	36.4	63.6	0.49
4-3p	4	6	10	1	21	47.6	52.4	0.49
4-5p	3	9	8	1	21	57.1	42.9	0.59
miR-1	8	5	6	3	22	59.1	40.9	0.51
6	5	7	5	5	22	54.5	45.5	0.62
13	5	4	9	4	22	40.9	59.1	0.48
34	1	10	5	5	21	52.4	47.6	0.50
miR-2	5	7	6	5	23	52.2	47.8	0.54
36	3	10	6	3	22	59.1	40.9	0.76
37	4	7	5	6	22	50.0	50.0	0.62
38	7	7	4	3	21	66.7	33.3	0.89
39	3	7	5	6	21	47.6	52.4	0.59
40	3	9	8	3	23	52.2	47.8	0.64
41	10	3	4	4	21	61.9	38.1	0.77
42	7	5	6	5	23	52.2	47.8	0.61
43	4	9	7	5	25	52.0	48.0	0.49
miR-3	3	10	8	2	23	56.5	43.5	0.62
45	7	5	8	3	23	52.2	47.8	0.62
46	7	6	5	4	22	59.1	40.9	0.56
miR-4	8	4	6	4	22	54.5	45.5	0.62
48	4	6	8	3	21	47.6	52.4	0.45
49	5	8	7	3	23	56.5	43.5	0.61
50	3	9	7	6	25	48.0	52.0	0.51
51	5	5	8	5	23	43.5	56.5	0.45
53	8	5	7	2	22	59.1	40.9	0.62
54	3	8	5	6	22	50.0	50.0	0.58
miR-5	6	6	6	5	23	52.2	47.8	0.71
57	7	8	6	4	25	60.0	40.0	0.75
58	3	5	6	6	20	40.0	60.0	0.42
60	4	5	7	4	20	45.0	55.0	0.65
miR-6	5	8	6	4	23	56.5	43.5	0.70
62	1	10	6	5	22	50.0	50.0	0.54
63	5	6	6	5	22	50.0	50.0	0.57
miR-7	8	4	5	8	25	48.0	52.0	0.50
67	4	3	9	6	22	31.8	68.2	0.50
miR-8	2	7	6	7	22	40.9	59.1	0.50
83	11	3	5	7	26	53.8	46.2	0.71
95	2	5	8	10	25	28.0	72.0	0.50
128	3	2	13	2	20	25.0	75.0	0.47
163	3	6	11	5	25	36.0	64.0	0.52
181	4	2	12	3	21	28.6	71.4	0.58
182	6	8	9	3	26	53.8	46.2	0.72
217	7	9	2	5	23	69.6	30.4	1.03

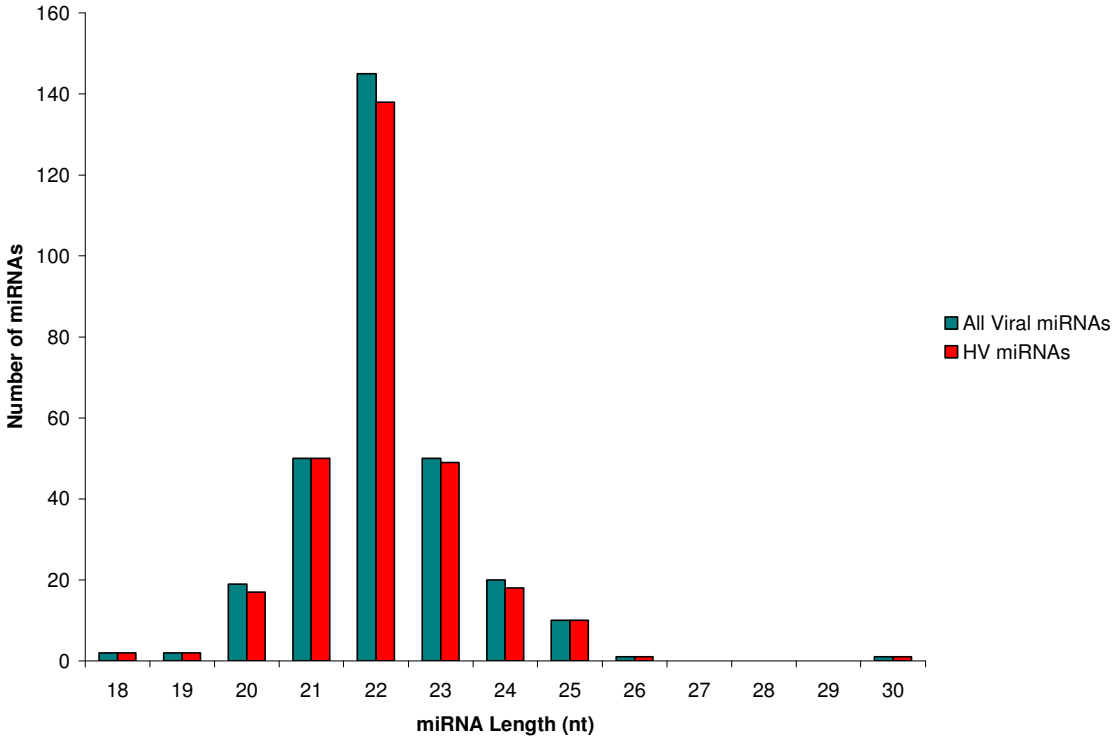

Figure 3.10: Length distribution of previously discovered viral miRNAs.

MDV-1 and MDV-2 which are serotypes of the same virus have been found to share any miRNAs (Yao *et al*., 2007).

3.4.2 Seed Conservation

Alignment of the 46 miRNAs$_{C\ Levy}$ with each other resulted in the observation that the predicted miRNA from Group 1 on the minus strand and Group 3 on the plus strand were identical. This could be due to evolutionary duplication, observed also in the *Mardivirus* member herpesvirus of turkeys (Yao *et al*., 2009). Functional orthologues of mammalian miR-155 have been found in other herpesviruses (1.5.3) but thus far, none has been found in OvHV-2 (Zhao *et al*., 2009). Alignment of the 46 miRNAs$_{C\ Levy}$ to all the miRNAs published in miRBase (Release 17; 16,772 entries - by using the miRBase search tool [mature miRNAs were searched for by SSEARCH with an E-value cut-off of 100; Supplemental DVD; miRBase]) resulted in 16 miRNAs$_{C\ Levy}$ having a seed match with 76 sequences in the database (Table 3.10); an alignment was determined a seed match if nucleotides 1-7, 1-8, or 2-8 from the 5' end of both sequences were the same, G:U pairings were acceptable. Half of the seed matches were not considered to be significant due to being miRNA* species (15) or miRNAs that belonged to poorly conserved gene families, none of which have been found in OvHV-2 host species (23). The remaining 38 matches which all mapped to the predicted miRNA in Group 217 on the minus strand (represented by 6,064 reads) were all members of the mir-216 gene family that is broadly conserved and found in most vertebrates (Figure 3.11). miR-216 targets PTEN (a tumour suppressor) and Ybx1 (a translation factor) which leads to cell survival, hypertrophy, sclerosis, and a decreased cellular response to stress - all symptoms observed in MCF (Figure 3.12) (Evdokimova *et al*., 2006, Kato *et al*., 2010, 2009). In Addition, Ybx1 promotes transcription of HLA II and stabilization of IL-2 mRNA (1.1.6, 1.2.1) (Chen *et al*., 2000, Didier *et al*., 1988). A decrease in Ybx1 and therefore a decrease in HLA II could support immune evasion. Without Ybx1, IL-2 mRNA is degraded more rapidly in T cells; this could explain the depleted levels of IL-2

Table 3.10: Seed conservation of predicted OvHV-2 miRNAs.

Group	Seed Matches	Organism	Seed Match	miRNA Family
Plus Strand				
3	0/60			
64	0/34			
96	2/117	soybean	gma-miR-4395	
		orang-utan	ppy-miR-1270	mir-1270
Minus Strand				
1	0/60			
3	1/52	red jungle fowl	gga-miR-1770	
4-3p	2/47	red flour beetle	tca-miR-279b-5p	mir-279
		mouse	mmu-miR-466c-5p	mir-466
4-5p	0/94			
miR-1	0/69			
6	0/57			
13	0/57			
34	0/95			
miR-2	0/61			
36	0/96			
37	0/64			
38	1/33	planarian	sme-miR-2168-5p	
39	1/202	sea squirt	cin-miR-4059-3p	
40	10/126	cow	bta-miR-23b-5p	mir-23
		human	hsa-miR-23a* hsa-miR-23b*	
		house mouse	mmu-miR-23a* mmu-miR-23b*	
		platypus	oan-miR-23b* oan-miR-23a*	
		rat	rno-miR-23a* rno-miR-23b*	
		zebra finch	tgu-miR-23*	
41	0/80			
42	0/61			
43	1/214	red jungle fowl	gga-miR-1736	
miR-3	0/74			
45	0/223			
46	0/19			
miR-4	0/62			
48	0/72			
49	0/187			

50	0/189			
51	0/102			
53	0/71			
54	1/164	sea lamprey	pma-miR-218a*	mir-218
miR-5	1/165	human	hsa-miR-4670-3p	
57	0/131			
58	0/26			
60	0/27			
miR-6	0/99			
62	0/142			
63	0/67			
miR-7	6/89	human	hsa-miR-524-3p hsa-miR-525-3p	mir-515
		orang-utan	ppy-miR-524-3p ppy-miR-525-3p	
		chimpanzee	ptr-miR-524 ptr-miR-525	
67	0/58			
miR-8	1/73	silkmoth	bmo-miR-745*	
83	0/142			
95	0/99			
128	5/106	fruit fly	dme-miR-4951-5p	
		red jungle fowl	gga-miR-1790 gga-miR-1809	
		platypus	oan-miR-125*	mir-125
		sea lamprey	pma-miR-4590	
163	4/89	*Arabidopsis thaliana*	ath-miR-447a ath-miR-447b ath-miR-447c-3p	mir-447
		human	hsa-miR-3191	mir-3190
181	1/154	mouse	mmu-miR-450a-2*	mir-450
182	1/192	*C. elegans*	cel-miR-40*	mir-36
217	38/120	lancelet	bfl-miR-216	mir-216
		cow	bta-miR-216a bta-miR-216b	
		dog	cfa-miR-216a cfa-miR-216b	
		sea squirt	cin-miR-216	
		sea squirt	csa-miR-216a csa-miR-216b	
		zebrafish	dre-miR-216a dre-miR-216b	

217 (cont.)	38/120 (cont.)	horse	eca-miR-216a eca-miR-216b	mir-216
		pufferfish	fru-miR-216b	
		red jungle fowl	gga-miR-216 gga-miR-216b	
		gorilla	ggo-miR-216	
		human	hsa-miR-216a hsa-miR-216b	
		ring-tailed lemur	lca-miR-216	
		owl limpet	lgi-miR-216a	
		gray short-tailed opossum	mdo-miR-216	
		Rhesus macaque	mml-miR-216a mml-miR-216b	
		house mouse	mmu-miR-216a mmu-miR-216b	
		platypus	oan-miR-216	
		sea lamprey	pma-miR-216b	
		bonobo	ppa-miR-216	
		orang-utan	ppy-miR-216 ppy-miR-216b	
		chimpanzee	ptr-miR-216b	
		rat	rno-miR-216a rno-miR-216b-5p	
		boar	ssc-miR-216	
		zebra finch	tgu-miR-216a tgu-miR-216b	
		green spotted pufferfish	tni-miR-216b	
		Western clawed frog	xtr-miR-216	

```
                    U   CCA UU  AA U
Group 217     5'-UAAUCUC GCU   A  GU  A -3'
miR-216       5'-UAAUCUC GCU   A  UG  A -3'
                    A   GGC AC  UG
```

Figure 3.11: Alignment of the putative OvHV-2 miRNA found in Group 217 on the minus strand against the vertebrate miRNA miR-216.

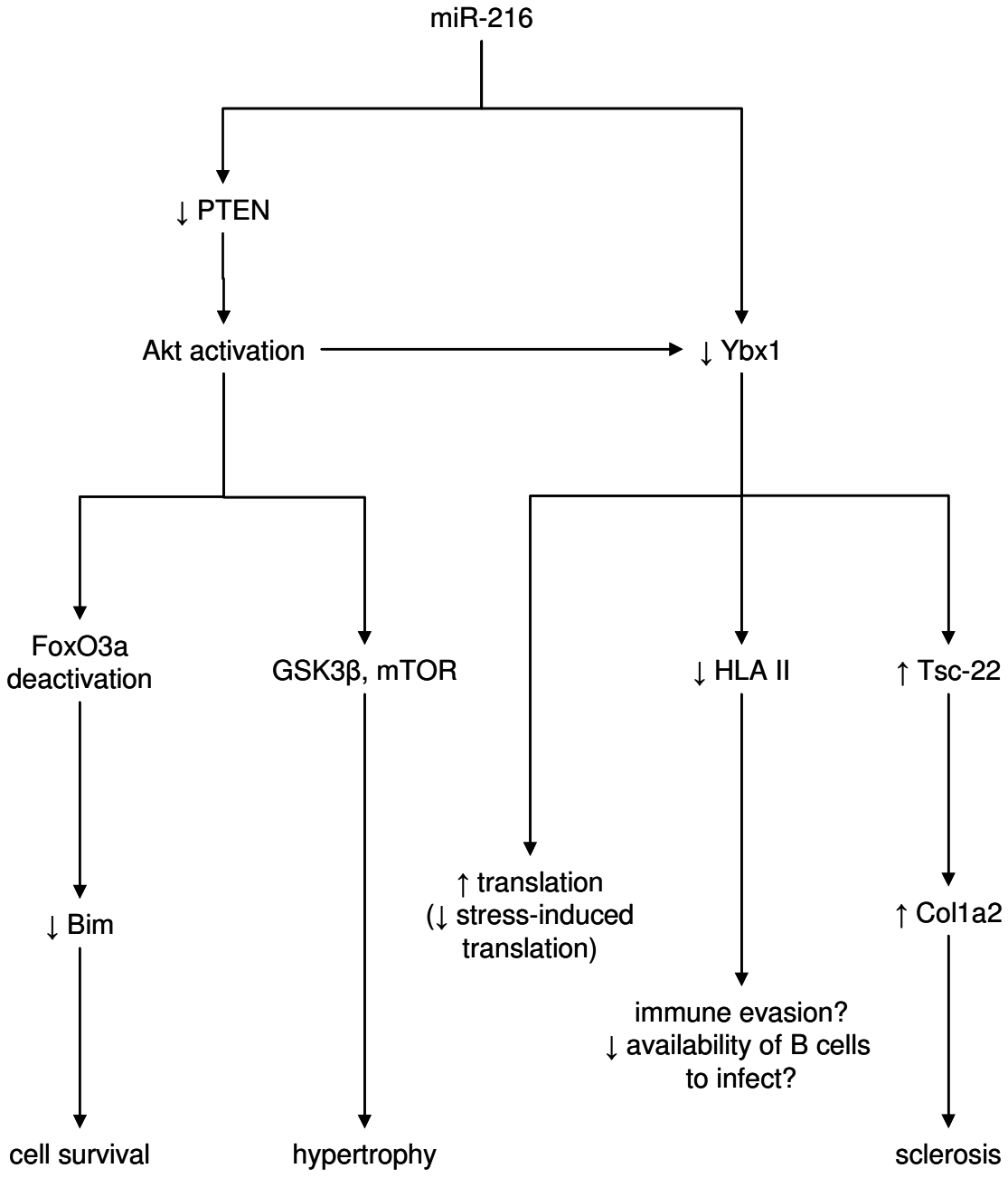

Figure 3.12: Schematic of cellular miR-216 regulation of cellular targets.

observed in OvHV-2-infected T cells. The abundance of the predicted OvHV-2 miRNA in Group 217 and the described targets and downstream affects of miR-216 are compelling evidence to support that Group 217 is a genuine OvHV-2 miRNA that may mimic a cellular miRNA and that may have a role in the pathogenesis of MCF. The remaining predicted miRNAs appear unique to OvHV-2; i.e. they have no cellular homologues.

3.4.3 OvHV-2 miRNAs Predicted by LC Sciences

The LC Sciences analysis predicted 37 out of the 46 $miRNAs_{C\ Levy}$, plus an additional 27. The addition of the four candidate miRNAs that were originally passed over for northern hybridization validation back into the list of predicted OvHV-2 miRNAs (3.5) was justified given that they were also predicted to be $miRNAs_{LC\ Sciences}$. LC Sciences predicted 11 miRNAs on the plus strand of the OvHV-2 genome, but only one of them was also a $miRNA_{C\ Levy}$ (Group 3 - group numbers are from 3.3). The remaining plus strand $miRNAs_{LC\ Sciences}$ were not $miRNAs_{C\ Levy}$ based on their secondary structure; they were not predicted to fold into a stem-loop, there were asymmetrical bulges in the stem, or the tag was not contained in the stem. The two additional $miRNAs_{C\ Levy}$ (Group 64 and 96) were most likely missed by LC Sciences due to their exclusion of tags that were represented by less than three reads; both groups were represented by one.

The LC Sciences analysis predicted 53 miRNAs on the minus stand, 36 of which were also predicted by my study; i.e. $miRNAs_{C\ Levy}$. 16 out of the remaining 17 $miRNAs_{LC\ Sciences}$ were not $miRNAs_{C\ Levy}$ due to their secondary structure prediction; they did not form stem-loops or the sequenced tag was not contained within the stem. The remaining one was not considered by manual analysis due to The Genepool's size filter; excluding any tags outside of 22-26 nt in length. The additional seven $miRNAs_{C\ Levy}$ on the minus strand (Groups 4, 13, 83, 128, 163, 181, and 182) that were not predicted by LC Sciences is again most likely due to their read count filter.

Both LC Sciences and Glazov *et al*., 2010 filtered out underrepresented sequence tags (<3 for LC Sciences and <2 for Glazov *et al*., 2010). These read limits appear arbitrary and it seems premature to dismiss these tags before all naturally infected cell types have been analyzed. It may be that in epithelial cells or B cells these tags will be represented by a higher number of reads. Until then, these single read tags will continue to be considered predicted OvHV-2 miRNAs.

3.4.4 OvHV-2 Pre-miRNAs Predicted by Walz *et al*., 2010

In 2010, Walz *et al.* published an article describing their global analysis of evolutionary conserved pre-miRNAs of 14 gammaherpesviruses (including OvHV-2) using VMir (http://www.hpi-hamburg.de/forschung/abteilungen-forschungsgruppen/zellulaere-virusabwehr/software-download.html). The VMir analysis and their following filtering steps retained 90% of the known gammaherpesvirus pre-miRNAs known at the time (miRBase Release 13 - 146 viral miRNAs; 139 herpesvirus miRNAs) and predicted 88 candidate pre-miRNAs in OvHV-2 with a score given based on similarity to known viral pre-miRNAs (Figure 3.13; Supplemental DVD - Walz).

45 out of the 88 pre-miRNAs predicted by Walz *et al*. were not represented by sequenced tags in this study (31 on the plus strand and 14 on the minus strand). Out of the remaining 43 predicted pre-miRNAs that were represented by tags in this study, 37 coincided with the predicted miRNAs found by manual analysis (2 on the plus strand and 35 on the minus strand) including the 8 that were validated in this study. 27/64 miRNAs predicted by LC Sciences were not predicted by Walz *et al*., however 3 of these were found across from predicted pre-miRNAs by Walz *et al*. 9/46 miRNAs predicted by manual analysis were not predicted by Walz *et al*. (Figure 3.14). There were five pre-miRNAs predicted by Walz *et al*. that were not considered to be candidate miRNAs by me based on their secondary structure (Table 3.11). Given Walz *et al*.'s filtering process and the subsequent loss of 10% of known gammaherpesvirus miRNAs, it is possible that the nine miRNAs predicted in this study that Walz *et al*. did not detect were lost in the filtering process.

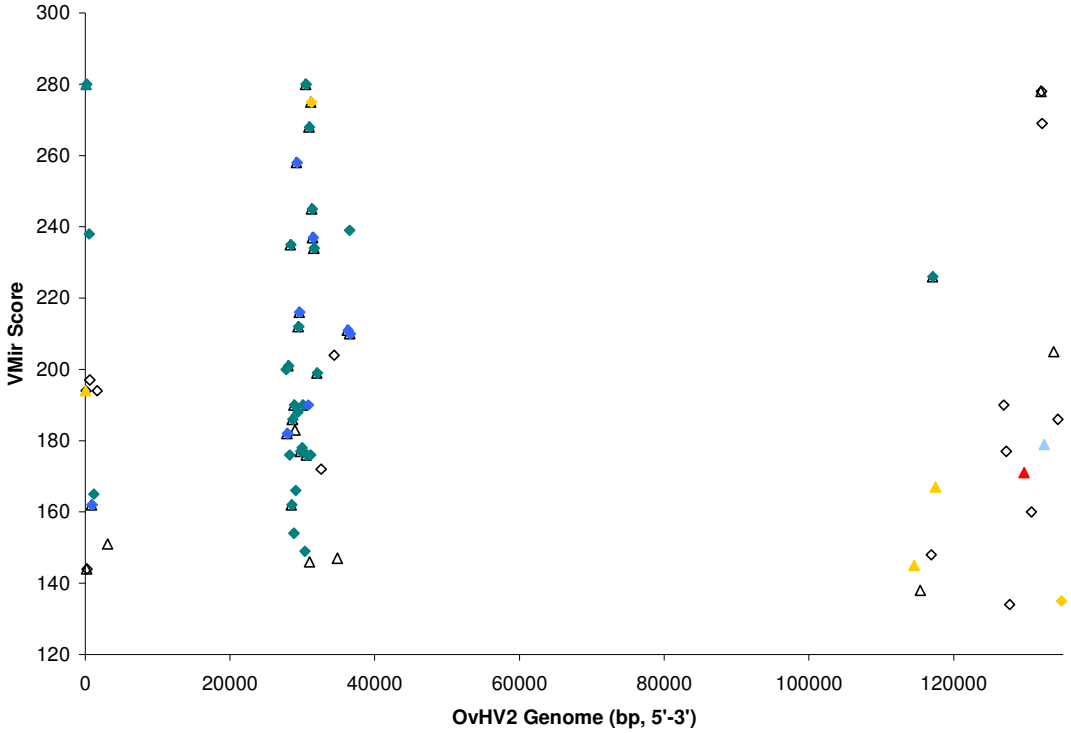

Figure 3.13: VMir scores for the 88 pre-miRNAs predicted by Walz *et al*., 2010.

Legend: ▲ Plus Strand ♦ Minus Strand. Legend: predicted by Walz *et al*. only (45), predicted by Walz *et al*. and represented by tags in The Genepool dataset but not predicted by me (5), predicted by Walz *et al*., LC Sciences and represented by tags in The Genepool dataset but not predicted by me (1), predicted by Walz *et al*. and me (1), predicted by Walz *et al*., LC Sciences, and me (36), validated ovhv2-miRs (predicted by all three [8].

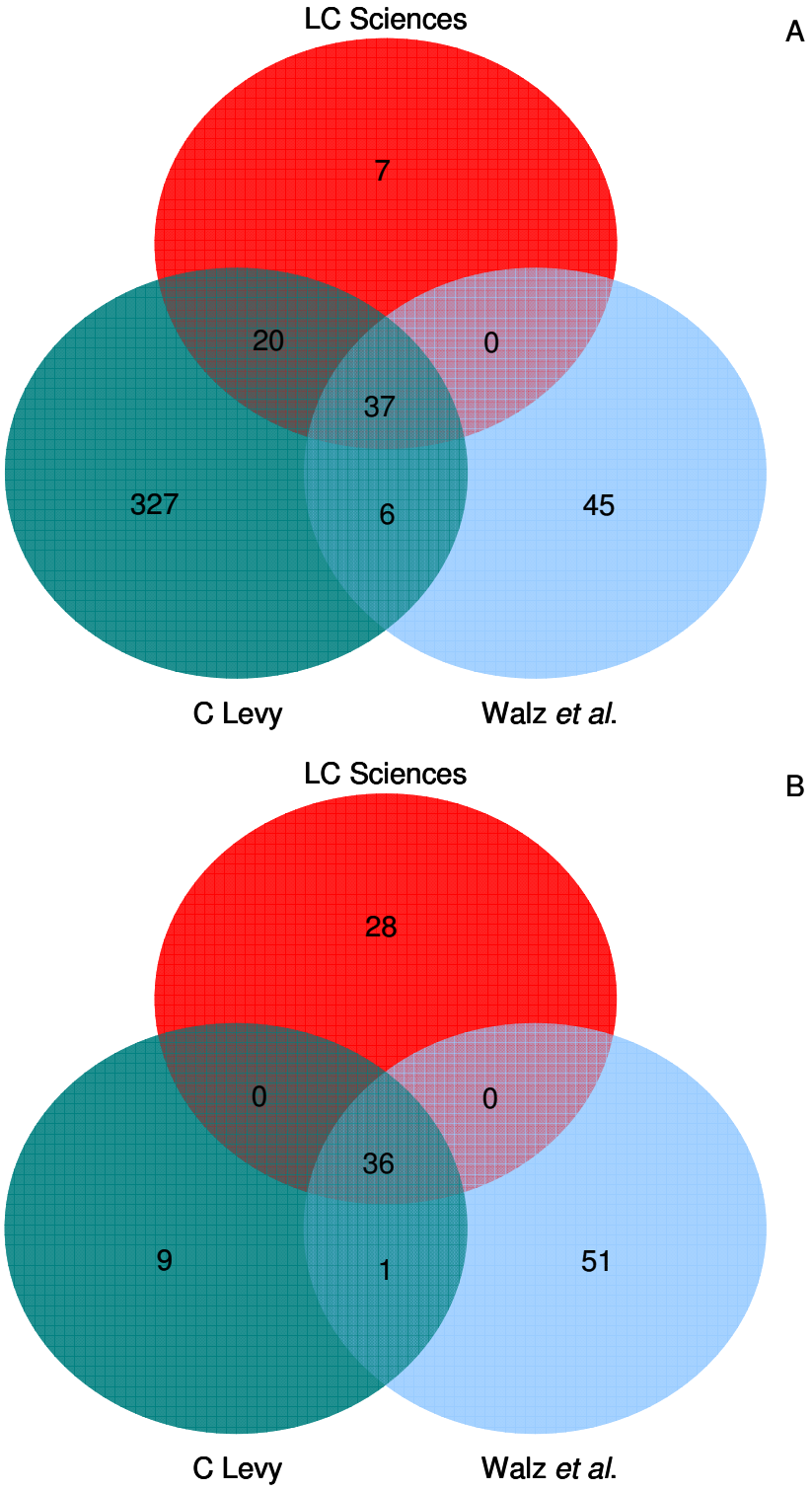

Figure 3.14: Venn diagram of predicted miRNAs by me, LC Sciences and Walz *et al.*; (A) includes all miRNA groups created in this study and (B) includes only those groups predicted to be miRNAs

Table 3.11: Pre-miRNAs predicted by Walz *et al*. that were not predicted in this study due to their secondary structure criteria.

	Walz *et al*. Predicted Pre-miRNAs		Corresponding Tags in This Study	
Group	Strand	Region (nt)	Strand	Tag 5' Start (nt)
2	+	52 – 124	+	101
59	-	31174 - 31271	-	31227
58	+	114512 - 114576	+	114555
63	+	117491 - 117588	+	117532
259	-	134805 - 134888	-	134811

The original data in this study was given to LC Sciences to compare their computational analysis to this study's manual analysis. Their analysis did not include a secondary structure component, which is a major element of miRNA biogenesis (1.5.1). Although a more time efficient method of analyzing high throughput sequencing, it appears that additional manual analysis will still be required of the investigator if they choose to use this kind of computational analysis. Walz *et al*., 2010 investigated conserved stem-loops in gammaherpesviruses. The prediction of 88 OvHV-2 pre-miRNAs by Walz *et al*., 2010 supports the finding that OvHV-2 might encode a large number of miRNAs. Again, the pre-miRNAs that they predicted may be real and just are not expressed in the cell line investigated in this study. The miRNAs predicted in this study and LC Sciences that were not predicted by Walz and colleagues may come from stem-loops that are not conserved in other gammaherpesviruses.

3.4.5 Passenger Strands or Additional miRNAs?

miRNAs* are reported to be present 100-fold less frequently than their duplexed miRNAs (Bartel, 2004). With this gauge, out of the 46 predicted OvHV-2 miRNAs detected in this study, 31 may by duplexed with a secondary miRNA (ranging from 1.1-fold decrease to 87.8-fold decrease) (Table 3.12). Three out of the 46 were duplexed with miRNAs* (ranging from 102.5-fold decrease to 379-fold decrease) and the remaining 12 could not be analyzed due to the passenger strand being undetected.

Table 3.12: Fold difference between OvHV-2 miRNAs and miRNAs*.

	Reads			
Group	miRNA	miRNA*	Fold Difference	Result
Plus Strand				
3	25	unknown	-----	-----
64	2	1	2.0	putative secondary miRNA
96	1	unknown	-----	-----
Minus Strand				
1	21	unknown	-----	-----
3	196	54	3.6	putative secondary miRNA
4	1	unknown	-----	-----
miR-1	10588	586	18.1	putative secondary miRNA
6	253	124	2.0	putative secondary miRNA
13	1	unknown	-----	-----
34	434	223	1.9	putative secondary miRNA
miR-2	39169	2201	17.8	putative secondary miRNA
36	6200	1825	3.4	putative secondary miRNA
37	6015	394	15.3	putative secondary miRNA
38	322	303	1.1	putative secondary miRNA
39	4717	377	12.5	putative secondary miRNA
40	1014	424	2.4	putative secondary miRNA
41	21686	881	24.6	putative secondary miRNA
42	740	408	1.8	putative secondary miRNA
43	31227	1720	18.2	putative secondary miRNA
miR-3	14694	420	35.0	putative secondary miRNA
45	6487	1459	4.4	putative secondary miRNA
46	9219	4065	2.3	putative secondary miRNA
miR-4	17508	6102	2.9	putative secondary miRNA
48	8095	152	53.3	putative secondary miRNA
49	2967	unknown	-----	-----
50	3794	273	13.9	putative secondary miRNA
51	24497	274	89.4	putative secondary miRNA
53	14966	146	102.5	miRNA*
54	1357	660	2.1	putative secondary miRNA
miR-5	11187	2241	5.0	putative secondary miRNA
57	5457	446	12.2	putative secondary miRNA
58	942	463	2.0	putative secondary miRNA
60	351	4	87.8	putative secondary miRNA
miR-6	10378	89	116.6	miRNA*
62	1535	18	85.3	putative secondary miRNA
63	517	33	15.7	putative secondary miRNA
miR-7	16574	2598	6.4	putative secondary miRNA
67	7834	2015	3.9	putative secondary miRNA
miR-8	46048	3732	12.3	putative secondary miRNA
83	1	unknown	-----	-----
95	1	unknown	-----	-----
128	1	unknown	-----	-----
163	1	unknown	-----	-----
181	1	unknown	-----	-----
182	1	unknown	-----	-----
217	6064	16	379	miRNA*

3.4.6 Ovhv2-miR Predicted Targets

OvHV-2 Gene Targets

It is beyond the remit of this thesis to explore the possible roles of these ovhv2-miRs in OvHV-2 gene regulation as there is very little, if any, means to tell a true target from a false positive when using bioinformatics to predict targets (Dr Finn Grey, communication) (2.8). Identification of true targets requires supporting evidence from microarray analysis or knockdown, -up, pull-down, or luciferase assays. However, there were a number of interesting targets predicted that warrant conjecture. OvHV-2 encodes a number of transcription factors such as Ov2, Ov6, ORF50, and ORF57. My analysis predicted that Ov2 is targeted by ovhv2-miR-2, -miR-4, and -miR-5, Ov6 is targeted by ovhv2-miR-3 and -miR-8, ORF50 is targeted by ovhv2-miR-3, -miR-5, -miR-6, and -miR-8, and ORF57 is targeted by ovhv2-miR-7 and -miR-8. The last three are immediate-early ORFs that may affect OvHV-2 gene expression and initiate OvHV-2 replication (1.1.6-7) (Boyne *et al*., 2006, Frame *et al*., 2008). Ov2 encodes a DNA binding protein homologous to cellular BATF, CREB, and Jun (Hart *et al*., 2007). CREB and Jun are both transcription factors associated with various cancers and BATF is a negative regulator of Jun (GeneCards®, KEGG PATHWAY Database; 2.6.3). OvHV-2 ORF20 (targeted by ovhv2-miR-2, -miR-5, -miR-6, -miR-7, and -miR-8) is homologous to ORFs of the same name in the gammaherpesviruses MHV-68 and KSHV, and BXRF1 in EBV, U_L76 in the betaherpesvirus HCMV, and U_L24 in the alphaherpesvirus HSV-1 (Nascimento *et al*., 2009). U_L24 is important for viral reactivation and replication; it mediates the distribution of cellular nucleolin (involved in ribosome production, and decondensing chromatin) and causes cell cycle arrest by indirectly inhibiting cyclin B signalling (4.1) (Nascimento *et al*., 2009). ORF73 (targeted by ovhv2-miR-6 and -miR-8) is conserved in all gammaherpesviruses and is required for the maintenance and segregation of latent viral genomes in dividing cells (1.1.6-7). OvHV-2 miRNAs could be used to down-regulate these ORFs to balance latency with reactivation and/or fine-tune their expression to control downstream protein expression. OvHV-2 encodes a number of viral homologues to cellular genes such as Ov2.5, Ov3, Ov4.5, and Ov9. My analysis predicted that Ov2.5 is targeted by ovhv2-

miR-4, Ov3 is targeted by ovhv2-miR-3, -miR-6, and -miR-8, Ov4.5 is targeted by ovhv2-miR-4 and -miR-8, and Ov9 is targeted by ovhv2-miR-5 and -miR-6. Ov2.5 encodes an IL-10 homologue which can also initiate transcription by activating the JAK-STAT pathway (GeneCards®). In addition, IL-10 can inhibit NF-κB which can lead to the development of abnormal immune cells, and suppress cytokine expression by T helper cells, antigen presentation by MHC class II, and macrophage activation. Ov3 encodes a homologue of SEMA7A which is a membrane-bound signalling protein found on activated lymphocytes (Hart *et al*., 2007). Ov4.5 and Ov9 both encode Bcl-2 homologues; Ov4.5 encodes a viral Bcl-2 similar to that found in EBV (BALF1) and Ov9 encodes a viral Bcl-2 protein that most closely resembles cellular BAX. BAX is anti-apoptotic and BALF1 acts indirectly to regulate BAX (Hardwick *et al*., 2003). Interestingly, over-expression of cellular anti-apoptotic Bcl-2 can lead to lymphoproliferation. OvHV-2 miRNA regulation of these ORFs could support immune evasion by balancing restriction of the infected cell's ability to respond to stress-stimuli with necessary transcription as well as balancing apoptotic factors so that an increased number of newly synthesized virions can accumulate before the host cell lyses.

Ov5 (predicted to be targeted by ovhv2-miR-1 and -miR-8) encodes a homologue of the transmembrane EBV G protein-coupled receptor BILF1 (Hart *et al*., 2007). BILF1 suppresses expression of MHC class I on the cell surface (by marking cell surface MHC class I and newly translated MHC class I for degradation) suppresses CXCL12 signalling (promotes T cell migration) by binding to its receptor CXCR4, and is involved in cell transformation (Lyngaa *et al*., 2010, Nijmeijer *et al*., 2010, Zuo *et al*., 2011). ORF58 (targeted by ovhv2-miR-3, -miR-5, -miR-7, and -miR-8) is a member of the BMRF2 gene family that is conserved in all gammaherpesviruses and is involved with viral spread to neighbouring cells (Gill *et al*., 2008). ORF58 is necessary for transport of ORF27 to the plasma membrane; this then initiates actin polymerization to form frond-like protrusions that carry newly exocytosed virions to adjacent uninfected cells. These ORFs could be targeted by miRNAs to influence virion production and spread or to maintain latency.

Five miRNAs$_{C\ Levy}$ are encoded directly opposite six OvHV-2 ORFs which suggests that these ORFs may be regulated by viral miRNAs (Table 3.13). They include ORFs that express three tegument proteins (ORF3, ORF33, ORF64) an immediate-early transcription factor (Ov6) a putative glycoprotein (ORF31) and a nuclear capsid localization factor (ORF32). However, none of these miRNAs$_{C\ Levy}$ were predicted by LC Sciences or Walz *et al*. (stem-loop secondary structure is not predicted to be conserved in other herpesviruses) and taken alongside their low read count (reads = 1) their genomic locations (far from the three miRNA clusters) and that some of the validated miRNAs in this study have been predicted to target some of these same ORFs without having to be directly opposite them, these tags may not represent expressed OvHV-2 miRNAs; validation by knock-down assays would be necessary.

Table 3.13: Predicted OvHV-2 miRNAs encoded opposite OvHV-2 Orfs; all from the minus strand.

Group	Reads	Target
13	1	Orf3
95	1	Orf31
		Orf32
		Orf33
128	1	Ov6
181	1	Orf64
182	1	

Bovine Gene Targets

Aside from the interesting predicted viral targets of the ovhv2-miRs, there were also a number of interesting predicted bovine targets.

ALDH3A2 and NDUFB5 (targeted by ovhv2-miR-1) are involved in cellular metabolism; ALDH3A2 catalyzes the oxidation of long-chain aliphatic aldehydes to fatty acids which are used for energy and NDUFB5 is involved in mitochondrial respiration as a subunit of NADH:ubiquinone oxidoreductase - a resultant depletion of ATP in the cytosol due to downregulation of these two proteins could trigger apoptosis

(Hardwick *et al*., 2003). PERP (also targeted by ovhv2-miR-1) activates the p53-dependent apoptotic pathway; transformed cell lines contain more p53 than normal cells, therefore it is conceivable that more available p53 would increase the incidence of PERP-activated apoptosis. Ovhv-2 miRNA targeting of these proteins could balance pro- and anti-apoptotic pathways.

A2M (targeted by ovhv2-miR-1) inhibits proteases and Splicing Factor 3B and SF3B14 (both targeted by ovhv2-miR-5) are associated with spliceosomes. ANK1 (also targeted by ovhv2-miR-1) links the lymphocyte membrane glycoprotein CD44 to the cytoskeleton. CD44 is a hyaluronic acid receptor, which when bound to its ligand leads to lymphocyte activation (proliferation). OvHV-2 miRNA targeting of these proteins could influence protein expression, and signal transduction to support viral persistence.

REPS2 (targeted by ovhv2-miR-1) inhibits growth factor signalling by causing the internalization of growth factor receptors. CEP350 (targeted by ovhv2-miR-3) anchors microtubules at the centrosome in preparation for cell division and CDC25C (targeted by ovhv2-miR-5) activates the Cdk1:cyclin B complex which initiates entry into mitosis. OvHV-2 miRNA targeting of these proteins would support cell growth and viral replication by delaying cytokinesis until the viral genome was duplicated and tethered to the cellular chromatin (1.1.6).

There were also a number of predicted cellular targets that could influence control of cellular processes. Exportin 4 (targeted by ovhv2-miR-1) shuttles proteins from the nucleus to the cytosol with the same cofactor associated with Exportin 5 in miRNA biogenesis (1.3.1) (GeneCards®); OvHV-2 miRNA targeting of Exportin 4 could increase the availability of its cofactor to associate with Exportin 5, thus supporting miRNA biogenesis. UBE2G1 (targeted by ovhv2-miR-5) is an E2 ubiquitin-conjugating enzyme and NDFIP2 (targeted by ovhv2-miR-3) activates a number of E3 ubiquitin-ligases which have a vast number of regulatory roles in cell biology; of interest, implication in the regulation and differentiation of lymphoid cells, involvement in the

budding of many viruses, inhibition of TGF-β signalling by targeting Smad2 and TGFR1 for degradation (anti-apoptotic; Table 1.4) and inhibits activation-induced cell death in T cells. MYO19 (targeted by ovhv2-miR-4) is an actin filament transport molecule and KLHL31 and CREM (both targeted by ovhv2-miR-5) repress or initiate transcription. OvHV-2 miRNA targeting of these proteins could fine tune any number of biological processes.

CREB and CREM are both involved in human T cell lymphotropic virus type 1 (HTLV-1) infection (KEGG PATHWAY Database). HTLV-1 is a human retrovirus that causes adult T cell leukaemia (ATL) from infected $CD4^+$ T cells and uses CREB and CREM to initiate viral transcription (Lemasson *et al*., 2007). The evidence that another mammalian virus uses these cellular proteins for transcription supports the finding that OvHV-2 might encode a CREB-like protein (Ov2) and target it and CREM in order to control its transcription. Lastly, TLR7 (targeted by ovhv2-miR-1) is a single-stranded RNA receptor that is associated with the production of autoantibodies (Green *et al*., 2011). Activation by nucleic acids leads to activation of NF-κB, cytokine secretion, and inflammation (GeneCards®). Targeting of this protein by viral miRNAs could support immune evasion.

The pathology of MCF is thought to be due to the deregulation of cellular processes in the presence of OvHV-2. This deregulation leads to lymphoproliferation and cytotoxicity. OvHV-2 is now known to express miRNAs which could have an affect on many biological pathways. The small selection of predicted viral and cellular targets looked at above for just 8 of the 46 predicted miRNAs highlight a number of biological pathways that could be involved in various pathogenic effects, such as transcription factors and inhibitors of pathways that control the cell's ability to respond to stress and abnormalities. miRNAs are used as a means to fine tune biological processes and too much or too little of an effect could have significant consequences for the cell and the animal as a whole.

Chapter Four: Analysis of OvHV-2 ORF20 as an Ovhv2-miR Target

4.1 AIMS

The aim of this project was to determine if the predicted ovhv2-miR-5, -miR-6, and -miR7 target sites in the 3' UTR of OvHV-2 ORF20 were functional by dual luciferase assay.

4.2 INTRODUCTION

The breadth of potential ORF targeting by the ovhv2-miRs suggests that the virus may use self-encoded miRNAs to regulate gene expression (3.7). OvHV-2 ORF20 was selected for initial target validation because in related viruses, it is involved in controlling the cell cycle (a major feature in the pathogenesis of MCF; 3.8.5) and was predicted to be targeted by ovhv2-miR-5, -miR-6, and -miR-7 in the 3' UTR (Figure 4.1). Nascimento *et al*., 2009, 2007 characterized orf20 in MHV68 and three of its homologues across the herpesvirus subfamilies (HSV-1, HCMV, and KSHV) and found that it localized in the nucleus and caused G_2/M cell cycle arrest and eventually apoptosis. Through an as yet unknown mechanism, presence of orf20 was found to keep the Cdk1:cyclin B complex in its inactive state by maintaining phosphorylation of Cdk1. As discussed previously in section 3.4.6, activation of the Cdk1:cyclin B complex by CDC25C is necessary for the initiation of mitosis. Their evidence suggested that apoptosis was not directed by orf20. Cell cycle arrest has been suggested to benefit herpesvirus replication and immune evasion (Davy et al., 2007) (Figure 4.2).

Before a functional analysis of ovhv2-miRs on OvHV-2 ORF20, the cellular localization of orf20 was characterized to assess its similarity to the characterized homologues in other herpesviruses. Immunocytochemical staining of cells transfected with a tagged orf20 expressing-plasmid was used to determine the occupied cellular compartment. A dual luciferase assay was used for the functional analysis because knockdown of luciferase expression that contains a miRNA target site upon treatment with the corresponding miRNA is easily measurable and has the additional benefit of co-

expressing firefly luciferase unaffected by miRNA treatment to control for discrepancies in expression readings.

4.3 RESULTS

4.3.1 Cellular Localization of Orf20

BHK cells were transfected with tagged ORF20-expressing plasmids to determine the protein's cellular localization. AlHV-1 ORF20 was used due to the conservation of this ORF in all herpesviruses (1.2, 3.8.5) AlHV-1 ORF20 and OvHV-2 ORF20 have 60% sequence identity at the amino acid level (Figure 4.3) and the availability of the cloned FLAG-tagged gene (Aschman, 2008). To insert ORF20-FLAG into the pLZ3-CIng-ps-linker plasmid, a 5' *Xho*I and 3' *Nhe*I restriction site was added to the insert by PCR, using *Pfu* DNA polymerase (2.1.2, Appendix 2-3). PLZ3-CIng-ps-linker was used for co-localization purposes as it contains nEGFP (nuclear enhanced green fluorescent protein) and an internal ribosome entry site (IRES) to allow co-expression. The transfection of BHK cells was optimized using the EGFP expressing plasmid pEGFP-N1 by varying the ratio of plasmid DNA to the lipid transfection reagent, Lipofectamine 2000 (2.4.4, Appendix 3). The transfected cells were viewed, and the optimal conditions were determined by florescence microscopy. Florescence was observed in every well but the optimal ratio was determined to be 1:8. Successful transfection of BHKs with pLZ3-CIng-ps-linker[ORF20-FLAG] was observed by expression of nEGFP (Figure 4.4) and orf20 was observed to localize in both the nucleus and cytoplasm based on staining for FLAG (2.4.6) (Figure 4.5). This suggests that OvHV-2 orf20 could act similarly to MHV-68 orf20 as it also localizes in the nucleus.

4.3.2 OvHV-2 miRNA Regulation of ORF20

To determine if the predicted target sites for ovhv2-miR-5, -miR-6, and -miR-7 in the 3' UTR of OvHV-2 ORF20 were functional, a dual luciferase assay was designed so that a measure of miRNA silencing could be made (2.5.1). pEGFP-N1 was used as a transfection control, and a psiCHECK™ vector with the complementary sequence to

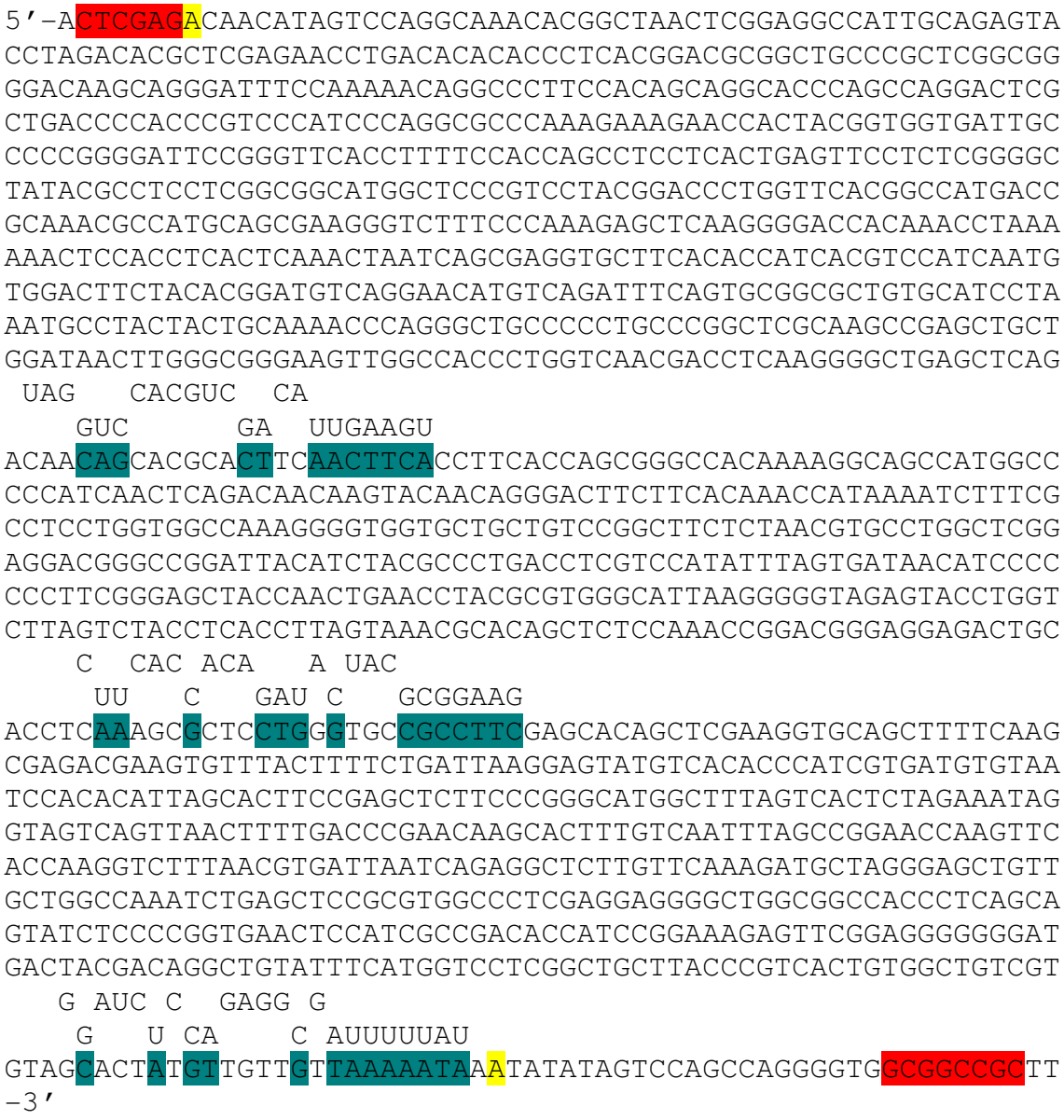

Figure 4.1: OvHV-2 ORF20 3' UTR (boundaries are in yellow) isolated by PCR; 5' *Xho*I and 3' *Not*I restriction sites are in red and putative ovhv2-miR target sites (from 5' → 3', miR-5, miR-7, and miR-6) are in green.

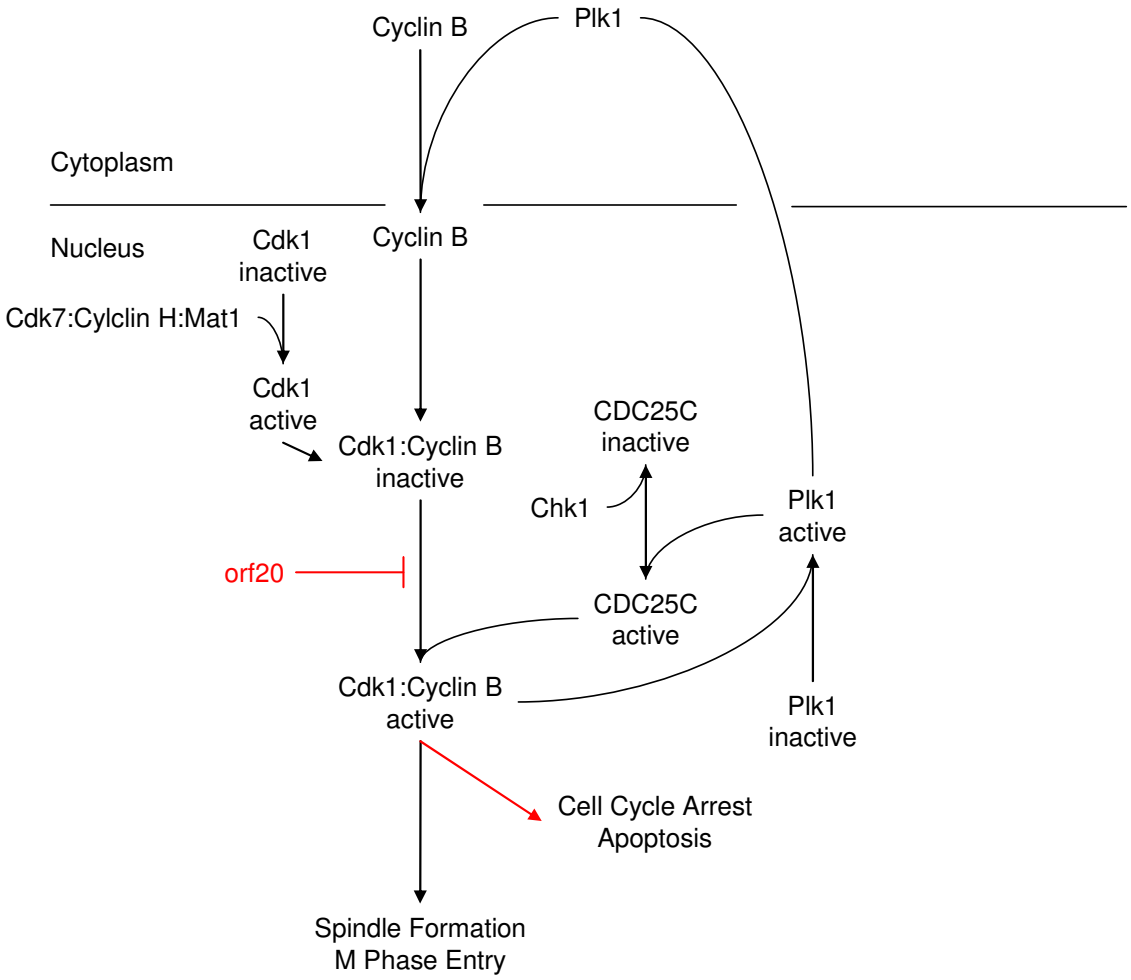

(Adapted from Prof. L. N. Johnson; http://biop.ox.ac.uk/www/lj2001/).

Figure 4.2: Simplified schematic of M phase initiation by Cdk1:cyclin B and the observed affect in the presence of herpesvirus orf20.

```
CLUSTAL 2.1 multiple sequence alignment


AlHV-1 MFP-LLGQSACAALNSLPAKRKKAGLQAHRKVYKQLLQYHSFTKINKFLELKHPDPKKVK 59
OvHV-2 MFQSILSQRPICALSSLPAKRKVAGLNAHRKVYKQLMLYTSFGKVNKFLGLQHICPKKVK 60
       **  :*.* . .**.******* ***:*********: * ** *:**** *:*  *****

AlHV-1 YRLFFEVSLGPRIVDVIVLTSYETERVCYVVELKTCLGSEFNFTSVRAAQRTQGLCQLYD 119
OvHV-2 YKLFFEVSLGPRIADIIVLASQGEQRMCYIIELKTCLGAHFVPNPIKLAQRSQGLCQLHD 120
       *:***********.*:***:*   :*:**::*******:.*  ..:: ***:******:*

AlHV-1 STKYLSNNAPLGGERWEVRAHLLFKSQSAMKTLYVEHPGFQFNQLQCTTGALSVFLKSRE 179
OvHV-2 STKYLCNNAPRGEERWVVQAHLLFKSQVSLKTLHSEHPTFPFALIQSKEEALSAFLRLRE 180
       *****.**** * *** *:******** ::***: *** * *  :*..  ***.**: **

AlHV-1 DVACRQLLYQGLQCAALAKKMRVLGTKSTKRARDKPTQVSRVPAQRSPVQKARGRKQAES 239
OvHV-2 DAEFKQVLRQGCPPAEVAKGMRLLGPKPQERARYKPPKVPRAQAQRLALPKARGRKQNAS 240
       *.  :*:* **   * :** **:**.*. :*** **.:*.*. *** .: *******  *

AlHV-1 HKKGASKGRAG 250
OvHV-2 HKKGAVKNGA- 250
       ***** *. *
```

Figure 4.3: Amino acid conservation between AlHV-1 ORF20 and OvHV-2 ORF20 using ClustalW2 (2.6.3).

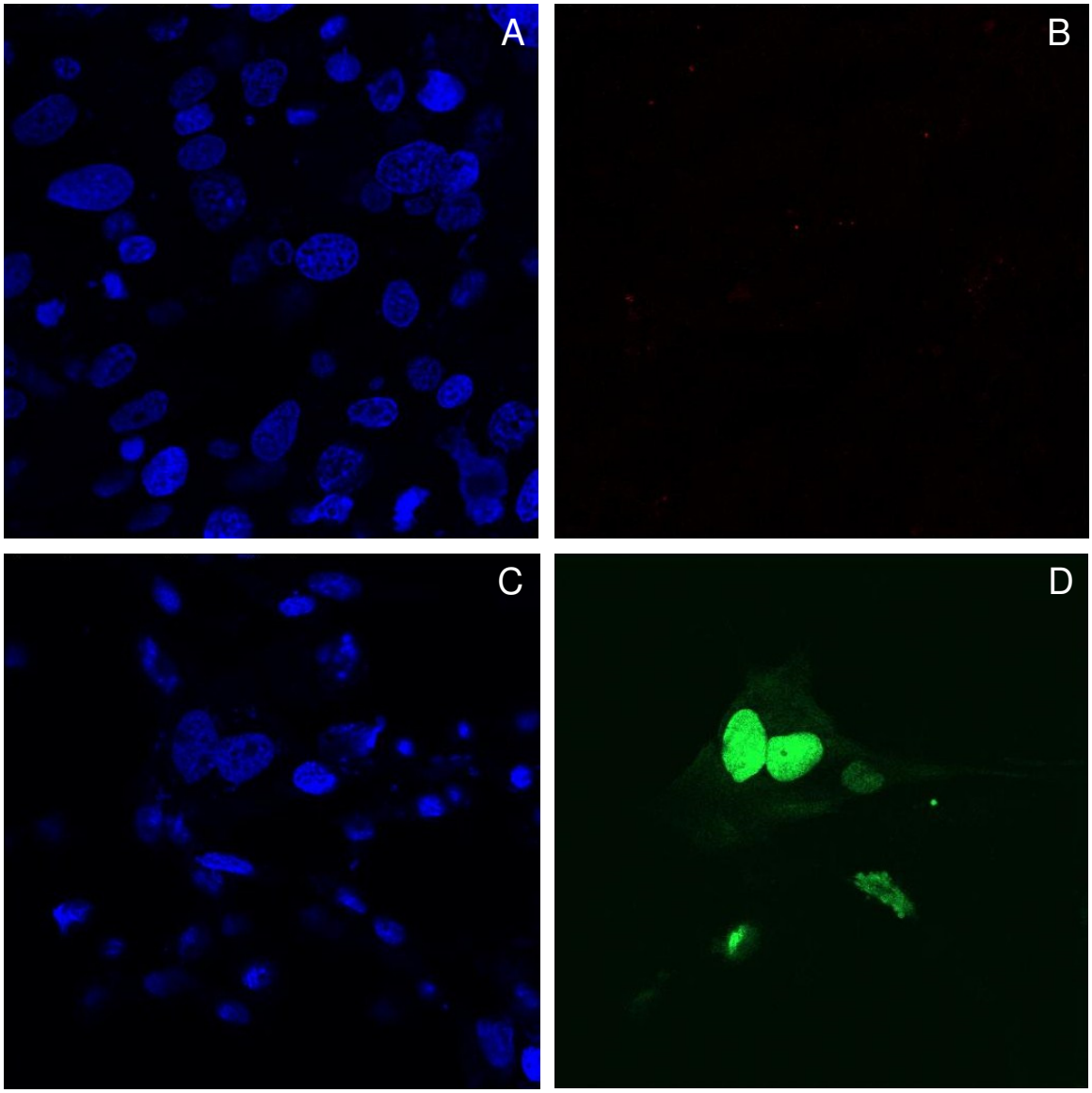

Figure 4.4: Confocal images of BHK transfection controls after 48 hrs; (A-B) non-transfected cells - (A) shows Topro-3 nuclear staining and (B) shows the same cells for FLAG staining; (C-D) pLZ3-CIng-ps-linker transfected cells - (C) shows Topro-3 nuclear staining and (D) shows nuclear-localized GFP.

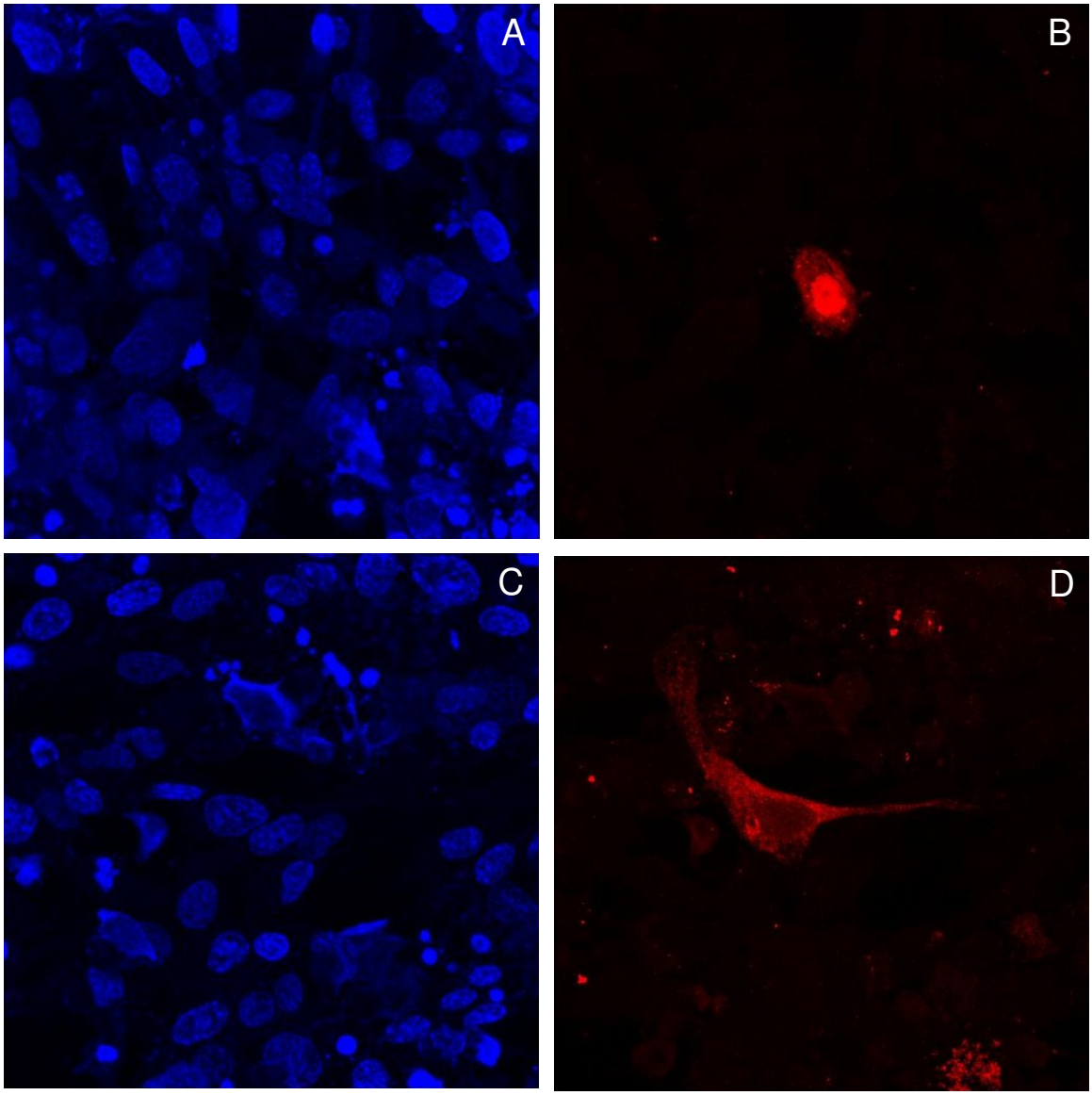

Figure 4.5: Confocal images of BHK transfection with pLZ3-CIng-ps-linker[ORF20-FLAG] after 48 hrs; (A-B) nuclear localized orf20 - (A) shows Topro-3 nuclear staining and (B) shows the same cells for FLAG staining; (C-D) cytoplasm localized orf20 - (C) shows Topro-3 nuclear staining and (D) shows staining of FLAG.

mcmv-miR-M23-2 (kindly donated by Dr Amy Buck, University of Edinburgh) co-transfected with a mimic of mcmv-miR-M23-2 was used as a positive control. Mimics of OvHV-2 miRNAs that were not predicted to target ORF20 (ovhv2-miR-1, -miR-2, and -miR-3) were used as additional negative controls (Table 4.1).

The non-transfected and mock transfected samples were used to correct for background luciferase readings; the average of the six firefly readings was subtracted from all the other firefly readings (the same was done with the *Renilla* readings). The reading ratio of *Renilla* to firefly (*R*/F) was used to normalize the *Renilla* readings. The negative control psiCHECK™ co-transfected with ovhv2-miR-5, -miR-6, and -miR7 mimics showed significant up-regulation with a miRNA mimic concentration of 50 nM ($p = 0.008$), but there was no significant difference when treated with 5 nM or 25 nM miRNA mimics ($p_{5nM} = 0.037$ and $p_{25nM} = 0.072$) (Figure 4.6, Table 4.2). The positive control psiCHECK™[comp. miR-M23-2] co-transfected with mcmv-miR-M23-2 mimic showed significant down-regulation for all three mimic concentrations ($p_{5nM} = 0.00004$, $p_{25nM} = 0.00009$, and $p_{50nM} = 0.000001$). Dual luciferase assay readings can be found in the Supplemental DVD; Luciferase Assay - 3 replicates.

The negative control psiCHECK™[ORF20 3' UTR] co-transfected with ovhv2-miR-1, -miR-2, and -miR3 mimics showed no significant difference for all three mimic concentrations ($p_{5nM} = 0.558$, $p_{25nM} = 0.122$, and $p_{50nM} = 0.280$) (Figure 4.7, Table 4.3). psiCHECK™[ORF20 3' UTR] co-transfected with ovhv2-miR-5, -miR-6, and -miR-7 mimics also showed no significant difference for all three mimic concentrations ($p_{5nM} = 0.490$, $p_{25nM} = 0.435$, and $p_{50nM} = 0.337$).

The dual luciferase assay was repeated with higher concentrations of miRNA mimic and using a GloMax® luminometer that could read 96-well plates allowed for six replicates in the hopes of decreasing the variability observed between three replicates (Table 4.4).

Table 4.1: miRNA silencing dual luciferase triplicate assay co-transfection conditions.

Well	Vector	miR mimic	[miR Mimic]
Controls			
1-3	untransfected		
4-6	mock transfected		
7-9	pEGFP-N1		
10-12	psiCHECK™		
22-24	psiCHECK™	miR-5, -6, -7	5 nM
25-27	psiCHECK™	miR-5, -6, -7	25 nM
28-30	psiCHECK™	miR-5, -6, -7	50 nM
31-33	psiCHECK™[comp. miR-m23-2]		
34-36	psiCHECK™[comp. miR-m23-2]	miR-m23-2	5 nM
37-39	psiCHECK™[comp. miR-m23-2]	miR-m23-2	25 nM
40-42	psiCHECK™[comp. miR-m23-2]	miR-m23-2	50 nM
43-45	psiCHECK™[ORF20 3' UTR]		
46-48	psiCHECK™[ORF20 3' UTR]	miR-1, -2, -3	5 nM
49-51	psiCHECK™[ORF20 3' UTR]	miR-1, -2, -3	25 nM
52-54	psiCHECK™[ORF20 3' UTR]	miR-1, -2, -3	50 nM
Test			
55-57	psiCHECK™[ORF20 3' UTR]	miR-5, -6, -7	5 nM
58-60	psiCHECK™[ORF20 3' UTR]	miR-5, -6, -7	25 nM
61-63	psiCHECK™[ORF20 3' UTR]	miR-5, -6, -7	50 nM

Table 4.2: miRNA silencing dual luciferase sextuplicate assay co-transfection conditions.

Well	Vector	miR Mimic	[Mimic]
Controls			
1-6	Untransfected		
7-12	mock transfected		
13-18	psiCHECK™[comp. miR-m23-2]		
19-24	psiCHECK™[comp. miR-m23-2]	miR-m23-2	100 nM
25-30	psiCHECK™[ORF20 3' UTR]		
31-36	psiCHECK™[ORF20 3' UTR]	scrambled	50 nM
37-42	psiCHECK™[ORF20 3' UTR]	scrambled	100 nM
Test			
43-48	psiCHECK™[ORF20 3' UTR]	miR-5, -6, -7	50 nM
49-54	psiCHECK™[ORF20 3' UTR]	miR-5, -6, -7	100 nM
55-60	psiCHECK™[ORF20 3' UTR]	miR-5	100 nM
61-66	psiCHECK™[ORF20 3' UTR]	miR-6	100 nM
67-72	psiCHECK™[ORF20 3' UTR]	miR-7	100 nM

The luminometer readings were corrected and normalized in the same way described previously (Supplemental DVD; Luciferase Assay - 6 replicates). The positive control psiCHECK™[comp. miR-m23-2] treated with 100 nM mcmv-miR-M23-2 mimic showed significant down-regulation (Figure 4.8, Table 4.5).

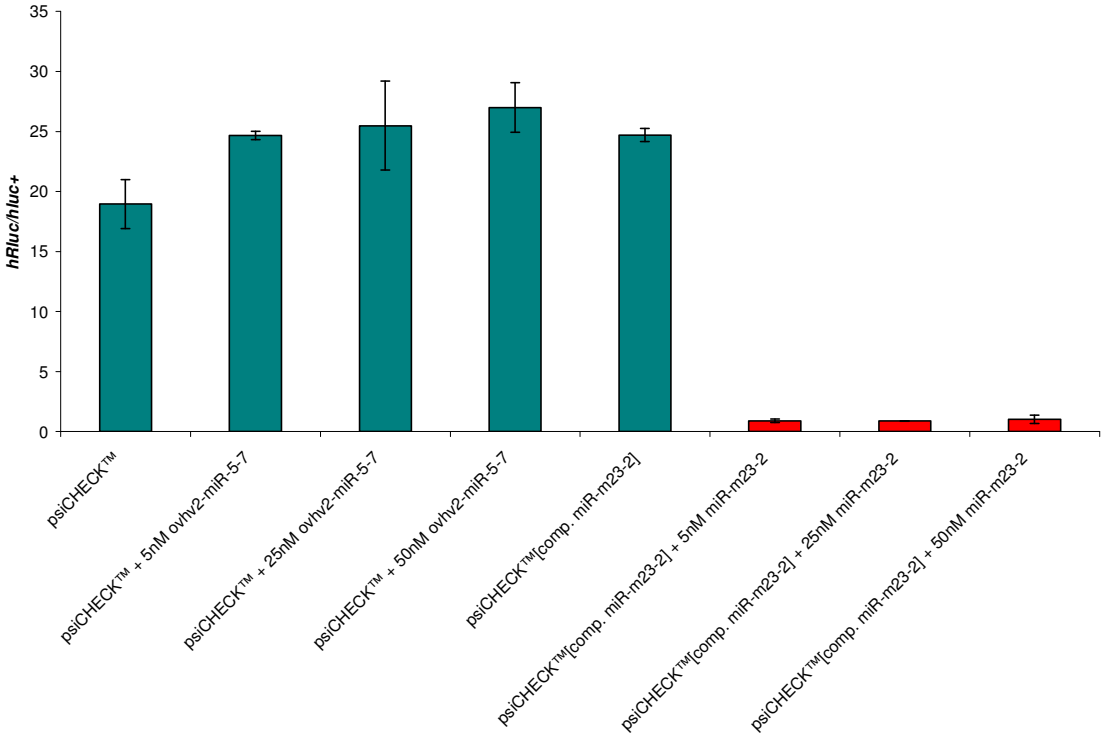

Figure 4.6: Controls for OvVH-2 ORF20 3' UTR miRNA silencing triplicate dual luciferase assay; untreated or control-treated samples are shown in green while the experimentally-treated are shown in red.

Table 4.3: P-values for triplicate dual luciferase controls.

Control Vector	Treatment	P-value	Result
psiCHECK™	5 nM ovhv2-miR-5-7	0.037	Not Significant
	25 nM ovhv2-miR-5-7	0.072	Not Significant
	50 nM ovhv2-miR-5-7	0.008	Significant
psiCHECK™[comp. miR-m23-2]	5 nM mcmv-miR-m23-2	0.00004	Significant
	25 nM mcmv-miR-m23-2	0.00009	Significant
	50 nM mcmv-miR-m23-2	0.000001	Significant

Legend: A two-tailed, independent t-test, $\alpha = 0.025$ was used against the psiCHECK™ vector and a one-tailed, independent t-test $\alpha = 0.050$ was used against the psiCHECK™[comp. miR-m23-2] vector.

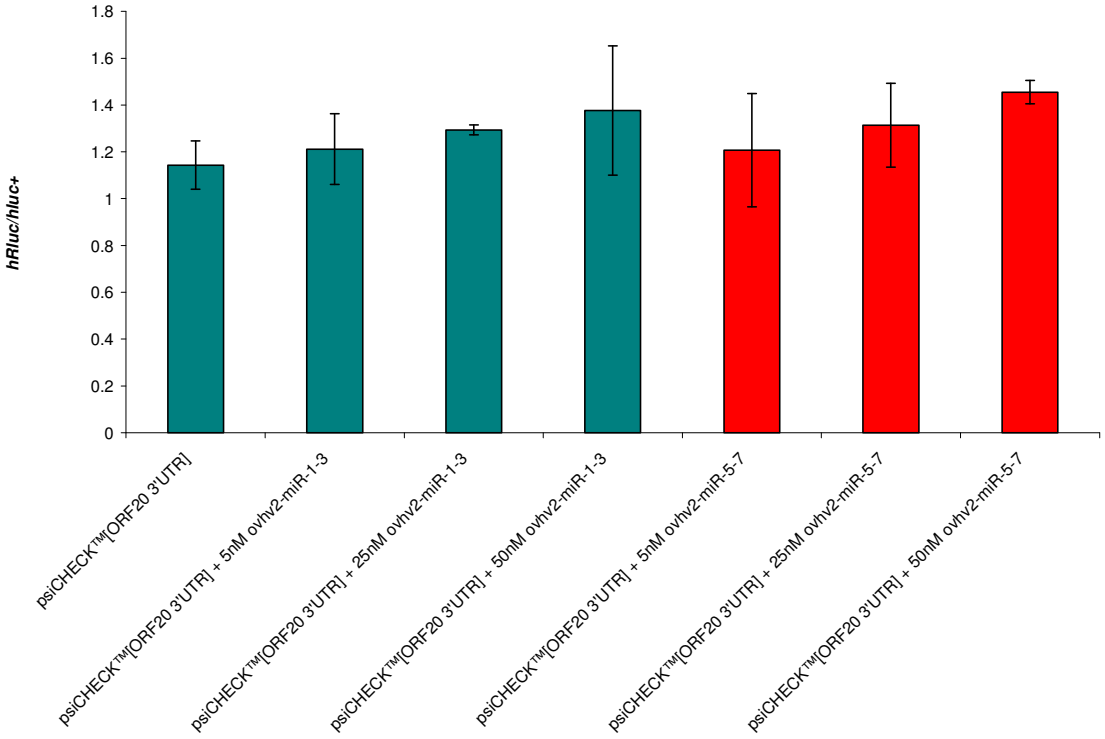

Figure 4.7: Negative control and sample for miRNA silencing triplicate dual luciferase assay; untreated or control-treated samples are shown in green while the experimentally-treated are shown in red.

Table 4.4: P-values for triplicate dual luciferase assay.

Control Vector	Treatment	P-value	Result
psiCHECK™[ORF20 3' UTR]	5 nM ovhv2-miR-1-3	0.558	Not Significant
	25 nM ovhv2-miR-1-3	0.122	Not Significant
	50 nM ovhv2-miR-1-3	0.280	Not Significant
5 nM ovhv2-miR-1-3	5 nM ovhv2-miR-5-7	0.490	Not Significant
25 nM ovhv2-miR-1-3	25 nM ovhv2-miR-5-7	0.435	Not Significant
50 nM ovhv2-miR-1-3	50 nM ovhv2-miR-5-7	0.337	Not Significant

Legend: A two-tailed, independent t-test, $\alpha = 0.025$ was used against the psiCHECK™[ORF20 3' UTR] vector and a one-tailed, independent t-test $\alpha = 0.050$ was used against the control mimics ovhv2-miR-1, -miR-2, and -miR-3.

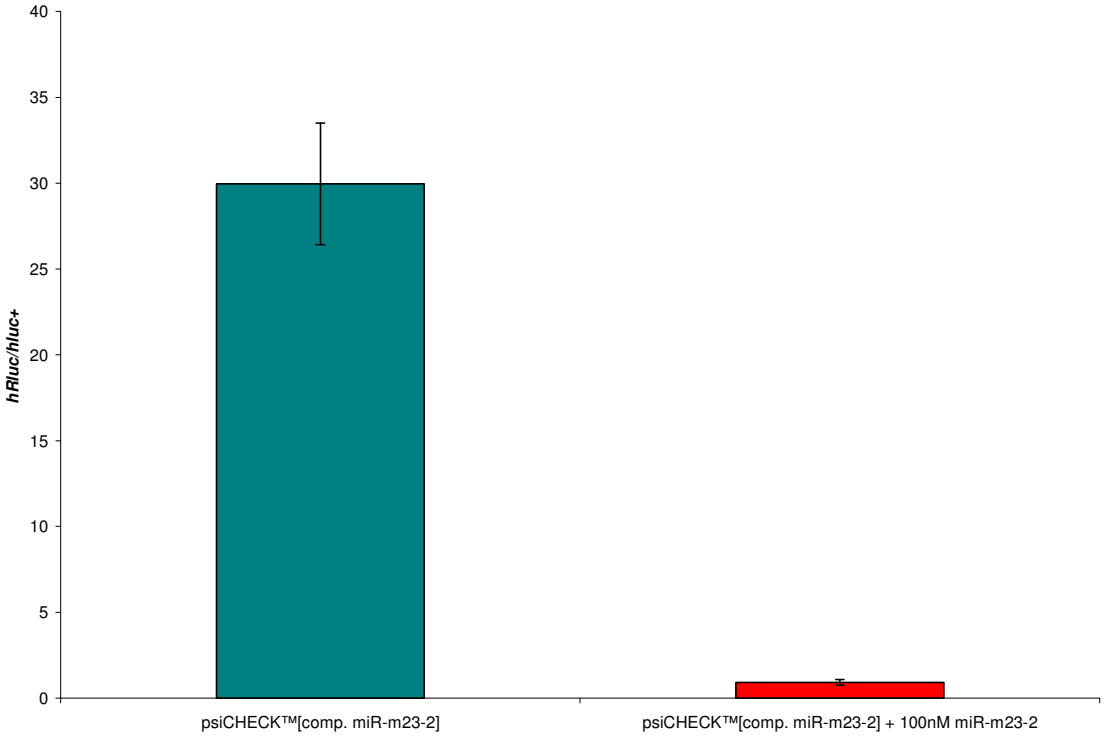

Figure 4.8: Positive control for miRNA silencing sextuplicate dual luciferase assay; untreated or control-treated samples are shown in green while the experimentally-treated are shown in red.

Table 4.5: P-values for sextuplicate dual luciferase control.

Control Vector	Treatment	P-value	Result
psiCHECK™[comp. miR-m23-2]	100 nM mcmv-miR-m23-2	0.000003	Significant

Legend: A one-tailed, independent t-test $\alpha = 0.050$ was used against the psiCHECK™[comp. miR-m23-2] vector.

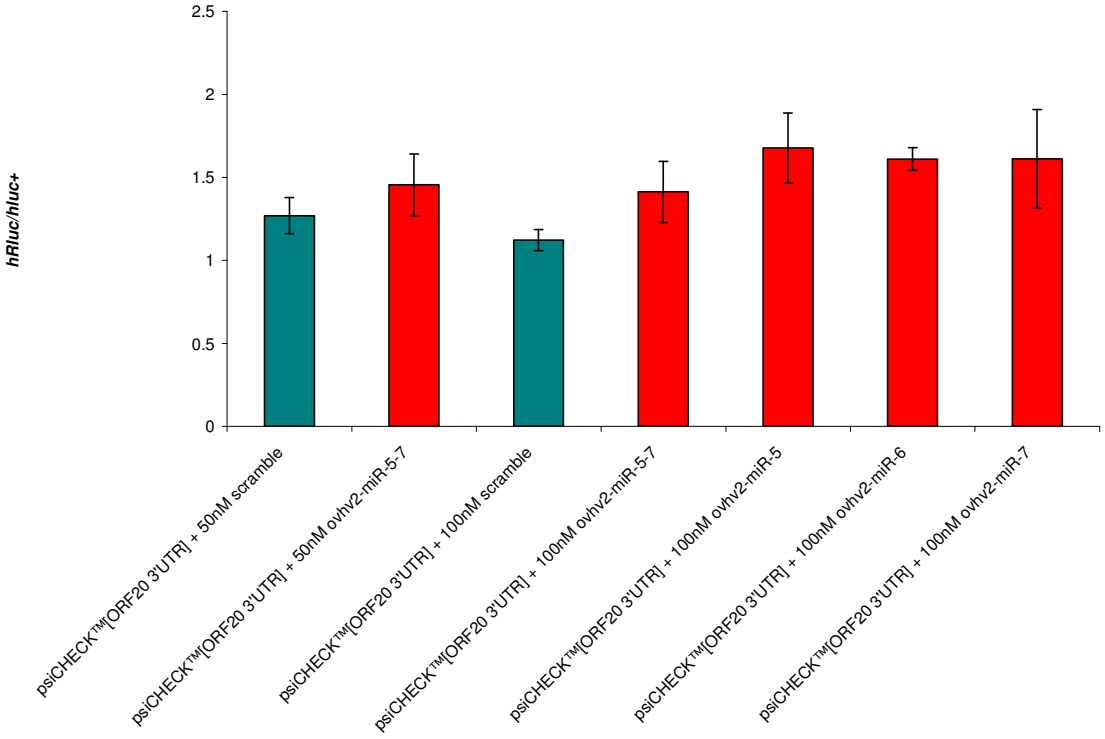

Figure 4.9: miRNA silencing sextuplicate dual luciferase assay, untreated or control-treated samples are shown in teal while the experimentally-treated are shown in red.

Table 4.6: P-values for sextuplicate dual luciferase assay.

Control Vector	Treatment	P-value	Result
psiCHECK™[ORF20 3' UTR] + 50 nM scramble	50 nM ovhv2-miR-5-7	0.034	Signigicant
psiCHECK™[ORF20 3' UTR] + 100 nM scramble	100 nM ovhv2-miR-5-7	0.005	Significant
	100 nM ovhv2-miR-5	0.0004	Significant
	100 nM ovhv2-miR-6	0.00000009	Significant
	100 nM ovhv2-miR-7	0.004	Significant

Legend: A one-tailed, independent t-test $\alpha = 0.050$ was used.

The negative control psiCHECK™[ORF20 3' UTR] was co-transfected with a scrambled miRNA mimic which was used to compare luciferase levels with the same plasmid that had been co-transfected with targeting mimics. Regardless of concentration, all luciferase levels read from samples treated with targeting mimics were significantly higher than the controls ($p_{50nM\ ovhv2\text{-}miR\text{-}5\text{-}7} = 0.034$, $p_{100nM\ ovhv2\text{-}miR\text{-}5\text{-}7} = 0.005$, $p_{100nM\ ovhv2\text{-}miR\text{-}5} = 0.0004$, $p_{100nM\ ovhv2\text{-}miR\text{-}6} = 0.00000009$, and $p_{100nM\ ovhv2\text{-}miR\text{-}7} = 0.004$) (Figure 4.9, Table 4.6).

4.4 DISCUSSION

Two dual-luciferase assays (one in triplicate with manual mixing of the assay reagents and one with six replicates with automatic mixing of the assay reagents) were performed to elucidate the ability of ovhv2-miR-5, -miR-6, and -miR-7 to knock down OvHV-2 ORF20. The negative and positive controls used in the assays showed that the assays worked. Addition of non-specific mimics (those not predicted to target transcripts expressed from the vector) resulted in a noticeable increase (significant in one case of six) in luciferase expression. 5 nM and 25 nM mimic treatment increased luciferase expression by ~32% (not significant; $p_{5nM} = 0.037$ and $p_{25nM} = 0.072$) while 50nM mimic treatment gave rise to a 43% increase (significant; $p = 0.008$). There was a ~ 97% knockdown observed for psiCHECK™[comp. miR-m23-2] treated with mcmv-miR-m23-2 mimic in both assays, however knock-down of ORF20 was not observed. The luciferase expression of psiCHECK™ and psiCHECK™[comp. miR-m23-2] were not significantly different ($p = 0.032$) however psiCHECK™[ORF20 3' UTR] luciferase expression was significantly lower ($p_{psiCHECK™} = 0.004$ and $p_{psiCHECK™[comp.\ miR\text{-}m23\text{-}2]} = 0.0001$) (Table 4.7). This may be due to the size of the target region inserted into the vector; psiCHECK™[comp. miR-m23-2] had the addition of ~21 bp downstream of the *Renilla* luciferase whereas psiCHECK™[ORF20 3' UTR] had ~1530 bp.

Table 4.7: P-values of the three test vectors.

	Triplicate Study			Sextuplicate Study		
Vector	psiCHECK™	M23-2	ORF20	M23-2	$ORF20_{50nM\ scramble}$	$ORF20_{100nM\ scramble}$
psiCHECK™	-------	-------	-------	-------	-------	-------
psiCHECK™[comp. miR-m23-2]	0.032	-------	-------	-------	0.000006	0.000006
psiCHECK™[ORF20 3' UTR]	0.004	0.0001	-------	------	-------	-------

Legend: Two-tailed, independent t-test p-values comparing luciferase expression levels of the three test plasmids ($\alpha = 0.025$); psiCHECK™, psiCHECK™[comp. M23-2] (M23-2) and psiCHECK™[ORF20 3' UTR] (ORF20).

In the triplicate assay, there was no significant difference (Table 4.3) in luciferase expression of psiCHECK™[ORF20 3' UTR] when treated with control miRNA mimics or targeting miRNA mimics. The sextuplicate assay resulted in a significant increase (Table 4.6) of luciferase expression when treated with targeting mimics; all three together or individually. 50 nM ovhv2-miR mimics caused a luciferase expression increase of 15% and 100 nM ovhv2-miR mimics caused an increase of 26%. Transfection with individual ovhv2-miRs resulted in a 49% increase with ovhv2-miR-5, a 43% increase with ovhv2-mir-6, and a 44% increase with ovhv2-miR-7. Based on these results, it does not appear that ovhv2-miR-5, -miR-6, or -miR-7 downregulate OvHV2 ORF20 by binding to the 3' UTR. It is feasible however that they may still target ORF20 and affect its rate of translation. It does not appear that the three ovhv2-miRs synergize as the greater effect was observed when they were expressed individually. Further repeats of these assays are currently being conducted in the lab.

It is interesting that two factors that interact with the Cdk1:cyclin B mechanism of the cell cycle have been predicted as OvHV-2 miRNA targets; OvHV2 ORF20 and cellular CDC25C (both are predicted to be targets of ovhv2-miR-5). As stated previously, the mechanism of regulation of the cell cycle by orf20 is unknown, but the presence of orf20 inhibits the activation of the Cdk1:cyclin B complex by maintaining Cdk1 in its phosphorylated form. CDC25C is the protein that activates the complex by

dephosphorylating Cdk1. It is possible that orf20 interacts with CDC25C to cause cell cycle arrest while OvHV-2 expressed miRNAs fine tune this interaction for the benefit of the virus's survival.

If ovhv2-miR-5, -miR-6, and -miR-7 do target the 3' UTR of ORF20, it does not appear that they downregulate it. If they do, it may be that their binding to the transcript impedes other suppressing factors allowing more efficient translation (as seen in the sextuplicate assay). Again, OvHV-2 miRNA targeting of ORF20 is still being looked at in the lab, but this also shows the inherent difficulty in the study of miRNAs. Although bioinformatic analysis predicted three miRNA target sites in the 3' UTR of ORF20, there is the very real possibility that ORF20 is a false target. Before hypotheses about OvHV-2 miRNA regulation can be made, true targets need to be identified, and that work is continuing.

Chapter Five: Analysis of OvHV-2 Transcriptome

5.1 AIMS

To characterize OvHV-2 gene expression by using high throughput sequencing to identify the mRNA transcripts expressed in the bovine LGL cell line BJ1035, and bioinformatics to determine the genes transcribed.

5.2 INTRODUCTION

At present, high throughput sequencing transcriptomic investigations involving herpesviruses has only covered the changes in the cellular transcriptome in response to a gammaherpesvirus protein expressed during the lytic cycle (orf37 in KSHV and MHV-68) (Clyde *et al*., 2011). Previous studies on OvHV-2 gene expression have so far focused on a handful of genes and have determined that their expression differs depending on if the virus is undergoing lytic or latent replication or has infected a reservoir or susceptible host. In the reservoir host, OvHV-2 maintains a low-level of ORF expression and can clearly be defined as latent; in susceptible species, ORF expression is increased - BJ1035s contain a mixed population of OvHV-2 activity, with a low level of reactivity occurring (5.4, Thonur *et al*., 2006). The Illumina Solexa GAII used in the identification of the OvHV-2 miRNAs (Chapter Three) provided the opportunity to take the first look at the OvHV-2 transcriptome in a susceptible host. This method was used as it is reported to be more sensitive than microarray. Analysis of the specific activation of certain ORFs could lead to insight on the mechanism of MCF.

5.3 RESULTS

5.3.1 RNA Extraction

Three RNA samples were extracted from BJ1035 cells (2.1.11) and sent to The Genepool to isolate the mRNA, construct and sequence cDNA libraries made up of 21 nt tags, and map to the OvHV2 genome (2.1.13).

5.3.2 Sequencing Analysis

For the three RNA samples, the sequenced reads were mapped to the OvHV-2 genome using the default settings of MAQ with a mapping quality of 30 (2.1.13; Table 5.1).

Table 5.1: Summary of Solexa high throughput sequencing results.

		Mapped to OvHV-2		
Sample	Total Reads	Reads	Plus Strand	Minus Strand
1	7,230,508	31,512 (0.44%)	12,077	19,435
2	16,450,709	30,229 (0.18%)	6,536	23,693
3	16,335,916	47,108 (0.29%)	19,667	27,441

There were 2,046 unique tags mapped to the OvHV-2 genome; 1,507 tags were found in at least two samples and 697 tags contained point mutations between samples at the same genome location (Supplemental DVD; Tables 5.1 and 5.2).

5.3.3 Determining OvHV-2 Open Reading Frame Parameters

The coordinates for the 73 predicted OvHV-2 genes were compiled using the OvHV-2 genome published in GenBank (AY839756; 2.9; Hart et al., 2007) (Supplemental DVD; Table 5.3). This genome was isolated from BJ1035 cells, the same cell line used in this study.

5.3.4 OvHV-2 Expression Profile in BJ1035 Cells

Using the compiled gene locations (5.3.3) sequenced tags for the three RNA samples could be assigned to OvHV-2 ORFs (Figure 5.1). Attention was given to genes that were expressed more (i.e. had a higher read count) than genes in the rest of each sample. Initially, highly expressed genes were attempted to be isolated by determining the mean read count and taking those genes that were expressed a given standard deviation above the mean. This however resulted in too few highlighted genes in some samples and too many in others (Table 5.3). Using the TATA and polyA signal coordinates (5.3.1) the sum of the reads for each viral ORF was determined and the mean for the three samples was taken to analyze the relative ORF expression levels throughout the genome (Figure 5.2, Table 5.2).

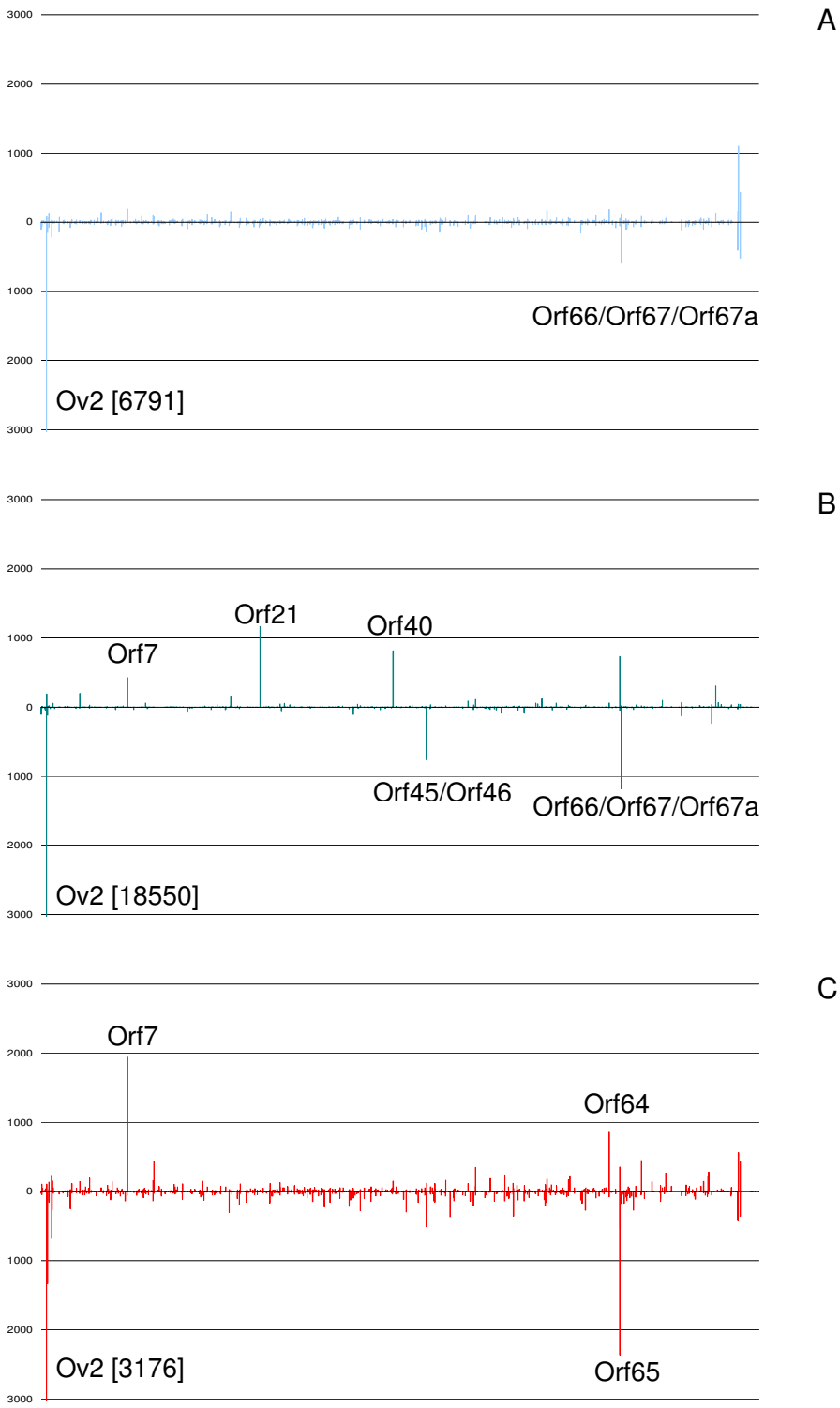

Figure 5.1: Frequency of Solexa sequenced tags mapped along the OvHV-2 genome for samples 1-3 (A-C) with highly expressed tags labelled with the ORFs predicted in that location.

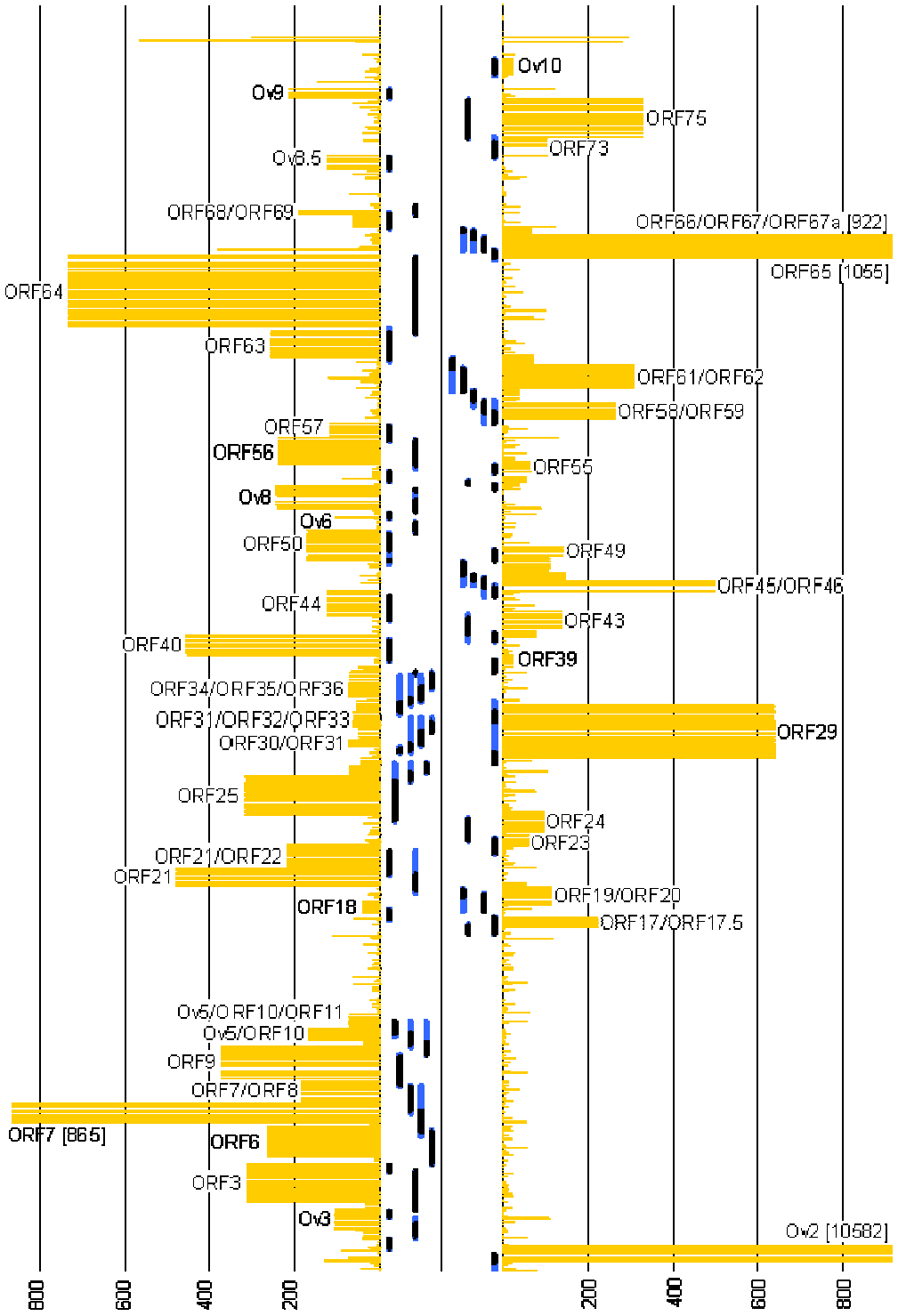

Figure 5.2: Mean read frequency of the three samples in Figure 5.1 with the mean sum of the reads contained within ORFs, along the OvHV-2 genome with labelled peaks of interest; predicted ORFs are shown between the plus and minus tag frequencies - ORF in blue and the coding region in black.

Table 5.2: OvHV-2 ORF transcription levels in BJ1035 cells.

ORF	Reads				
	Sample 1	Sample 2	Sample 3	Mean	Standard Deviation
Ov2	7263	18700	5784	10582.3	7068.9
Ov2.5	103	2	0	35.0	58.9
Ov3	90	26	192	102.7	83.7
Ov3.5	35	2	53	30.0	25.9
ORF3	392	53	487	310.7	228.1
ORF3/Ov4.5	0	0	0	0.0	0.0
Ov4.5	14	1	17	10.7	8.5
ORF6	255	25	511	263.7	243.1
ORF6/ ORF7	46	17	2	21.7	22.4
ORF7	213	433	1949	865.0	945.2
ORF7/ORF8	267	64	214	181.7	105.3
ORF7/ORF8/ORF9	0	2	0	0.7	1.2
ORF9	318	8	780	368.7	388.5
Ov5	63	6	27	32.0	28.8
Ov5/ORF10	165	11	325	167.0	157.0
Ov5/ORF10/ORF11	81	4	122	69.0	59.9
ORF17/ORF17.5	153	38	478	223.0	228.2
ORF17	0	0	6	2.0	3.5
ORF18	74	5	34	37.7	34.6
ORF19/ORF20	165	4	174	114.3	95.7
ORF20	147	1	5	51.0	83.2
ORF21	158	1181	91	476.7	610.9
ORF21/ORF22	129	64	456	216.3	210.1
ORF23	64	73	39	58.7	17.6
ORF23/ORF24	16	0	12	9.3	8.3
ORF24	107	6	175	96.0	85.0
ORF25	338	15	597	316.7	291.6
ORF25/ORF26	117	1	81	66.3	59.4
ORF25/ORF26/ORF27	36	4	80	40.0	38.2
ORF29	254	31	473	252.7	221.0
ORF30	0	1	1	0.7	0.6
ORF30/ORF31	114	29	84	75.7	43.1
ORF31	0	0	0	0.0	0.0
ORF31/ORF32	17	15	106	46.0	52.0
ORF31/ORF32/ORF33	86	4	87	59.0	47.6
ORF34	76	22	53	50.3	27.1
ORF34/ORF35	28	2	50	26.7	24.0
ORF34/ORF35/ORF36	76	8	127	70.3	59.7
ORF34/ORF35/ORF36/ORF37	78	4	114	65.3	56.1
ORF37	0	0	0	0.0	0.0
ORF37/ORF38	40	0	58	32.7	29.7
ORF39	54	22	11	29.0	22.3

ORF40	163	834	361	452.7	344.8
ORF42/ORF43	77	7	141	75.0	67.0
ORF43	70	19	322	137.0	162.2
ORF44	166	16	186	122.7	92.9
ORF45/ORF46	208	852	603	554.3	324.7
ORF46	21	0	1	7.3	11.8
ORF46/ORF47/ORF48	84	4	356	148.0	184.5
ORF47/ORF48	1	0	0	0.3	0.6
ORF48	213	16	94	107.7	99.2
ORF49	56	3	367	142.0	196.6
ORF50	126	25	318	156.3	148.8
Ov6	3	1	0	1.3	1.5
Ov7	22	0	3	8.3	11.9
Ov8	166	164	427	252.3	151.3
ORF52	22	28	59	36.3	19.9
ORF53	75	61	22	52.7	27.5
ORF54	30	6	4	13.3	14.5
ORF55	70	45	71	62.0	14.7
ORF56	218	37	457	237.3	210.7
ORF56/ORF57	58	1	46	35.0	30.0
ORF57	144	42	161	115.7	64.4
ORF58/ORF59	239	190	367	265.3	91.4
ORF58/ORF59/ORF60	48	0	47	31.7	27.4
ORF60	47	1	60	36.0	31.0
ORF60/ORF61/ORF62	0	0	0	0.0	0.0
ORF61/ORF62	244	71	612	309.0	276.3
ORF62	78	6	121	68.3	58.1
ORF63	197	42	530	256.3	249.4
ORF63/orf64	20	4	53	25.7	25.0
ORF64	688	109	1398	731.7	645.6
ORF65	170	69	2926	1055.0	1621.1
ORF65/ORF66/ORF67/ORF67a	0	0	0	0.0	0.0
ORF66/ORF67/ORF67a	871	1201	695	922.3	256.9
ORF67/ORF67a	9	19	170	66.0	90.2
ORF67a	0	0	0	0.0	0.0
ORF68	56	37	89	60.7	26.3
ORF68/ORF69	100	19	447	188.7	227.4
ORF69	24	11	0	11.7	12.0
Ov8.5	95	9	262	122.0	128.6
ORF73	115	129	65	103.0	33.6
ORF73/ORF75	0	0	0	0.0	0.0
ORF75	519	22	446	329.0	268.4
Ov9	108	6	524	212.7	274.4
Ov10	62	8	7	25.7	31.5

Among the 52 annotated OvHV-2 polyA signals from the NCBI Database (AY839756) two signals were used; AATAAA (77%) and ATTAAA (23%). A search through the genome for these two sequences resulted in an additional 138 polyA signals; AATAAA (59%) and ATTAAA (41%) (Supplemental DVD; Table 5.4). 29 of the additional polyA signals were found within predicted ORFs (Table 5.4).

5.4 DISCUSSION

The transcriptome of OvHV-2 in BJ1035 cells was sequenced to examine viral gene expression in the susceptible host. In the process of determining the relative levels of OvHV-2 gene expression, additional polyA signals were found throughout the entire length of the genome (Figure 5.3). Many were found to cluster close together, some with a published polyA signal; these may reinforce the "stopping" signal to RNA polymerase. Others were found within ORFs so may denote shorter or longer transcripts stemming from a single promoter. Interestingly, though there was observed transcript expression for ORF18, there was no published polyA site, and even with the newly discovered sites, the closest polyA site was within ORF21/ORF22 (3622 bp away). There were also a number found in regions without predicted ORFs; it may be that they belong to unidentified ORFs. Although the current number of predicted OvHV-2 ORFs is well within the normal range for gammaherpesviruses (73 protein coding ORFs compared to an average of 78±6, n=12 gammaherpesviruses with full sequenced genomes) it is possible that it could encode more.
(GenBank; http://www.ncbi.nlm.nih.gov/Taxonomy/Browser/wwwtax.cgi?id=10374)

To support this hypothesis, sequenced mRNA tags were found to map to these undesignated regions (Figure 5.4). Some of these undefined transcripts could also represent pri-miRNAs, although interestingly, there were no transcripts detected corresponding to the location of ovhv2-miR-1, -miR-3, or -miR-4. This could be due to the location of *Nla*III restriction sites in the genome, which were used to produce the transcript tags that make up the transcriptome. This could also explain why there were no transcripts found for one or more exons for Ov2, Ov2.5, and Ov6.

Table 5.3: Number of peaks to be labelled if based on mean read count and standard deviation.

	Standard Deviations on Either Side of Mean							
Sample	**0.25**	**0.5**	**0.75**	**1**	**1.25**	**1.5**	**1.75**	**2**
1	44	19	9	6	6	6	6	4
2	9	7	6	4	3	3	1	1
3	121	82	51	35	29	23	18	17

Table 5.4: Unpublished polyA signals found within predicted ORFs.

Gene Name	Strand	PolyA Signal (5' Start)	Tag Frequency 5' of PolyA Signal				
			Sample 1	Sample 2	Sample 3	Mean	Variance
Ov2	-	2804	162	27	41	77	74
Ov2.5	+	4393	84	2	0	29	48
ORF3	+	9990	191	245	570	335	205
ORF7/ORF8	+	18007	213	433	1949	865	945
		20279	426	63	175	221	186
ORF9	+	23194	310	4	773	362	387
Ov5	+	24266	0	0	1	0	1
ORF21	+	43166	403	1214	467	695	451
ORF24	-	47856	207	13	294	171	144
ORF25/ORF26/ORF27	+	54411	467	18	705	397	349
ORF29	-	56059	49	1	103	51	51
		56655	248	159	689	365	284
		59731	103	24	319	149	153
ORF31/ORF32	+	58289	17	15	106	46	52
ORF43	-	69140	0	0	0	0	0
		69370	466	96	391	318	196
ORF45/ORF46	-	72698	182	801	572	518	313
		73565	23	0	1	8	13
ORF48	-	75990	16	0	97	38	52
ORF50	+	76171	1	0	1	1	1
Ov6	+	79556	3	1	0	1	2
		80192	18	0	0	6	10
ORF53	-	84655	63	67	154	95	51
ORF54	+	85614	112	9	212	111	102
ORF60	-	93779	14	0	0	5	8
ORF63	+	100305	827	366	1603	932	625
ORF65	-	108282	91	61	2896	1016	1628
ORF68	+	112942	435	814	646	632	190
ORF73	-	119325	115	129	65	103	34

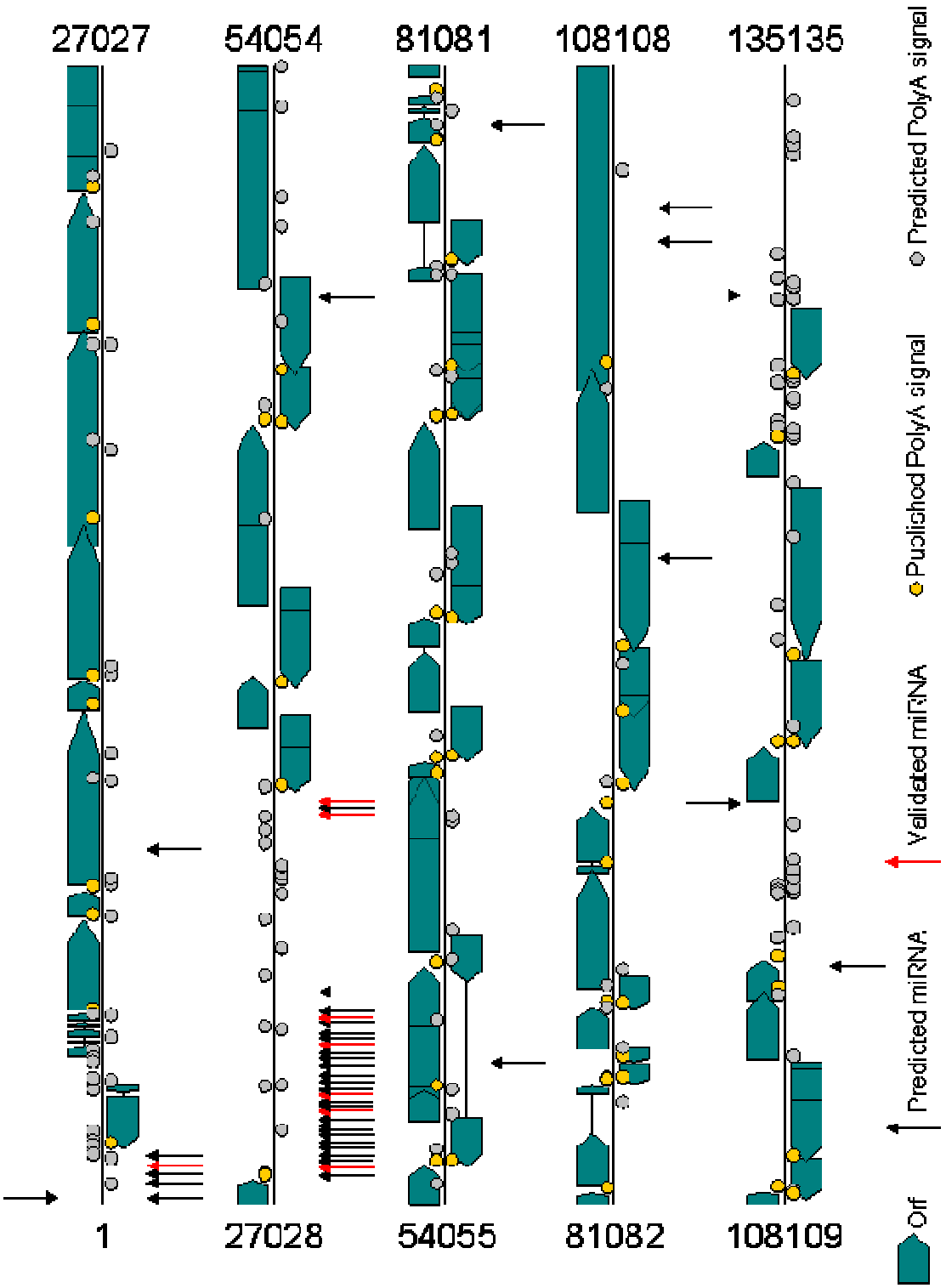

Figure 5.3: OvHV-2 genome schematic detailing the location of polyA signals in relation to predicted ORFs and miRNAs; circles representing polyA signals to the left of the genome line are on the positive strand, those to the right are on the minus strand.

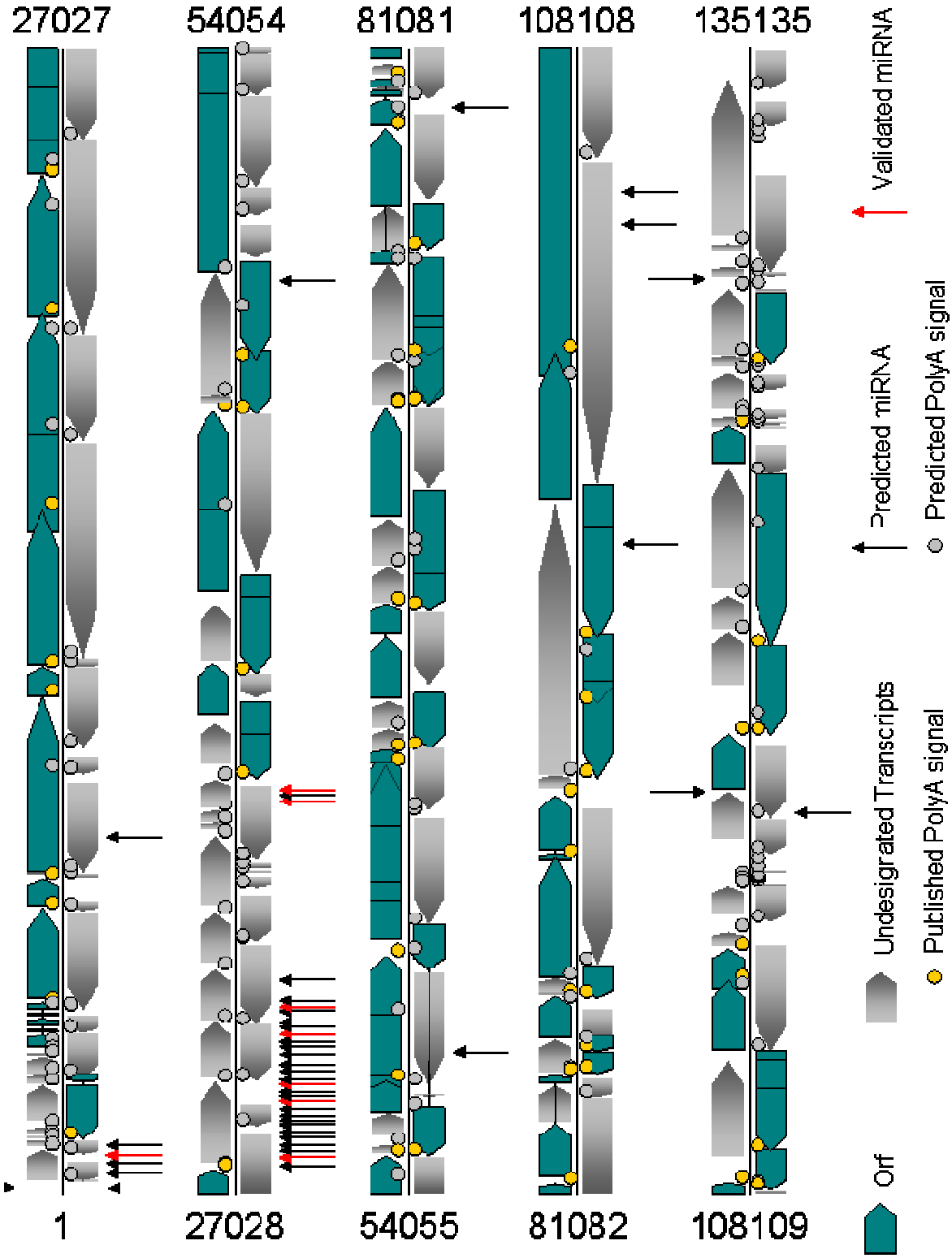

Figure 5.4: OvHV-2 genome schematic detailing the location of undesignated transcripts in relation to predicted ORFs, miRNAs and polyA signals.

Within the three samples sequenced, the most highly expressed OvHV-2 genes were Ov2, ORF7, ORF21, ORF40, ORF45/ORF46, ORF64, ORF65, and ORF66/ORF67/ORF67a (Table 5.5).

Table 5.5: Highly expressed OvHV-2 genes in BJ1035 cell line.

Name	Strand	Description
Ov2	-	basic leucine zipper; putative transcription factor
ORF7	+	terminase subunit; interacts with ORF29 and ORF67a
ORF21	+	thymidine kinase; tegument protein associated with capsid
ORF40	+	helicase-primase
ORF45	-	Unknown
ORF46	-	uracil-DNA glycosylase
ORF64	+	tegument protein
ORF65	-	capsid protein
ORF66	-	Unknown
ORF67	-	U_L34, nuclear egress tegument protein
ORF67a	-	packaging protein; interacts with terminase

It has been observed that the first ORF encoded in gammaherpesvirus genomes is often involved in cell transformation (Coulter *et al*., 2001, Damania *et al*., 2000). Although no sequence homology has been observed between genera and very little between species, these ORFs encode membrane-bound proteins that oligomerize and stimulate lymphocyte activation pathways. The genome location of Ov2, its homology to cellular transcription factors (3.8.5) and its observed high transcript expression in immortalized T cells supports the role of Ov2 in the pathogenesis of MCF; the alphaherpesvirus MDV-1 also expresses a Jun-like protein called Meq which is expressed in transformed cells and lymphomas (Burnside *et al*., 2006). Currently, Aayesha Riaz is undertaking *in situ* hybridizations to determine whether Ov2 is expressed primarily in latent or reactivated cells as well as conducting dual luciferase assays to see if the predicted target site by ovhv2-miR-4 in the 3' UTR of Ov2 is functional. Initially, the assays reported that there was no regulation by ovhv2-miR-4, but further analysis identified a T → C point mutation in the region complementary to the seed sequence (Riaz, A., unpublished

results). This could be due to RNA editing and explain the high expression of Ov2 observed in the transcriptome.

This transcript profile appears to differ from that described by Thonur *et al*, 2006 who focused on the "unique" genes (Ov2-Ov10) and genes used as markers for latency (ORF73) and reactivation (ORF9 and ORF50) using Gardella gels and Southern blots. They found that the OvHV-2 genome was predominately circular and in a latent state in ovine T cells (reservoir species) with restricted gene expression; most notably Ov3.5 and ORF73. Treatment with doxorubicin caused a shift towards linear genomes and reactivation with expression of all "unique" genes and ORF9 and ORF50 along with ORF73. The BJ1035 cell line contained both circular and linear viral genomes, with an unusual transcript profile from that observed in latent or productive virus in sheep; all the "unique" genes were expressed (Ov8 and Ov8.5 being the most highly expressed and Ov2 the least) as in the reactivated ovine cells, but ORF50 was undetectable as in the latent ovine cells. Treatment with doxorubicin did not have as strong of an effect on the bovine cells, though expression of Ov3 increased and ORF50 was detected. In this study, all the genes focussed on by Thonur *et al*. were expressed in the BJ1035 cells, but to differing degrees; Ov2 was expressed over 40 times more than Ov8, and ORF50 was detectable without treatment with doxorubicin. Although the cells were grown in the same conditions in both studies, there are a number of explanations for why different levels of gene expression were observed. First, the experimental methodology differed; Thonur *et al*. used Southern blots whereas I used high throughput sequencing. Secondly, OvHV-2 may not exert the same control over gene expression in bovine cells as it does in sheep cells. Alternatively, given what seems to be a mix of latent and productive virus in bovine cells, it may be that over the four years between the studies, the cell line holds a different ratio of latent:reactivated virus. Based on the selection of genes with high expression in this study (those involved in viral DNA replication and packaging) and a comparably low expression of ORF73, an increase in reactivated virus is surmised. It would be beneficial to determine the ratio of latent:reactivated virus-

infected cells and determine which cell-state is expressing each of the highly abundant transcripts detected.

This preliminary study of the OvHV-2 transcriptome suggests that the deregulation of host cells that contribute to the development of MCF may be due to a deregulation of the virus itself. Although sheep and cattle are related and therefore both can carry OvHV-2, there may be enough of a difference in their molecular biology which enables the virus to maintain a symbiotic relationship with one and a harmful relationship with the other.

Chapter Six: Conclusion

Malignant catarrhal fever and its etiological agent OvHV-2 present an interesting scientific conundrum and challenge. Infection with OvHV-2 in sheep shows no overt clinical symptoms, but can cause a fatal disease in cattle brought upon by the activation of an immune response that involves lymphoproliferation and non-classical MHC restricted non-antigen-specific cytotoxicity. The key question in MCF is why infection of two closely related ruminant species results in such differing disease outcomes.

This project was concerned with understanding how OvHV-2 interacts with bovine lymphocytes at the molecular level to affect lymphocyte growth and differentiation, i.e. how OvHV-2 causes disease. Major candidates for virus-control of viral and cellular gene expression are virus-encoded miRNAs, which can, and have been found to, target transcription factors (1.5.2-3). miRNAs are involved in numerous biological pathways and the study of them and their function brings to light subtle interactions that can have far reaching effects. The previous discoveries of miRNAs in herpesviruses and their involvement in regulating viral replication, the cell cycle, and viral pathogenesis, supported the hypothesis that OvHV-2 may also express these regulatory RNAs. Identification and characterization of these may lead to an understanding of why there is a difference in persistence between reservoir and susceptible species and of the mechanisms behind the various clinical symptoms of MCF.

During this study, it was known that the pathogenic effects of OvHV-2 infection were derived from virally-infected, immortalized T cells. Thus, the bovine cell line BJ1035 was used, representing the $CD4^+$ T cell population infected and immortalized by OvHV-2.

Forty six OvHV-2 miRNAs were predicted by high throughput sequencing and bioinformatics; eight of which had additional supporting evidence by northern hybridization and are currently named ovhv2-miR-1 - miR-8. This represents the first report of the expression of virally encoded miRNAs in the *Macavirus* genus of herpesviruses. The success of this study was dependent upon the use of a number of

complementary techniques; next generation high throughput sequencing provided the amplification and identification of real transcripts transcribed by the cell, bioinformatics provided the prediction of miRNA biogenic secondary structure, and northern hybridization provided the verification that the transcripts sequenced were present as ~22-mers. Each technique by itself would not have been enough to prove the presence of miRNAs. An additional marker for miRNA prediction has been found in a sequence motif (CTCCGCCC) ~200 bp upstream of *C. elegans* miRNAs (Ohler *et al*., 2004). This particular sequence is not present upstream of any of the predicted OvHV-2 miRNAs found in this study, but it does suggest that there may be mammalian or viral sequence motifs yet to be discovered with a similar role.

These miRNAs are located throughout the genome (mostly on the minus strand), in regions that do not contain predicted ORFs. The majority of the miRNAs are localized in three clusters; one cluster is located at the left-hand end of the genome, 5' of Ov2, the other two are in the 9.3 kb non-coding region between ORF11 and ORF17/17.5. This clustering of miRNAs has been observed in other herpesviruses however to date no other herpesvirus has been shown to contain as many miRNAs as predicted in this study (3.4).

All but one of the predicted OvHV-2 miRNAs are novel, i.e. shares no seed homology with any other miRNA present in the miRBase database. The exception shares a conserved seed sequence with the well conserved vertebrate miRNA miR-216, and may act as a mimic to increase the regulatory activity of that miRNA in virus-infected host cells (3.8.2).

Using blastn, many viral and cellular targets were predicted for the eight ovhv2-miRs, however thus far no target has been identified experimentally. There is increasing interest in the role of miRNAs in host-virus interactions, cellular biology, and as treatments for disease. However, miRNAs can only be used as a tool once their function is known, which is why the identification of the targets of virus-encoded miRNAs is essential. Several mechanisms have been used to identify miRNA targets (3.3.6) and the

bioinformatics used in this study is a good starting point, but definitive evidence that a predicted target site is functional is necessary to begin to understand the role they play in their environment. There are several possible approaches to functionally identifying mRNAs targeted by individual miRNAs: RISC pull-down assays followed by microarray analysis have already been discussed (3.7) and improvements to this approach are continually being developed. This allows the mRNAs targeted by the miRNA to be directly identified. An alternative approach involves miRNA sponges whereby a transgene expresses a small RNA complementary to a miRNA of interest which then binds to its target, thus decreasing the miRNA's effect on the cell allowing resultant changes in phenotype or transcriptome to be assessed. Functional studies using these methods are currently being adopted in our laboratory. It is my suggestion that the predicted OvHV-2 miRNAs in the first cluster be focussed on initially as it may be involved in the transformation and pathology of the virus; this cluster is in a similar location to the oncogenic-associated miRNA cluster in MDV-1 and may be expressed from the same promoter as the Meq-like Ov2 (Burnside et al., 2006).

In addition to miRNA identification, a first examination of the OvHV-2 transcriptome was undertaken. The results confirm Thonur *et al*.'s observations that in susceptible species there is an increase in ORF expression; however the ORF expression observed in this study differed from that previously reported. It may be that in susceptible hosts, latency is not as tightly controlled leading to varying expression profiles and thus, the different symptoms and severities of MCF observed.

The high levels of OvHV-2 gene expression in T cells of susceptible species may be the trigger that initiates the development of MCF. It may be beneficial to analyze the OvHV-2 transcriptomes from sheep and a susceptible host exhibiting clinical signs of MCF for a direct comparison. In this way, specific viral ORFs associated with pathogenesis may be identified. Until then, the data in this study has highlighted a number of viral ORFs that could be investigated for interactions in the myriad of pathways that could lead to the deregulation of the host's immune system.

Given additional time, a comparison with other gammaherpesviruses could garner additional information; do they have undesignated polyA sites, and/or do they encode ORFs in similar locations to the "empty" regions in the OvHV2 genome? The sequence of these regions could also be used to search for homologues in other viruses or host species.

While the aim of this project was focussed on OvHV-2 miRNA and mRNA, the process of sequencing the RNA samples also provided small RNA and transcriptome data for cattle; http://www.mirz.unibas.ch/cloningprofiles/ provides miRNA profiles for a large number of cell types, including T cells. The small RNA data could be analyzed for the reads of the 662 published bovine miRNAs and this profile could be compared to that of an uninfected T cell. One point of interest for this comparison would be expression of the cellular miR-17/92 cluster which targets PTEN (3.8.2) (Xiao *et al*., 2008). This targeting is associated with lymphoproliferation and autoimmunity so it would be expected for this cluster to be more highly expressed in BJ1035 cells than uninfected T cells. The transcriptome of uninfected cattle could be sequenced as well and any differences between the two could aid in our understanding of the changes made to the cellular environment by OvHV-2.

OvHV-2 and MCF remain difficult to study due to a lack in a cell culture system and the variance of disease developed by susceptible species ranging from those that recover and those that die days after the onset of clinical symptoms. The finding that OvHV-2 encodes and expresses miRNAs in immortalized cells and the predicted viral and cellular targets found with bioinformatics for a small number of them supports the hypothesis that OvHV-2 miRNAs may have a role in viral and cellular gene expression, viral persistence, and MCF pathogenesis. The ovhv2-miRs can be used as a tool to study the biological pathways affected by this virus and should increase our understanding of OvHV-2 biology.

Bibliography

Abend, J. R., T. Uldrick, *et al*. (2010). "Regulation of tumor necrosis factor-like weak inducer of apoptosis receptor protein (TWEAKR) expression by Kaposi's sarcoma-associated herpesvirus microRNA prevents TWEAK-induced apoptosis and inflammatory cytokine expression." Journal of Virology **84**(23): 12139-12151.

Ackermann, M. (2006). "Pathogenesis of gammaherpesvirus infections." Veterinary Microbiology **113**(3-4): 211-222.

Alwine, J. C., W. L. Steinhart, *et al*. (1974). "Transcription of herpes simplex type 1 DNA in nuclei isolated from infected HEp-2 and KB cells." Virology **60**(1): 302-307.

Ambros, V., B. Bartel, *et al.* (2003). "A uniform system for microRNA annotation." Rna-a Publication of the RNA Society **9**(3): 277-279.

Aparicio, O., N. Razquin, *et al*. (2006). "Adenovirus virus-associated RNA is processed to functional interfering RNAs involved in virus production." Journal of Virology **80**(3): 1376-1384.

Arvin, A. M. (1996). "Varicella-zoster virus." Clinical Microbiology Reviews **9**(3): 361-381.

Ascherio, A. and K. L. Munger (2010). "Epstein-Barr virus infection and multiple sclerosis: A review." Journal of Neuroimmune Pharmacology **5**(3): 271-277.

Aschman, N. (2008). Characterisation of the protein encoded by Orf20 of alcelaphine herpesvirus 1. Edinburgh, University of Edinburgh: 1-33.

Babcock, G. J. and D. A. Thorley-Lawson (2000). "Tonsillar memory B cells, latently infected with Epstein-Barr virus, express the restricted pattern of latent genes previously found only in Epstein-Barr virus-associtated tumors." Proceedings of the National Academy of Sciences of the United States of America **97**(22): 12250-12255.

Babcock, G. J., L. L. Decker, *et al*. (1999). "Epstein-Barr virus-infected resting memory B cells, not proliferating lymphoblasts, accumulate in the peripheral blood of immunosuppressed patients." Journal of Experimental Medicine **190**(4): 567-576.

Backovic, M. and T. Jardetzky (2011). Class III Viral Membrane Fusion Proteins. Cell Fusion in Health and Disease Ii: Cell Fusion in Disease. Berlin, Springer-Verlag Berlin. **714**: 91-101.

Bartel, D. P. (2004). "MicroRNAs: Genomics, biogenesis, mechanism, and function." Cell **116**(2): 281-297.

Bartel, D. P. and C. Z. Chen (2004). "Micromanagers of gene expression: the potentially widespread influence of metazoan microRNAs." Nature Reviews Genetics **5**(5): 396-400.

Barth, S., T. Pfuhl, *et al*. (2008). "Epstein-Barr virus-encoded microRNA miR-BART2 down-regulates the viral DNA polymerase BALF5." Nucleic Acids Research **36**(2): 666-675.

Basyuk, E., F. Suavet, *et al*. (2003). "Human let-7 stem-loop precursors harbour features of RNase III cleavage products." Nucleic Acids Research **31**(22): 6593-6597.

Baxter, S. I. F., A. Wiyono, *et al*. (1997). "Identification of ovine herpesvirus 2 infection in sheep." Archives of Virology **142**(4): 823-831.

Baxter, S. I. F., I. Pow, *et al*. (1993). "PCR Detection of the sheep-associated agent of malignant catarrhal fever." Archives of Virology **132**(1-2): 145-159.

Bellare, P. and D. Ganem (2009). "Regulation of KSHV lytic switch protein expression by a virus-encoded microRNA: An evolutionary adaptation that fine-tunes lytic reactivation." Cell Host & Microbe **6**(6): 570-575.

Boehmer, P. E. and I. R. Lehman (1997). "Herpes simplex virus DNA replication." Annual Review of Biochemistry **66**: 347-384.

Borza, C. M. and L. M. Hutt-Fletcher (2002). "Alternate replication in B cells and epithelial cells switches tropism of Epstein-Barr virus." Nature Medicine **8**(6): 594-599.

Boyne, J. R. and A. Whitehouse (2006). "Nucleolar trafficking is essential for nuclear export of intronless herpesvirus mRNA." Proceedings of the National Academy of Sciences of the United States of America **103**(41): 15190-15195.

Brault, S. A., B. H. Bird, *et al*. (2011). "Genetic heterogeneity and variation in viral load during equid herpesvirus 2 infection of fouls." Veterinary Microbiology **147**(3-4): 253-261.

Braun, D. K., G. Dominguez, *et al*. (1997). "Human herpesvirus 6." Clinical Microbiology Reviews **10**(3): 521-567.

Bridgen, A. and H. W. Reid (1991). "Derivation of a DNA clone corresponding to the viral agent of sheep-associated malignant catarrhal fever." Research in Veterinary Science **50**(1): 38-44.

Burnside, J., Bernberg, E., *et al*. (2006). "Marek's disease virus encodes microRNAs that map to *meq* and the latency-associated transcript." Journal of Virology **80**(17): 8778-8786.

Burrells, C. and H. W. Reid. (1991). "Phenotypic analysis of lymphoblastoid cell-lines derived from cattle and deer affected with sheep-associated malignant catarrhal fever." Veterinary Immunology and Immunopathology **29**(1-2): 151-161.

Cai, X. Z., A. Schafer, *et al.* (2006). "Epstein-barr virus microRNAs are evolutionarily conserved and differentially expressed." Plos Pathogens **2**(3): 236-247.

Cai, X. Z. (2004). "Human microRNAs are processed from capped, polyadenylated transcripts that can also function as mRNAs." RNA - A Publication of the RNA Society **10**(12): 1957-1966.

Carel, J. C., B. L. Myones, *et al*. (1990). "Structural requirements for C3d,g/Epstein-Barr virus receptor (CR2/CD21) ligand binding, internaliztion, and viral infection." Journal of Biological Chemistry **265**(21): 12293-12299.

Cerutti, L., N. Mian, *et al*. (2000). "Domains in gene silencing and cell differentiation proteins: the novel PAZ domain and redefinition of the Piwi domain." Trends in Biochemical Sciences **25**(10): 481-482.

Chang, Y., E. Cesarman, *et al*. (1994). "Identification of herpesvirus-like DNA-sequences in AIDS-associated Kaposi's sarcoma." Science **266**(5192): 1865-1869.

Chen, C. Y., R. Gherzi, *et al*. (2000). "Nucleolin and YB-1 are required for JNK-mediated interleukin-2 mRNA stabilization during T-cell activation

Chen, C. Z., L. Li, *et al*. (2004). "MicroRNAs modulate hematopoietic lineage differentiation." Science **303**(5654): 83-86.

Chen, Z. L., X. H. Zhao, *et al*. (2011). "microRNA-92a promotes lymph node metastasis of human esophageal squamous cell carcinoma via E-cadherin." Journal of Cellular Physiology **226**(6): 1479-1488.

Choy, E. Y. W., K. L. Siu, *et al*. (2008). "An Epstein-Barr virus-encoded microRNA targets PUMA to promote host cell survival." Journal of Experimental Medicine **205**(11): 2551-2560.

Clyde, K. and B. A. Glaunsinger (2011). "Deep sequencing reveals direct targets of gammaherpesvirus-induced mRNA decay and suggests that multiple mechanisms govern cellular transcript escape." Plos One **6**(5): e19655.

Collery, P. and A. Foley (1996). "An outbreak of malignant catarrhal fever in cattle in the Republic of Ireland." Veterinary Record **139**(1): 16-17.

Cook, C. G. and G. A. Splitter (1988). "Lytic function of bovine lymphokines-activated killer cells from a normal and a malignant catarrhal fever virus-infected animal." Veterinary Immunology and Immunopathology **19**(2): 105-118.

Costa, E. A., A. D. Viott, *et al*. (2010). "Transmission of ovine herpesvirus 2 from asymptomatic boars to sows." Emerging Infectious Diseases **16**(12): 2011-2012.

Costa, É. A., E. Bastianetto, *et al*. (2009). "An outbreak of malignant catarrhal fever in Murrah buffaloes in Minas Gerais, Brazil." Pesquisa Veterinária Brasileira **29**(5): 395-400.

Cotter, M. A. and E. S. Robertson (1999). "The latency-associated nuclear antigen tethers the Kaposi's sarcoma-associated herpesvirus genome to host chromosomes in body cavity-based lymphoma cells." Virology **264**(2): 254-264.

Coulter, L. J., H. Wright, *et al*. (2001). "Molecular genomic characterization of the viruses of malignant catarrhal fever." Journal of Comparative Pathology **124**(1): 2-19.

Crawford, T. B., D. O'Toole, *et al.* (1999). Malignant Catarrhal Fever. Current Veterinary Therapy, 4th Edition - Food Animal Practices. J. L. Howard. Philadelphia, PA, W.B. Saunders Company: 306-309.

Crough, T. and R. Khanna (2009). "Immunology of human cytomegalovirus: from bench to bedside." Clinical Microbiology Reviews **22**(1): 76-98.

Cui, C., A. Griffiths, *et al.* (2006). "Prediction and identification of herpes simplex virus 1-encoded microRNAs." Journal of Virology **80**(11): 5499-5508.

Cullen, B. R. (2006). "Viruses and microRNAs." Nature Genetics 38: S25-S30.

Cunha, C. W., D. L. Traul, *et al*. (2008). "Detection of ovine herpesvirus 2 major capsid gene transcripts as an indicator of virus replication in shedding sheep and clinically affected animals." Virus Research **132**(1-2): 69-75.

Damania, B., J. K. Choi, *et al*. (2000). "Signaling activities of gammaherpesvirus membrane proteins." Journal of Virology **74**(4): 1593-1601.

Dasgupta, A. and D. W. Wilson (1999). "ATP depletion blocks herpes simplex virus DNA packaging and capsid maturation." Journal of Virology **73**(3): 2006-2015.

Davison, A. J., R. Eberle, *et al*. (2009). "The order Herpesvirales." Archives of Virology **154**(1): 171-177.

Davy, C. and J. Doorbar (2007). "G2/M cell cycle arrest in the life cycle of viruses." Virology **368**(2): 219-226.

del Solar, G., R. Giraldo, *et al*. (1998). "Replication and control of circular bacterial plasmids." Microbiology and Moloecular Biology Reviews **62**(2): 434-464.

Didier, D. K., J. Schiffenbauer, *et al*. (1988). "Characterization of the cDNA encoding a protein binding to the major histocampatibility complex class II Y box." Proceedings of the National Academy of Sciences of the United States of America **85**(): 7322-7326.

Dittmer, D., M. Lagunoff, *et al*. (1998). "A cluster of latently expressed genes in Kaposi's sarcoma-associated herpesvirus." Journal of Virology **72**(10): 8309-8315.

Doench, J. G. and P. A. Sharp (2004). "Specificity of microRNA target selection in translational repression." Genes & Development **18**(5): 504-511.

Doench, J. G., C. P. Petersen, *et al.* (2003). "siRNAs can function as miRNAs." Genes & Development **17**(4): 438-442.

Dölken, L., A. Krmpotic, *et al*. (2010). "Cytomegalovirus microRNAs facilitate persistent virus infection in salivary glands." Plos Pathogens **6**(10): e1001150.

Elbashir, S. M., W. Lendeckel, *et al*. (2001). "RNA interference is mediated by 21- and 22-nucleotide RNAs." Nature **411**(6836): 494-498.

Ellis, J. A., D. T. O'Toole, *et al*. (1992). "Predominance of BoCD8-positive T lymphocytes in vascular lesions in a 1-year-old cow with concurrent malignant catarrhal fever and bovine viral diarrhea virus infection." Veterinary Pathology **29**(6): 545-547.

Epstein, M. A., B. G. Achong, *et al*. (1964). "Virus particles in cultured lymphoblasts from Burkitt's lymphoma." Lancet **1**(733): 702-703.

Evdokimova, V., P. Ruzanov, *et al*. (2006). "Akt-mediated YB-1 phosphorylation activates translation of silent mRNA species." Molecular and Cellular Biology **26**(1): 277-292.

Farrell, P. (2002). "Cell-switching and kissing." Nature Medicine **8**(6): 559-560.

Feederle, R., S. D. Linnstaedt, *et al*. (2011). "A viral microRNA cluster strongly potentiates the transforming properties of a human herpesvirus." Plos Pathogens **7**(2): e1001294.

Field, N., W. Low, *et al*. (2003). "KSHV vFLIP binds to IKK-gamma to activate IKK." Journal of Cell Science **116**(18): 3721-3728.

Fields (2007). Virology. Philadelphia, Lippincott Williams & Wilkins.

Fish, J. E., M. M. Santoro, *et al*. (2008). "MiR-126 regulates angiogenic signalling and vascular integrity." Developmental Cell **15**(2): 272-284.

Frame, F. M. and R. G. Dalziel (2008). "Transcriptional control by the R-transactivator protein of Alcelaphine Herpesvirus-1." Veterinary Research Communications **32**(3): 215-223.

Gaidatzis, D., E. van Nimwegen, *et al.* (2007). "Inference of miRNA targets using evolutionary conservation and pathway analysis." Bmc Bioinformatics 8.

Ganem, D. (1997). "KSHV and Kaposi's sarcoma: The end of the beginning?" Cell **91**(2): 157-160.

Garber, A. C., J. H. Hu, *et al*. (2002). "Latency-associated nuclear antigen (LANA) cooperatively binds to two sites within the terminal repeat, and both sites contribute to the ability of LANA to suppress transcription and to facilitate DNA replication." Journal of Biological Chemistry **277**(30): 27401-27411.

Gill, M. B., R. Edgar, *et al*. (2008). "A gamma-herpesvirus glycoprotein complex manipulates actin to promote viral spread." Plos One **3**(3): e1808.

Glazov, E. A., P. F. Horwood, *et al*. (2010). "Characterization of microRNAs encoded by the bovine herpesvirus 1 genome." Journal of General Virology **91**: 32-41.

Gottwein, E. and B. R. Cullen (2010). "A human herpesvirus microRNA inhibits p21 expression and attenuates p21-mediated cell cycle arrest." Journal of Virology **84**(10): 5229-5237.

Gottwein, E., N. Mukherjee, *et al*. (2007). "A viral microRNA functions as an orthologue of cellular miR-155." Nature **450**(7172): 1096-U17.

Götze, R., and J. Liess. (1930). Deutsche Tierärztliche Wochenschrift **37**: 433.

Grey, F., R. Tirabassi, *et al*. (2010). "A viral microRNA down-regulates multiple cell cycle genes through mRNA 5'UTRs." Plos Pathogens **6**(6): e1000967.

Grey, F., H. Meyers, *et al*. (2007). "A human cytomegalovirus-encoded microRNA regulates expression of multiple viral genes involved in replication." Plos Pathogens **3**(11): 1593-1602.

Griffiths-Jones, S., H. K. Saini, *et al*. (2008). "miRBase: tools for microRNA genomics." Nucleic Acids Research **36**(Database Issue): D154-158.

Griffiths-Jones, S., R. J. Grocock, *et al*. (2006). "miRBase: microRNA sequences, targets and gene nomenclature." Nucleic Acids Research **34**(Database Issue): D140-D144.

Griffiths-Jones, S. (2004). "The microRNA Registry." Nucleic Acids Research **32**(Database Issue): D109-D111.

Grishok, A., A. E. Pasquinelli, *et al*. (2001). "Genes and mechanisms related to RNA interference regulate expression of the small temporal RNAs that control *C. elegans* developmental timing." Cell **106**(1): 23-34.

Grundhoff, A. and C. S. Sullivan (2011). "Virus-encoded microRNAs." Virology **411**(2): 325-343.

Haddad, R. S. and L. M. Hutt-Fletcher (1989). "Depletion of glycoprotein gp85 from virosomes made with Epstein-Barr virus proteins abolishes their ability to fuse with virus receptor-bearing cells." Journal of Virology **63**(12): 4998-5005.

Hammond, S. M., E. Bernstein, *et al*. (2000). "An RNA-directed nuclease mediates post-transcriptional gene silencing in Drosophila cells." Nature **404**(6775): 293-296.

Han, J. J., Y. Lee, *et al*. (2006). "Molecular basis for the recognition of primary microRNAs by the Drosha-DGCR8 complex." Cell **125**(5): 887-901.

Hansen, A., S. Henderson, *et al*. (2010). "KSHV-encoded miRNAs target MAF to induce endothelial cell reprogramming." Genes & Development **24**(2): 195-205.

Hardwick, J. M. and D. S. Bellows (2003). "Viral versus cellular BCL-2 proteins." Cell Death and Differentiation **10**(Suppl. 1): S68-S76.

Hart, J., M. Ackermann, *et al*. (2007). "Complete sequence and analysis of the ovine herpesvirus 2 genome." Journal of General Virology **88**(1): 28-39.

Henson, B. W., E. M. Perkins, *et al*. (2009). "Self-assembly of Epstein-Barr virus capsids." Journal of Virology **83**(8): 3877-3890.

Hu, J. H., A. C. Garber, *et al*. (2002). "The latency-associated antigen of Kaposi's sarcoma-associated herpesvirus supports latent DNA replication in dividing cells." Journal of Virology **76**(22): 11677-11687.

Hunt, R. (2011). Virology - Chapter Eleven: Herpes viruses, University of South Carolina School of Medicine. **2011**. http://pathmicro.med.sc.edu/virol/herpes.htm

Hüssy, D., F. Janett, *et al*. (2002). "Analysis of the pathogenetic basis for shedding and transmission of ovine gamma herpesvirus 2." Journal of Clinical Microbiology **40**(12): 4700-4704.

Hüssy, D., N. Stäuber, *et al*. (2001). "Quantitative fluorogenic PCR assay for measuring ovine herpesvirus 2 replication in sheep." Clinical and Diagnostic Laboratory Immunology **8**(1): 123-128.

Hutvágner, G. and P. D. Zamore (2002). "A microRNA in a multiple-turnover RNAi enzyme complex." Science **297**(5589): 2056-2060.

Hutvágner, G., J. McLachlan, *et al*. (2001). "A cellular function for the RNA-interference enzyme Dicer in the maturation of the let-7 small temporal RNA." Science **293**(5531): 834-838.

Jackson, A. L., S. R. Bartz, *et al*. (2003). "Expression profiling reveals off-target gene regulation by RNAi." Nature Biotechnology **21**(6): 635-637.

Johnson, D. C., T. W., *et al*. (2011). "Herpes simplex virus glycoproteins gB and gD function in a redundant fashion to promote secondary envelopment." Journal of Virology **85**(10): 4910-4926.

Johnston, R. J. and O. Hobert (2003). "A microRNA controlling left/right neuronal asymmetry in *Caenorhabditis elegans*." Nature **426**(6968): 845-849.

Jurak, I., M. F. Kramer, *et al*. (2010). "Numerous conserved and divergent microRNAs expressed by herpes simplex viruses 1 and 2." Journal of Virology **84**(9): 4659-4672.

Kato, M., L. Wang, *et al*. (2010). "Post-transcriptional up-regulation of Tsc-22 by Ybx1, a target of miR-216a, mediates TGF-β-induced collagen expression in kidney cells." Journal of Biological Chemistry **285**(44): 34004-34015.

Kato, M., S. Putta, *et al*. (2009). "TGF-β activates Akt kinase through a microRNA-dependent amplifying circuit targeting PTEN." Nature Cell Biology **11**(7): 881-U263.

Kaufmann, S. H. E. (1996). "γ/δ and other unconventional T lymphocytes: What do they see and what do they do?" Proceedings of the National Academy of Sciences **93**(6): 2272-2279.

Kelly, B. J., C. Fraefel, *et al*. (2009). "Functional roles of the tegument proteins of herpes simplex virus type 1." Virus Research **145**(2): 173-186.

Ketting, R. F., S. E. J. Fischer, *et al*. (2001). "Dicer functions in RNA interference and in synthesis of small RNA involved in developmental timing in *C. elegans*." Genes & Development **15**(20): 2654-2659.

Khvorova, A., A. Reynolds, *et al*. (2003). "Functional siRNAs and miRNAs exhibit strand bias." Cell **115**(2): 209-216.

Kim, O., H. Li, *et al*. (2003). "Demonstration of sheep-associated malignant catarrhal fever virions in sheep nasal secretions." Virus Research **98**(2): 117-122.

Kim, Y. K., J. Yu, *et al*. (2009). "Functional links between clustered microRNAs: Suppression of cell-cycle inhibitors by microRNA clusters in gastric cancer." Nucleic Acids Research **37**(5): 1672-1681.

Kozomara, A. and S. Griffiths-Jones (2011). "miRBase: integrating microRNA annotation and deep-sequencing data." Nucleic Acids Research **39**(Database Issue): D152-D157.

Kurtze, H. (1950). Deutsche Tierärztliche Wochenschrift **57**: 261.

Lai, E. C. (2002). "MicroRNAs are complementary to 3'UTR sequence motifs that mediate negative post-transcriptional regulation." Nature Genetics **30**(4): 363-364.

Latimer, E., J. C. Zong, *et al*. (2011). "Detection and evaluation of novel herpesviruses in routine and pathological samples from Asian and African elephants: Identification of two new probosciviruses (EEHV-5 and EEHV-6) and two new gammaherpesviruses (EGHV-3B and EGHV-5)." Veterinary Microbiology **147**(1-2): 28-41.

Lau, N. C., L. P. Lim, *et al*. (2001). "An abundant class of tiny RNAs with probably regulatory roles in *Caenorhabditis elegans*." Science **294**(5543): 858-862.

Lee, J. Y., J. J. Song, *et al*. (2010). "Transcriptional profiling of host gene expression in chicken embryo lung cells infected with laryngotracheitis virus." BMC Genomics **11**: 445.

Lee, R. C. and V. Ambros (2001). "An extensive class of small RNAs in *Caenorhabditis elegans*." Science **294**(5543): 862-864.

Lee, R. C., R. L. Feinbaum, *et al*. (1993). "The *C. elegans* herterchronic gene lin-4 encodes small RNAs with antisense complementarity to lin-14." Cell **75**(5): 843-854.

Lee, Y., C. Ahn, *et al*. (2003). "The nuclear RNase III Drosha initiates microRNA processing." Nature **425**(6956): 415-419.

Leight, E. R. and B. Sugden (2000). "EBNA-1: A protein pivotal to latent infection by Epstein-Barr virus." Reviews in Medical Virology **10**(2): 83-100.

Lemasson, I., M. R. Lewis, *et al*. (2007). "Human T-cell leukemia virus type 1 (HTLV-1) bZIP protein interacts with the cellular transcription factor CREB to inhibit HTLV-1 transcription." Journal of Virology **81**(4): 1543-1553.

Lewis, B. P., I. H. Shih, *et al*. (2003). "Prediction of mammalian microRNA targets." Cell **115**(7): 787-798.

Li, H., G. Karney, *et al*. (2008). "Long distance spread of malignant catarrhal fever virus from feedlot lambs to ranch bison." Canadian Veterinary Journal **49**(2): 183-185.

Li, H., N. S. Taus, *et al*. (2004). "Shedding of ovine herpesvirus 2 in sheep nasal secretions: The predominant mode of transmission." Journal of Clinical Microbiology **42**(12): 5558-5564.

Li, H., G. Snowder, *et al*. (1999). "Production of malignant catarrhal fever virus-free sheep." Veterinary Microbiology **65**(2): 167-172.

Li, H., G. Snowder, *et al*. (1998). "Transmission of ovine herpesvirus 2 in lambs." Journal of Clinical Microbiology **36**(1): 223-226.

Li, Q. X., M. K. Spriggs, *et al*. (1997). "Epstein-Barr virus uses HLA class II as a cofactor for infection of B lymphocytes." Journal of Virology **71**(6): 4657-4662.

Li, Q. X., S. M. Turk, *et al*. (1995). "The Epstein-Barr virus (EBV) BZLF2 gene product associates with the gH and gL homologs of EBV and carries an epitope critical to infection of B cells but not of epithelial cells." Journal of Virology **69**(7): 3987-3994.

Li, R., Y. Li, *et al*. (2008). "SOAP: short oligonucleotide alignment program." Bioinformatics **24**(5): 713-714.

Li, Y. P., J. M. Gottwein, *et al*. (2011). "MicroRNA-122 antagonism against hepatitis C virus genotypes 1-6 and reduced efficacy by host RNA insertion or mutations in the HCV 5'UTR." Proceedings of the National Academy of Sciences of the United States of America **108**(12): 4991-4996.

Liggitt, H. D. and J. C. DeMartini (1980). "The pathomorphology of malignant catarrhal fever: I. Generalized lymphoid vasculitis." Veterinary Pathology **17**(1): 58-72.

Lin, H. R. and D. Ganem (2011). "Viral microRNA target allows insight into the role of translation in governing microRNA target accessibility." Proceedings of the National Academy of Sciences of the United States of America **108**(13): 5148-5153.

Lingel, A., B. Simon, *et al*. (2003). "Structure and nucleic-acid binding of the *Drosophila* argonaute 2 PAZ domain." Nature **426**(6965): 465-469.

Liu, J. D., M. A. Valencia-Sanchez, *et al*. (2005). "MicroRNA-dependent localization of targeted mRNAs to mammalian P-bodies." Nature Cell Biology **7**(7): 719-U118.

Liu, J. D., M. A. Carmell, *et al*. (2004). "Argonaute2 is the catalytic engine of mammalian RNAi." Science **305**(5689): 1437-1441.

Lizasa, H., B. E. Wulff, *et al*. (2010). "Editing of Epstein-Barr virus-encoded BART6 microRNAs controls their Dicer targeting and consequently affects viral latency." Journal of Biological Chemistry **285**(43): 33358-33370.

Lo, A. K. F., K. F. To, *et al*. (2007). "Modulation of LMP1 protein expression by EBV-encoded microRNAs." Proceedings of the National Academy of Sciences of the United States of America **104**(41): 16164-16169.

Løken, T., M. Aleksandersen, *et al*. (1998). "Malignant catarrhal fever caused by ovine herpesvirus-2 in pigs in Norway." Veterinary Record **143**(17): 464-467.

Lu, C. C., Z. H. Li, *et al*. (2010). "MicroRNAs encoded by Kaposi's sarcoma-associated herpesvirus regulate viral life cycle." Embo Reports **11**(10): 784-790.

Lu, F., W. Stedman, *et al*. (2010). "Epigenetic regulation of Kaposi's sarcoma-associated herpesvirus latency by virus-encoded microRNAs that target Rta and the cellular Rb12-DNMT pathway." Journal of Virology **84**(6): 2697-2706.

Lund, E., S. Guttinger, *et al*. (2004). "Nuclear export of microRNA precursors." Science **303**(5654): 95-98.

Lung, R. W. M., J. H. M. Tong, *et al*. (2009). "Modulation of LMP2A expression by a newly identified Epstein-Barr virus-encoded microRNA miR-BART22." Neoplasia **11**(11): 1174-U89.

Lyngaa, R., K. Norregaard, *et al*. (2010). "Cell transformation mediated by the Epstein-Barr virus G protein-coupled receptor BILF1 is dependent on constitutive signalling." Oncogene **29**(31): 4388-4398.

Maniataki, E and Z. Mourelatos (2005). "A human, ATP-independent, RISC assembly machine fuelled by pre-miRNA." Genes & Development **19**(24): 2979-2990.

McCormick, C. and D. Ganem (2005). "The kaposin B protein of KSHV activates the p38/MK2 pathway and stabilizes cytokine mRNAs." Science **307**(5710): 739-741.

McGeoch, D. J., F. J. Rixon, *et al*. (2006). "Topics in herpesvirus genomics and evolution." Virus Research **117**(1): 90-104.

McGeoch, D. J. and A. J. Davison (1999). The molecular evolutionary history of the herpesviruses. Origin and Evolution of Viruses. E. Domingo, R. Webster and J. Holland. London, Academic Press: 441-465.

Meier-Trummer, C. S., B. Ryf, *et al*. (2010). "Identification of peripheral blood mononuclear cells targeted by ovine herpesvirus 2 in sheep." Veterinary Microbiology **141**(3-4): 199-207.

Meier-Trummer, C. S., H. Rehrauer, *et al*. (2009). "Malignant catarrhal fever of cattle if associated with low abundance of IL-2 transcript and a predominately latent profile of ovine herpesvirus 2 gene expression." Plos One **4**(7): e6265.

Meister, G. and T. Tuschl (2004). "Mechanisms of gene silencing by double-stranded RNA." Nature **431**(7006): 343-349.

Mettam, R. W. M. (1923). "Snotsiekte in cattle." Ninth and Tenth Reports of the Director Veterinary Education and Research, Union S. Africa. p 395.

Metzler, A. E. (1991). "The malignant catarrhal fever complex." Comparative Immunology Microbiology and Infectious Diseases **14**(2): 107-124.

Miller, N. and L. M. Hutt-Fletcher (1988). "A monoclonal-antibody to glycoprotein gp85 inhibits fusion but not attachment of Epstein-Barr virus." Journal of Virology **62**(7): 2366-2372.

Molesworth, S. J., C. M. Lake, *et al*. (2000). "Epstein-Barr virus gH is essential for penetration of B cells but also plays a role in attachment of virus to epithelial cells." Journal of Virology **74**(14): 6324-6332.

Moore, D. A., P. Kohrs, *et al*. (2010). "Outbreak of malignant catarrhal fever among cattle associated with a state livestock exhibition." Journal of the American Veterinary Medical Association **237**(1): 87-92.

Mourelatos, Z., J. Dostie, *et al*. (2002). "miRNPs: a novel class of ribonucleoproteins containing numerous microRNAs." Genes & Development **16**(6): 720-728.

Muller-Doblies, U. U., J. Egli, *et al*. (2001). "Epidemiology of malignant catarrhal fever in Switzerland." Schweizer Archiv Fur Tierheilkunde **143**(4): 173-183.

Murphy, E., J. Vanicek, *et al*. (2008). "Suppression of immediate-early viral gene expression by herpesvirus-coded microRNAs: Implications for latency." Proceedings of the National Academy of Sciences of the United States of America **105**(14): 5453-5458.

Muylkens, B., D. Coupeau, *et al*. (2010). "Marek's disease virus microRNA designated Mdv1-pre-miR-M4 targets both cellular and viral genes." Archives of Virology **155**(11): 1823-1837.

Mwangi, W. N., L. P. Smith, *et al*. (2011). "Clonal structure of rapid-onset MDV-driven $CD4^+$ lymphomas and responding $CD8^+$ T cells." Plos Pathogens **7**(5): e1001337.

Nachmani, D., N. Stern-Ginossar, *et al*. (2009). "Diverse herpesvirus microRNAs target the stress-induced immune ligand MICB to escape recognition by natural killer cells." Cell Host & Microbe **5**(4): 376-385.

Nascimento, R., J. D. Dias, *et al*. (2009). "The conserved UL24 family of human alpha, beta and gamma herpesviruses induces cell cycle arrest and inactivation of the cyclinB/cdc2 complex." Archives of Virology **154**(7): 1143-1149.

Nascimento, R. and R. M. E. Parkhouse (2007). "Murine gammaherpesvirus 68 ORF20 induces cell-cycle arrest in G(2) by inhibiting the Cdc2-cyclin B complex." Journal of General Virology **88**: 1446-1453.

Nelson, D. D., W. C. Davis, *et al*. (2010). "$CD8^+$/$perforin^+$/$WC1^-$ γδ T cells, not $CD8^+$ αβ T cells, infiltrate vasculitis lesions of American bison (*Bison bison*) with experimental sheep-assiciated malignant catarrhal fever." Veterinary Immunology and Immunopathology **136**(3-4): 284-291.

Nevels, M., A. Nitzsche, *et al*. (2011). "How to control an infectious bead string: nucleosome-based regulation and targeting of herpesvirus chromatin." Reviews in Medical Virology **21**(3): 154-180.

Nijmeijer, S., R. Leurs, *et al*. (2010). "The Epstein-Barr virus-encoded G protein-coupled receptor BILF1 hetero-oligomerizes with human CXCR4, scavenges $G\alpha_i$ proteins, and constitutively impairs CXCR4 functioning." Journal of Biological Chemistry **285**(38): 29632-296-41.

Nykanen, A., B. Haley, *et al*. (2001). "ATP requirements and small interfering RNA structure in the RNA interference pathway." Cell **107**(3): 309-321.

Ohler, U., S. Yekta, *et al*. (2004). "Patterns of flanking sequence conservation and a characteristic upstream motif for microRNA gene identification." RNA - A Publication of the RNA Society **10**(9): 1309-1322.

Okamura, K., M. D. Phillips, *et al*. (2008). "The regulatory activity of microRNA star species has substantial influence on miRNA and 3'UTR evolution." Nature Structural & Molecular Biology **15**(4): 354-363.

Olsen, P. H. and V. Ambros (1999). "The lin-4 regulatory RNA controls developmental timing in *Caenorhabditis elegans* by blocking LIN-14 protein synthesis after the initiation of translation." Developmental Biology **216**(2): 671-680.

O'Toole, D., H. Li, *et al*. (1997). "Chronic and recovered cases of sheep-associated malignant catarrhal fever in cattle." Veterinary Record **140**(20): 519-524.

Otsubo, T., Y. Akiyama, *et al*. (2011). "MicroRNA-126 inhibits Sox2 expression and contributes to gastric carcinogenesis." Plos One **6**(1): e16617

Pall, G. S. and A. J. Hamilton (2008). "Improved northern blot method for enhanced detection of small RNA." Nature Protocols **3**(6): 1077-1084.

Pan, X., B. Zhang, *et al.* (2007). "Characterizing viral microRNAs and its application on identifying new microRNAs in viruses." Journal of Cellular Physiology **211**(1): 10-18.

Pasquinelli, A. E., B. J. Reinhart, *et al*. (2000). "Conservation of the sequence and temporal expression of let-7 heterochronic regulatory RNA." Nature **408**(6808): 86-89.

Paulus, C., A. Nitzsche, *et al*. (2010). "Chromatinisation of herpesvirus genomes." Reviews in Medical Virology **20**(1): 34-50.

Petrocca, F., R. Visone, *et al*. (2008). "E2F1-regulated microRNAs impair TGFβ-dependent cell-cycle arrest and apoptosis in gastric cancer." Cancer Cell **13**(3): 272-286.

Pfeffer, S., A. Sewer, *et al.* (2005). "Identification of microRNAs of the herpesvirus family." Nature Methods **2**(4): 269-276.

Pfeffer, S., M. Zavolan, *et al.* (2004). "Identification of virus-encoded microRNAs." Science **304**(5671): 734-736.

Plowright, W., R. D. Ferris, *et al*. (1960). "Blue wildebeest and the ætiological agent of malignant catarrhal fever." Nature **188**(4757): 1167-1169.

Poffenberger, K. L. and B. Roizman (1985). "A noninverting genome of a viable herpes-simplex virus-1-presence of head-to-tail linkages in packaged genomes and requirements for circularization after infection." Journal of Virology **53**(2): 587-595.

Powers, J. G., D. C. VanMetre, *et al*. (2005). "Evaluation of ovine herpesvirus 2 infections, as detected by competitive inhibition ELISA and polymerase reaction assay in dairy cattle without clinical signs of malignant catarrhal fever." Journal of the American Veterinary Medical Association **227**(4): 606-611.

Qin, Z. Q., P. Kearney, *et al*. (2010). "Kaposi's sarcoma-associated herpesvirus (KSHV)-encoded microRNA specifically induce IL-6 and IL-10 secretion by macrophages and monocytes." Journal of Leukocyte Biology **87**(1): 25-34.

Ratcliff, F., B. D. Harrison, *et al.* (1997). "A similarity between viral defences and gene silencing in plants." Science **276**(5318): 1558-1560.

Reinhart, B. J., F. J. Slack, *et al*. (2000). "The 21-nucleotide let-7 RNA regulates developmental timing in *Caenorhabditis elegans*." Nature **408**(6772): 901-906.

Roizmann, B., R. C. Desrosiers, *et al*. (1992). "The family Herpesviridae - an update." Archives of Virology **123**(3-4): 425-449.

Rosbottom, J., R. G. Dalziel, *et al*. (2002). "Ovine herpesvirus 2 lytic cycle replication and capsid production." Journal of General Virology **83**(12): 2999-3002.

Rossi, J. J. (2005). "RNAi and the P-body connection." Nature Cell Biology **7**(7): 643-644.

Rossiter, P. B. (1983). "Antibodies to malignant catarrhal fever virus in cattle with non-wildebeest-associated malignant catarrhal fever." Journal of Comparative Pathology **93**(1): 93-97.

Rossiter, P. B. (1981). "Antibodies to malignant catarrhal fever virus in sheep." Journal of Comparative Pathology **91**(2): 303-311.

Russell, G. C., J. P. Stewart, *et al*. (2009). "Malignant catarrhal fever: A review." Veterinary Journal **179**(3): 324-335.

Samols, M. A., R. L. Skalsky, *et al.* (2007). "Identification of cellular genes targeted by KSHV-encoded microRNAs." Plos Pathogens **3**(5): 611-618.

Samols, M. A., J. H. Hu, *et al.* (2005). "Cloning and identification of a microRNA cluster within the latency-associated region of Kaposi's sarcoma-associated herpesvirus." Journal of Virology **79**(14): 9301-9305.

Sanford, S. E. and P. B. Little (1977). "The gross and histopathological lesions of malignant catarrhal fever in three captive sika deer (*Cervus nippon*) in southern Ontario." Journal of Wildlife Disease **13**(1): 29-32.

Schock, A., R. A. Collins, *et al.* (1998). "Phenotype, growth regulation and cytokine transcription in Ovine herpesvirus-2 (OvHV-2)-infected bovine T-cell lines." Veterinary Immunology and Immunopathology **66**(1): 67-81.

Schwarz, D. S., G. Hutvágner, *et al*. (2003). "Asymmetry in the assembly of the RNAi enzyme complex." Cell **115**(2): 199-208.

Simon, S., H. Li, *et al*. "The vascular lesions of a cow and bison with sheep-associated malignant catarrhal fever contain ovine herpesvirus 2-infected $CD8^+$ T lymphocytes." Journal of General Virology **84**(8): 2009-2013.

Skalsky, R. L., M. A. Samols, *et al*. (2007). "Kaposi's sarcoma-associated herpesvirus encodes an ortholog of miR-155." Journal of Virology **81**(23): 12836-12845.

Song, J. J., S. K. Smith, *et al*. (2004). "Crystal structure of argonaute and its implications for RISC slicer activity." Science **305**(5689): 1434-1437.

Song, J. J., J. D. Liu, *et al*. (2003). The crystal structure of the Argonaute2 PAZ domain reveals an RNA binding motif in RNAi effector complexes." Nature Structural Biology **10**(12): 1026-1032.

Stampfer, S. D., H. A. Lou, *et al*. (2010). "Structural basis of local, pH-dependent conformational changes in glycoprotein B from herpes simplex virus type 1." Journal of Virology **84**(24): 12924-12933.

Stark, A., J. Brennecke, *et al.* (2005). "Animal microRNAs confer robustness to gene expression and have a significant impact on 3' UTR evolution." Cell **123**(6): 1133-1146.

Stern-Ginossar, N., N. Saleh, *et al*. (2009). "Analysis of human cytomegalovirus-encoded microRNA activity during infection." Journal of Virology **83**(20): 10684-10693.

Stern-Ginossar, N., N. Elefant, *et al*. (2007). "Host immune system gene targeting by a viral miRNA." Science **317**(5836): 376-381.

Stoker, M., I. Macpherson (1964). "Syrian hamster fibroblast cell line BHK21 and its derivatives." Nature **203**(495): 1355-1357.

Szekely, L., F. Chen, *et al*. (1998). "Restricted expression of Epstein-Barr virus (EBV)-encoded, growth transformation-associated antigens in an EBV- and human herpesvirus type 8-carrying body cavity lymphoma line." Journal of General Virology **79**(6): 1445-1452.

Tahbaz, N., F. A. Kolb, *et al*. (2004). "Characterization of the interactions between mammalian PAZ PIWI domain proteins and Dicer." EMBO Reports **5**(2): 189-194.

Tang, S., A. Patel, *et al*. (2009). "Novel less-abundant viral microRNAs encoded by herpes simplex virus 2 latency-associated transcript and their roles in regulating ICP34.5 and ICP0 mRNAs." Journal of Virology **83**(3): 1433-1442.

Tang, S., A. S. Bertke, *et al*. (2008). "An acutely and latently expressed herpes simplex virus 2 viral microRNA inhibits expression of ICP34.5, a viral neurovirulence factor." Proceedings of the National Academy of Sciences of the United States of America **105**(31): 10931-10936.

Taus, N. S., D. A. Schneider, *et al*. (2010). "Sheep (*Ovis aries*) airway epithelial cells support ovine herpesvirus 2 lytic replication *in vivo*." Veterinary Microbiology **145**(1-2): 47-53.

Tay, Y., J. Q. Zhang, *et al*. (2008). "MicroRNAs to Nanog, Oct4 and Sox2 coding regions modulate embryonic stem cell differentiation." Nature **455**(7216): 1124-U12.

Thonur, L., G. C. Russell, *et al.* (2006). "Differential transcription of ovine herpesvirus 2 genes in lymphocytes from reservoir and susceptible species." Virus Genes **32**(1): 27-35.

Traul, D. L., H. Li, *et al*. (2007). "Resistance to malignant catarrhal fever in American bison (*Bison bison*) is associated with MHC class IIa polymorphisms." Animal Genetics **38**(2): 141-146.

Uldrick, T. S. and D. Whitby (2011). "Update on KSHV epidemiology, Kaposi Sarcoma pathogenesis, and treatment of Kaposi Sarcoma." Cancer Letters **305**(2): 150-162.

Umbach, J. L., M. F. Kramer, *et al*. (2008). "MicroRNAs expressed by herpes simplex virus 1 during latent infection regulate viral mRNAs." Nature **454**(7205): 780-U108.

Verma, S. C., K. Lan, *et al*. (2007). Structure and function of latency-associated nuclear antigen. Kaposi Sarcoma Herpesvirus: New Perspectives. **312**: 101-136

Walz, N., T. Christalla, *et al.* (2010). "A global analysis of evolutionary conservation among known and predicted gammaherpesvirus microRNAs." Journal of Virology **82**(2): 716-728.

Wang, S. S., A. B. Aurora, *et al*. (2008). "The endothelial-specific microRNA miR-126 governs vascular integrity and angiogenesis." Developmental Cell **15**(2): 261-271.

Wang, X., W. J. Kenyon, *et al*. (1998). "Epstein-Barr virus uses different complexes of glycoproteins gH and gL to infect B lymphocytes and epithelial cells." Journal of Virology **72**(7): 5552-5558.

Wang, X. and L. M. Hutt-Fletcher (1998). "Epstein-Barr virus lacking glycoprotein gp42 can bind to B cells but is not able to infect." Journal of Virology **72**(1): 158-163.

Wiebusch, L., A. Neuwirth, *et al*. (2008). "Cell cycle-independent expression of immediate-early gene 3 results in G_1 and G_2 arrest in murine cytomegalovirus-infected cells." Journal of Virology **82**(20): 10188-10198.

Wightman, B., I. Ha, *et al*. (1993). "Posttranscriptional regulation of the heterochronic gene lin-14 by lin-4 mediates temporal pattern-formation in *C. elegans*." Cell **75**(5): 855-862.

Wightman, B., T. R. Burglin, *et al*. (1991). "Negative regulatory sequences in the lin-14 3'-untranslated region are necessary to generate a temporal switch during *Caenorhabditis elegans* development." Genes & Development **5**(10): 1813-1824.

Xia, T., A. O'Hara, *et al*. (2008). "EBV microRNAs in primary lymphomas and targeting of CXCL-11 by ebv-mir-BHRF1-3." Cancer Research **68**(5): 1436-1442.

Xiao, C. C., L. Srinivasan, *et al*. (2008). "Lymphoproliferative disease and autoimmunity in mice with increased miR-17-92 expression in lymphocytes." Nature Immunology **9**(4): 405-414.

Xu, N., T. Papagiannakopoulos, *et al*. (2009). "MicroRNA-145 regulates Oct4, Sox2, and KLF4 and represses pluripotency in human embryonic stem cells." Cell **137**(4): 647-658.

Xu, P. Z., S. Y. Vernooy, *et al*. (2003). "The *Drosophila* miRNA miR-14 suppresses cell death and is required for normal fat metabolism." Current Biology **13**(9): 790-795.

Xu, S., C. Y. Xue, *et al*. (2011). "Marek's disease virus type 1 microRNA miR-M3 suppresses cisplatin-induced apoptosis by targeting Smad2 of the transforming growth factor beta signal pathway." Journal of Virology **85**(1): 276-285.

Yan, K. S., S. Yan, *et al*. (2003). "Structure and conserved RNA binding of the PAZ domain." Nature **426**(6965): 469-474.

Yao, Y. X., Y. G. Zhao, *et al*. (2009). "Novel microRNAs (miRNAs) encoded by herpesvirus of turkeys: Evidence of miRNA evolution by duplication." Journal of Virology **83**(13): 6969-6973.

Yao, Y. X., Y. G. Zhao, *et al*. (2007). "Marek's disease virus type 2 (MDV-2)-encoded microRNAs show no sequence conservation with those encoded by MDV-1." Journal of Virology **81**(13): 7164-7170.

Yekta, S., I. H. Shih, *et al*. (2004). "MicroRNA-directed cleavage of HOXB8 mRNA." Science **304**(5670): 594-596.

Yi, R., Y. Qin, *et al*. (2003). "Exportin-5 mediates the nuclear export of pre-microRNAs and short hairpin RNAs." Genes & Development **17**(24): 3011-3016.

Yu, X. K., S. Shah, *et al*. (2011). "Biochemical and structural characterization of the capsid-bound tegument proteins of human cytomegalovirus." Journal of Structural Biology **174**(3): 451-460.

Zeng Y. and B. R. Cullen (2005). "Efficient processing of primary microRNA hairpins by drosha requires flanking nonstructured RNA sequences." Journal of Biological Chemistry **280**(30): 27595-27603.

Zeng Y., R. Yi, *et al*. (2003). "MicroRNAs and small interfering RNAs can inhibit mRNA expression by similar mechanisms." Proceedings of the National Academy of Sciences of the United States of America **100**(17): 9779-9784.

Zdobnov, E. M. and R. Apweiler (2001). "InterProScan - an integration platform for the signature-recognition methods in InterPro." Bioinformatics **17**(9): 847-848.

Zhang, B. H., X. P. Pan, *et al.* (2006). "Evidence that miRNAs are different from other RNAs." Cellular and Molecular Life Sciences **63**(2): 246-254.

Zhao, Y. G., H. T. Xu, *et al*. (2011). "Critical role of the virus-encoded microRNA-155 ortholog in the induction of Marek's disease lymphomas." Plos Pathogens **7**(2): e1001305

Zhao, Y. G., Y. X. Yao, *et al*. (2009). "A functional microRNA-155 ortholog encoded by the oncogenic Marek's disease virus." Journal of Virology **83**(1): 489-492.

Zheng, S. Q., Y. X. Li, *et al*. (2011). "miR-101 regulates HSV-1 replication by targeting ATP5B." Antiviral Research **89**(3): 219-226.

Zhong, W. D., H. Wang, *et al*. (1996). "Restricted expression of Kaposi sarcoma-associated herpesvirus (human herpesvirus 8) genes in Kaposi sarcoma." Proceedings of the National Academy of Sciences of the United States of America **93**(13): 6641-6646.

Ziegelbauer, J. M., C. S. Sullivan, *et al*. (2009). "Tandem array-based expression screens identify host mRNA targets of virus-encoded microRNAs." Nature Genetics **41**(1): 130-134.

Zuker, M. (2003). "Mfold web server for nucleic acid folding and hybridization prediction." Nucleic Acids Research **31**(13): 3406-3415.

Zuo, J. M., L. L. Quinn, *et al*. (2011). "The Epstein-Barr virus-encoded BILF1 protein modulates immune recognition of endogenously processed antigen by targeting major histocompatibility complex class I molecules trafficking on both the exocytic and endocytic pathways." Journal of Virology **85**(4): 1604-1614.